CHEMICAL
RESEARCH,
DEVELOPMENT &
ENGINEERING
CENTER

CRDEC-CR-87059

EXTINCTION MEASUREMENTS ON ALUMINUM AND CARBON SMOKE PARTICLES FROM FAR INFRARED TO FAR ULTRAVIOLET

by Donald R. Huffman
UNIVERSITY OF ARIZONA
Tucson, AZ 85721

March 1987

U.S. ARMY
ARMAMENT
MUNITIONS
CHEMICAL COMMAND

Aberdeen Proving Ground, Maryland 21010-5423

UNCLASSIFIED
SECURITY CLASSIFICATION OF THIS PAGE

AD-A179 003

REPORT DOCUMENTATION PAGE

1a. REPORT SECURITY CLASSIFICATION UNCLASSIFIED	1b. RESTRICTIVE MARKINGS
2a. SECURITY CLASSIFICATION AUTHORITY	3 DISTRIBUTION/AVAILABILITY OF REPORT Approved for public release; distribution is unlimited.
2b. DECLASSIFICATION/DOWNGRADING SCHEDULE	
4. PERFORMING ORGANIZATION REPORT NUMBER(S) CRDEC-CR-87059	5. MONITORING ORGANIZATION REPORT NUMBER(S)
6a. NAME OF PERFORMING ORGANIZATION University of Arizona 6b. OFFICE SYMBOL (If applicable)	7a. NAME OF MONITORING ORGANIZATION
6c. ADDRESS (City, State, and ZIP Code) Tucson, AZ 85721	7b. ADDRESS (City, State, and ZIP Code)
8a. NAME OF FUNDING/SPONSORING ORGANIZATION CRDEC 8b. OFFICE SYMBOL (If applicable) SMCCR-RSP-B	9. PROCUREMENT INSTRUMENT IDENTIFICATION NUMBER DAAK11-80-K-0083
8c. ADDRESS (City, State, and ZIP Code) Aberdeen Proving Ground, MD 21010-5423	10. SOURCE OF FUNDING NUMBERS PROGRAM ELEMENT NO. / PROJECT NO. / TASK NO. / WORK UNIT ACCESSION NO.

11. TITLE (Include Security Classification)
Extinction Measurements on Aluminum and Carbon Smoke Particles from Far Infrared to Far Ultraviolet

12. PERSONAL AUTHOR(S)
Huffman, Donald R.

13a. TYPE OF REPORT	13b. TIME COVERED	14. DATE OF REPORT (Year, Month, Day)	15. PAGE COUNT
Contractor	FROM 80 09 TO 83 08	1987 March	184

16. SUPPLEMENTARY NOTATION
COR: Robert H. Frickel, SMCCR-RSP-B, (301) 671-3854

17. COSATI CODES			18. SUBJECT TERMS (Continue on reverse if necessary and identify by block number)
FIELD	GROUP	SUB-GROUP	Smoke, Carbon, Ultraviolet, Particles, Extinction, Optical constants, Aluminum, Infrared,
15	06	03	

19. ABSTRACT (Continue on reverse if necessary and identify by block number)

For various practical uses of the extinction properties of small particles, one must know the appropriate optical constants of the particulate medium and be able to properly calculate extinction from the optical constants. To know how well one can succeed in this, however, it is desirable to have carefully controlled tests comparing measured extinction for the small particles and calculated extinction. This report presents such findings for two different particulate systems - small aluminum particles and small carbon particles. (key words)

Since the parts of this work comprise the Ph.D. dissertations of two different individuals, it is convenient to present the results in two entirely separate parts. Part I is "The Extinction by Small Aluminum Particles," written by Janice Rathmann, and Part II is "The Optical Properties of Carbon," by Otto Edoh. Although there is a duplication of some introductory material, there is value in retaining the completeness of each work.

(Continued on reverse)

20 DISTRIBUTION/AVAILABILITY OF ABSTRACT	21. ABSTRACT SECURITY CLASSIFICATION
☒ UNCLASSIFIED/UNLIMITED ☐ SAME AS RPT. ☐ DTIC USERS	UNCLASSIFIED
22a. NAME OF RESPONSIBLE INDIVIDUAL TIMOTHY E. HAMPTON	22b. TELEPHONE (Include Area Code) (301) 671-2914 22c. OFFICE SYMBOL SMCCR-SPS-T

DD FORM 1473, 84 MAR — 83 APR edition may be used until exhausted. All other editions are obsolete.

SECURITY CLASSIFICATION OF THIS PAGE
UNCLASSIFIED

In both of these studies (aluminum and carbon), a critical review of optical constants was made with supplementary measurements done as necessary to produce what appears to be a sufficiently accurate set of optical constants for use in calculations. For aluminum, available optical constants appeared to be adequate, although new measurements relating to the unavoidable amorphous aluminum oxide coating were made. In the case of carbon, both glassy and crystalline carbon (graphite) were considered, with supplemental measurements required on the former. Extinction measurements were then made and compared with simple calculational models such as the Mie theory for spheres and a random distribution of ellipsoidal shapes in the Rayleigh approximation.

The essential conclusion we have reached in both of these studies is that shape effects, which are very difficult to calculate properly, play a dominant role in the infrared extinction of these two materials. Although difficult to calculate, the extinction deduced from measurements tends to be orders of magnitude higher than one calculates using sphere theory.

PREFACE

The work described in this report was authorized under Contract No. DAAK11-80-K-0083. This work was started in September 1980 and completed in August 1983.

The use of trade names or manufacturers' names in this report does not constitute an official endorsement of any commercial products. This report may not be cited for purposes of advertisement.

This report has been approved for release to the public.

BLANK

CONTENTS

(CONTENTS CONTINUED)

Part I

THE EXTINCTION BY SMALL ALUMINUM PARTICLES

Written by Janice Rathmann

EXTINCTION MEASUREMENTS ON ALUMINUM AND CARBON SMOKE PARTICLES
FROM FAR INFRARED TO FAR ULTRAVIOLET

1. ABSTRACT

Absorption measurements were performed from .12μm to 250μm on small particles of Al produced by the standard inert gas evaporation technique. These were done because experimental results of Granqvist et.al. revealed a discrepancy of over three orders of magnitude with the predictions of both the classical Drude theory for spherical particles and the quantum mechanical Gor'kov Eliashberg theory. Our measurements serve to confirm the results of Granqvist et.al. in the far IR and to extend the data to the UV. In the present paper the "anomalous" absorption is explained with a model using the classical Drude theory by taking into account a distribution of ellipsoidal shapes and an amorphous oxide layer, which is found to cover the particles. In order to determine the optical constants of amorphous aluminum oxide required in the calculation, a new technique applicable to powdered materials was used. Our model with the shape distribution was found to give excellent agreement with the experimental results. Several models proposed by other authors to explain the "anomalous" far IR absorption were also considered, but did not agree as well with the data.

2. INTRODUCTION

The absorption of light by several sizes of small aluminum particles was measured in the far infrared (from 3 cm^{-1} to 150 cm^{-1}) by Tanner, Sievers, and Buhrman (1975). For the smallest particle size they observed a multiple peak structure which they interpreted in terms of quantum size effects (QSE) predicted by the Gor'kov Eliashberg theory (1965). Granqvist et.al. (1976) repeated the experiment using an improved sample fabrication technique that produced smaller particles of a more uniform size. The structure that was expected to occur due to QSE was not seen and the absorption they measured was three orders of magnitude higher than either the Gor'kov Eliashberg theory or the classical Drude theory predict (see Fig. 1.). The failure to see structure caused by QSE is understandable since the size distribution of particles was not sharp enough (Granqvist et. al. 1976, Granqvist 1978). In fact Devaty and Sievers (1980) point out that it is very unlikely that QSE can be seen with present particle preparation techniques. The anomalously high absorption is not as

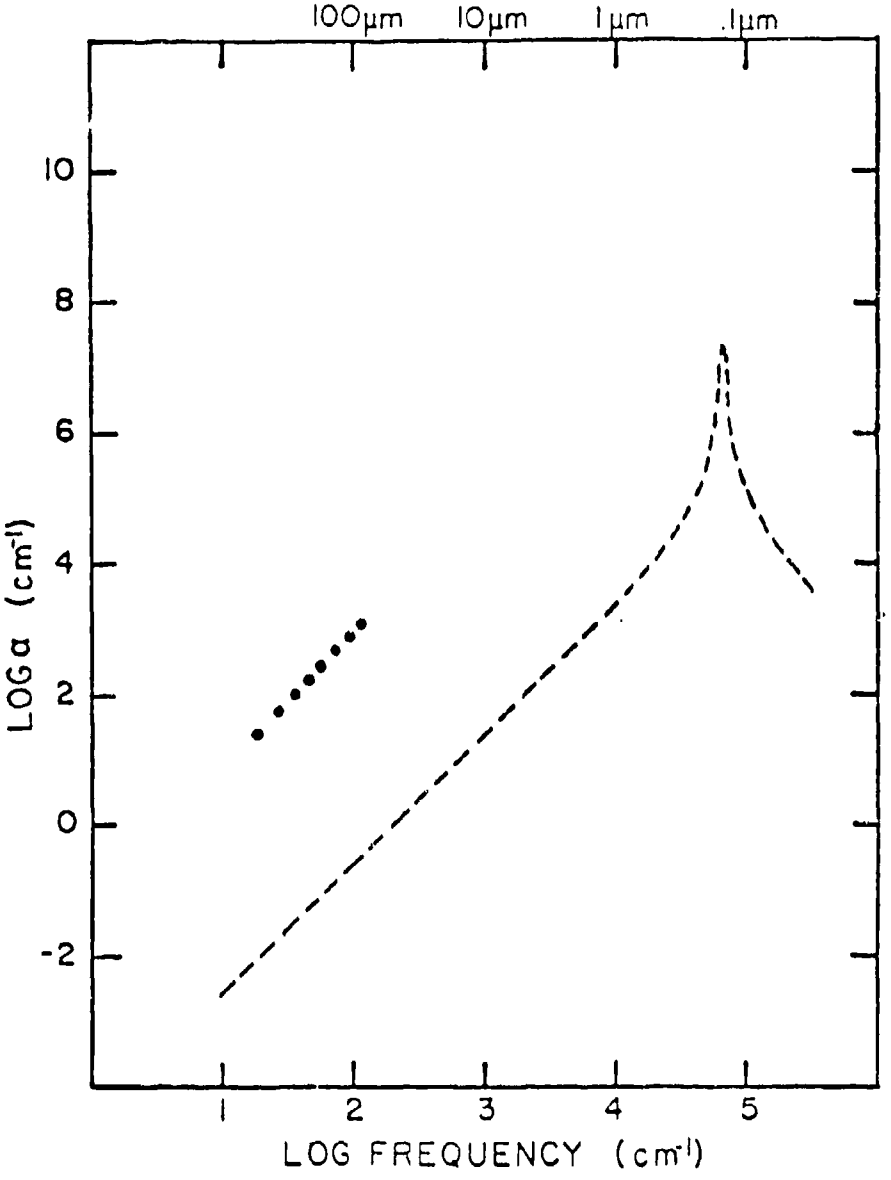

Fig. 1. Absorption Coefficient of Al

The data of Granqvist et al. (solid circles) and calculated absorption for spheres (dashed line)

easily explained. There have been many theories proposed to account for this, including the following.

1) The aluminum particles produced by Granqvist et.al. have an amorphous oxide coating on them (they purposely let in oxygen in the inert gas evaporation process to ensure electrical neutrality of the particles). It has been suggested by Simanek (1977) that the absorption occurs primarily in the oxide coating. His model requires the particles to aggregate into clusters so that in effect the sample consists of randomly oriented cylinders of aluminum oxide with aluminum particles embedded within.

2) Glick and Yorke (1978) suggest that a large part of the absorption in the far infrared should be due to phonon excitation. The Gor'kov Eliashberg theory and most of the others assume purely electronic absorption. They say the structure of the lattice absorption should closely parallel the structure in the phonon density of states of crystalline aluminum and expect the electronic absorption to have no appreciable structure. The absorption they calculate is in better agreement with the data of Granqvist et.al. (as far as it extends) than either the Gor'kov Eliashberg theory or the Drude theory.

3) Another theory (Lushnikov, Maksimenko, and Simonov 1978, and Maksimenko, Simonov and Lushnikov 1977) says that when the particle size is close to or smaller than the mean free path of the material there are QSE due to

correlations between the one electron energy levels inside the particle (Coulomb interactions between conduction electrons). This theory produces some improvement but does not completely account for th three orders of magnitude difference that was observed experimentally.

4) Ruppin (1979) calculates the absorption due to agglomerated oxide coated Al particles using the Bruggeman theory and the Maxwell-Garnett theory. For small particles (50 Å in diameter) the agreement between his theory for elongated clusters and the experimental results of Granqvist et.al. is not very good. For larger particles (375 Å in diameter), he gets good agreement with the experiment when he uses the Bruggeman treatment for elongated chainlike clusters (with the ratio of the long axis to the short axis equal to 30) or for disclike clusters.

5) In a later paper, Simanek (1980) proposes that the anomalously high absorption is due to Mott's (1970) a.c. conductivity mechanism. The reason for this new model is that preliminary measurements by Sievers (1978) indicated that the absorption in the far infrared by pure amorphous aluminum oxide was far too low. In this new calculation the absorption is primarily due to defects (excess aluminum and oxygen vacancies) that occur at the interface between the aluminum and the oxide. Simanek again uses the model of long oxide cylinders with spherical metal grains mixed in. With the use of Mott's a.c. conductivity formulation he

calculates the absorption and claims to get good agreement with experiment.

In this study we have extended the measurements of Tanner et.al. and Granqvist et.al. by measuring the absorption of small aluminum particles from the far infrared to the vacuum ultraviolet (.12 μm to 250 μm). In an attempt to resolve the discrepancy between the theory and the experimental results use is made of a simple treatment of nonspherical shapes (Huffman and Bohren 1980). Although the aluminum particles produced are known to be almost spherical (Granqvist and Buhrman 1976) they clump together to form chains and clusters which behave much like single particles of nonspherical shape.

Due to the oxide coating on the particles it was necessary to consider two layer particles in the shape distribution calculation. This requires the optical constants of the amorphous oxide coating. In the infrared these were determined experimentally by doing absorption measurements and the results of Hagemann, Gudat, and Kunz (1974) were used in the ultraviolet.

3. THEORY

When dealing with the optical properties of small particle systems it is important to understand how light interacts with bulk solids. This chapter begins by introducing the terminology used when dealing with optical properties of matter. In the next section we will begin the discussion of small particles by looking at the Mie theory for spheres and find the Rayleigh limit for the case of Al particles. We then discuss the Rayleigh theory for ellipsoids and generalize it to take into account a distribution of ellipsoidal shapes. Finally, this shape distribution is used to calculate the absorption of small particles of Al_2O_3 and comparison is made with experimental results.

3.1 Optical Properties of Bulk Solids.

Maxwell's equations for the interaction of electromagnetic radiation with a nonmagnetic, isotropic material (in cgs units) are:

$$\nabla \cdot \vec{E} = 0 \tag{1}$$

$$\nabla \times \vec{E} = -\frac{1}{c}\frac{\partial \vec{H}}{\partial t} \tag{2}$$

$$\nabla \cdot \vec{H} = 0 \tag{3}$$

$$\nabla \times \vec{H} = \frac{\varepsilon}{c}\frac{\partial \vec{E}}{\partial t} + \frac{4\pi\sigma}{c}\vec{E} \tag{4}$$

where

E is the electric field vector,

H is the magnetic field vector,

c is the speed of light in vacuo,

ε is the dielectric constant, and

σ is the electrical conductivity.

We can find a wave equation for E by taking the curl of (2) and substituting (4) into the resulting expression,

$$\nabla^2 \vec{E} = \frac{\varepsilon}{c^2}\frac{\partial^2 \vec{E}}{\partial t^2} + \frac{4\pi\sigma}{c^2}\frac{\partial \vec{E}}{\partial t} \tag{5}$$

For monochromatic light, of wavevector $\vec{q}$ and frequency ω, a single plane wave can be used to describe the electric field vector,

$$\vec{E} = \vec{E}_o \exp i(\vec{q}\cdot\vec{r} - \omega t) \tag{6}$$

Substituting this into (5) we find,

$$q^2 = \frac{\omega^2}{c^2}\left(\varepsilon + \frac{i4\pi\sigma}{\omega}\right) \tag{7}$$

We can define a complex index of refraction m, such that,

$$\vec{q} = \frac{\omega}{c} m\hat{q} = \frac{\omega}{c}(n+ik)\,\hat{q} \tag{8}$$

where n is just the usual index of refraction, k is normally called the extinction coefficient, and $\hat{q}$ is a unit vector in the direction of $\vec{q}$. Substituting this in the wave equation (5), the expression for the electric field becomes,

$$\vec{E} = \vec{E}_0[\exp-(\tfrac{\omega}{c} k\hat{q}\cdot\vec{r})][\exp i(\tfrac{\omega}{c} n\hat{q}\cdot\vec{r}-\omega t)] \qquad (9)$$

We see that k determines the extent to which the amplitude of the light wave is attenuated in the material, i.e. it is a measure of the absorption by the material. c/n is the speed of light in the material.

From (7), we see that a complex dielectric constant can be defined,

$$q^2 = \frac{\omega^2}{c^2}\varepsilon = \frac{\omega^2}{c^2}(\varepsilon'+i\varepsilon'') \qquad (10)$$

where ε' and ε'' are the real and imaginary parts of ε, respectively. ε' is just the old ε from Maxwell's equations, and $\varepsilon''=4\pi\sigma/\omega$. By squaring (8) and comparing to (10) we can find the relationships between the complex dielectric constant and the complex index of refraction,

$$\begin{aligned} \varepsilon' &= n^2 - k^2 \\ \varepsilon'' &= 2nk \end{aligned} \qquad (11)$$

Either of these two sets of quantities $(\varepsilon',\varepsilon'')$ or (n,k), characterize the optical properties of the material. In discussions of optical properties of small particles we usually use the dielectric constant, ε.

3.2 Introduction to Small Particles and the Mie Theory.

When light is incident on a system of small particles it can either be scattered or absorbed. The sum is called extinction, i.e.,

extinction=scattering+absorption.

The amount of light transmitted through a collection of n spherical particles, with path length l can be written,

$$T = \exp\ (-NQ_{ext}\pi a^2)l \qquad (12)$$

where

N is the number of particles per unit volume=n/V and

a is the radius of the particle.

Q_{ext} is called the efficiency factor for extinction, and is equal to the sum of the absorption efficiency (Q_{abs}) and the scattering efficiency (Q_{scat}). These quantities will be discussed later in more detail. It is more convenient to write (12) in terms of the mass per unit area of particles, σ, where

$$\sigma = m/A = ml/V = (n4/3\pi a^3\rho)l/V$$

Here ρ is the bulk density of the material. Therefore, the transmission equation (12) becomes,

$$T = \exp\ (-3/4\ \frac{Q_{ext}}{\rho a}\ \sigma)$$

or

$$T = \exp\ (-\alpha\sigma/\rho) \qquad (13)$$

where $\alpha=3Q_{ext}/4a$ is the extinction cross section per unit volume of material.

In 1908 Gustav Mie developed a theory to calculate Q_{ext} and Q_{scat} for arbitrarily sized spherical particles. The derivation is given many places (see for example van de Hulst 1957); we will just quote the results. The extinction cross section for a sphere (where $C_{ext}= \pi a^2 Q_{ext}$) is,

$$C_{ext} = \frac{2\pi a^2}{x^2} \sum_{1}^{\infty} (2n+1)\ \mathrm{Re}\ (a_n+b_n) \qquad (14)$$

and the scattering cross section ($C_{scat}=\pi a^2 Q_{scat}$) is,

$$C_{scat} = \frac{2\pi a^2}{x^2} \sum_{1}^{\infty} (2n+1)(|a_n|^2+|b_n|^2) \qquad (15)$$

where x is the size parameter and is related to the wavelength of light (λ) through,

$$x = 2\pi a/\lambda \qquad (16)$$

The Mie coefficients a_n and b_n are complex (and complicated) expressions involving spherical Bessel and Hankel functions and their derivatives.

It turns out that (14) and (15) can be greatly simplified if the following two conditions hold,

i) $x<<1$,

ii) $|m|x<<1$.

The first condition requires that the size of the particle be small compared to the wavelength of light and the second

condition requires the phase shift of light within the particle to be negligible. We can see the simplification by looking at Fig. 2. where C_{ext}/vol (α) for Al vs. particle radius (a) has been plotted on a log-log scale, using the Mie theory, for several different wavelengths of light. For each of the wavelengths there is a flat region, where the extinction is almost independent of the size of the particle. Such a flat region occurs for a<100Å. This region is where the above two conditions are fulfilled and is due primarily to the a_1 term in the Mie theory. It is generally called the Rayleigh region, after Lord Rayleigh, who solved the problem for very small particles many years before the Mie theory. The large bump for the three curves with λ > 1μm is primarily due to the b_1 term in the Mie theory. Physically, it is caused by eddy current losses. Eddy currents are important when the diameter of the particle is close to, but less than, the skin depth of the particle material. For λ =.1 m the skin depth is less than the radius (for a=100Å) so that the interior of the particle is shielded from the external electric field. In this case, the eddy currents are confined to the surface so that the volume of material able to absorb energy is reduced.

We will, in general, assume $x<<1$ and $|m|x<<1$ so that eddy current losses and other higher order modes can be ignored, and therefore, Rayleigh theory can be used.

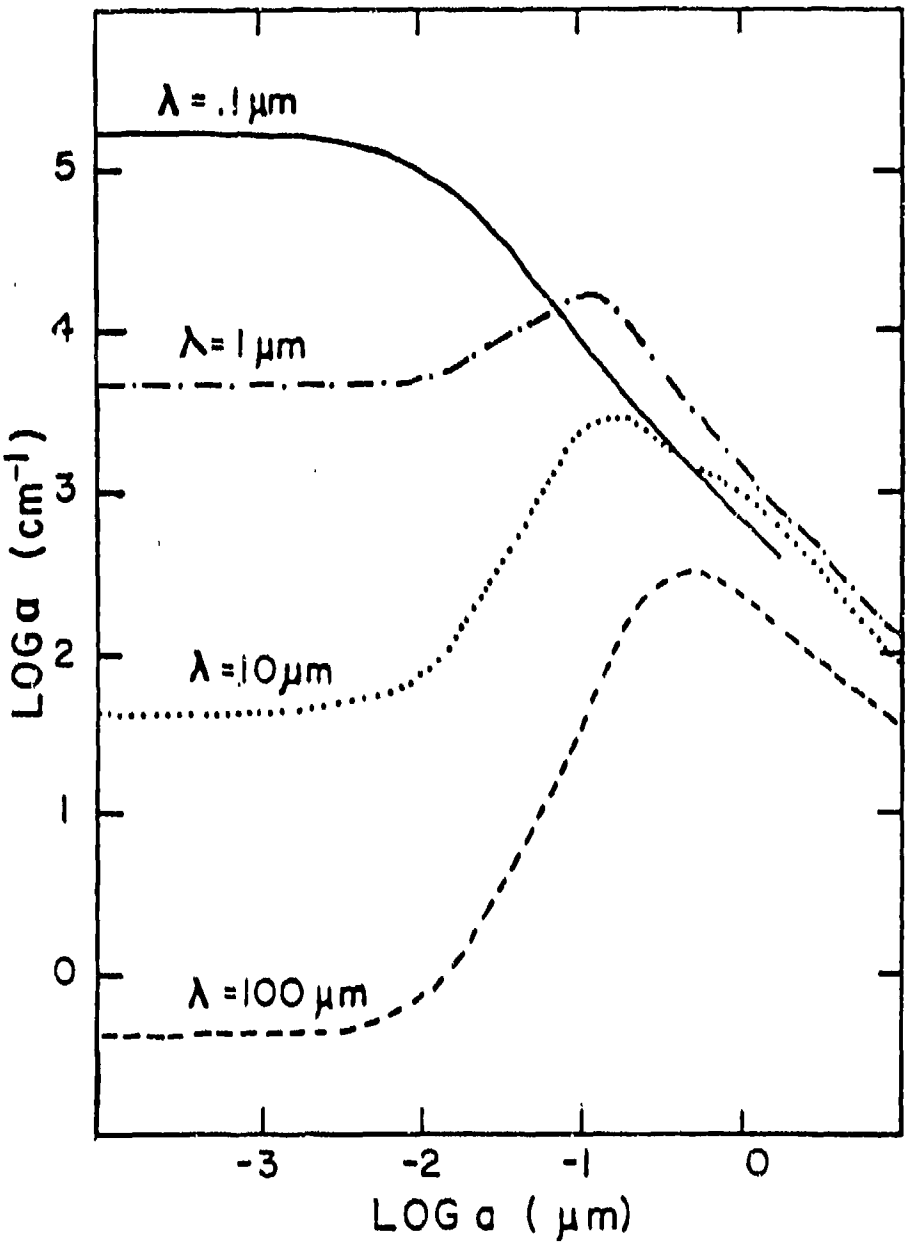

Fig. 2. Dependence of Absorption on Particle Size

Calculated absorption for spherical particles vs. particle radius using the Mie theory for various wavelengths of light

It can be shown that the absorption and scattering cross sections calculated in the Rayleigh limit are equivalent to considering the particle as an electric dipole in a uniform electric field (see, for example, van de Hulst 1957). The electric polarizability ($\tilde{\alpha}$), for a sphere embedded in a medium of dielectric constant ε_m, is (see Jackson 1962),

$$\tilde{\alpha} = \frac{\varepsilon-\varepsilon_m}{\varepsilon+2\varepsilon_m} \tag{17}$$

where ε is the complex dielectric constant of the particle, and a is the radius of the particle. C_{scat} and C_{abs} are related to the polarizability through the relations (van de Hulst 1957),

$$C_{scat} = \frac{8\pi}{3} k^4 |\tilde{\alpha}|^2 \tag{18}$$

$$C_{abs} = 4\pi k \, \mathrm{Im}\, \tilde{\alpha} \tag{19}$$

where $k = 2\pi/\lambda$. By substituting (17) into (18) and (19) we get,

$$C_{scat} = \frac{8}{3} \pi a^2 x^4 \left| \frac{\varepsilon-\varepsilon_m}{\varepsilon+2\varepsilon_m} \right|^2 \tag{20}$$

$$C_{abs} = 4\pi a^2 x \, \mathrm{Im} \, \frac{\varepsilon-\varepsilon_m}{\varepsilon+2\varepsilon_m} \tag{21}$$

In (20) we see the familiar result that the scattering is proportional to $1/\lambda^4$ (since $x = 2\pi a/\lambda$), provided ε and ε_m are slowly varying.

3.3 Rayleigh Theory for Ellipsoids.

So far in our discussion of small particles we have been dealing with spherical particles. Real particles, however, are not usually spherical. The Mie theory is useful for calculations for spheres but is quite cumbersome and not easily generalized to other shapes of particles (except infinite cylinders). As discussed in the previous section, an approximate expression for the absorption and scattering cross sections can be found by solving the electrostatic boundary value problem to obtain the polarizability.

We can generalize this to other shapes of particles, specifically to ellipsoids, by solving the boundary value problem in ellipsoidal coordinates. This derivation is given in Stratton (1941). The expression for the polarizability of an ellipsoid with semi-axes a,b,c, with the field parallel to the jth axis, is,

$$\tilde{\alpha}_j = \frac{V}{4\pi} \frac{\varepsilon-\varepsilon_m}{\varepsilon_m+L_j(\varepsilon-\varepsilon_m)} \qquad (22)$$

where

j=1,2,3 and

V is the volume of the ellipsoid, V= $4/3\pi abc$.

The L_j's are called depolarization factors and are related to the semi-axes of the ellipsoid. L_3, for example, is given by,

$$L_3 = \frac{abc}{2} \int \frac{dq}{(a^2+q)^{1/2}(b^2+q)^{1/2}(c+q)^{1/2}}$$

They are normalized such that, $L_1+L_2+L_3=1$. Using (18) and (19) we can get expressions for C_{scat} and C_{abs} for a single ellipsoid with arbitrary L_j,

$$C^j_{scat} = \frac{k^4}{6\pi} V^2 \left| \frac{\varepsilon-\varepsilon_m}{\varepsilon_m+L_j(\varepsilon-\varepsilon_m)} \right|^2 \tag{23}$$

$$C^j_{abs} = kV \, Im \left\{ \frac{\varepsilon-\varepsilon_m}{\varepsilon_m+L_j(\varepsilon-\varepsilon_m)} \right\} \tag{24}$$

where the superscript j means the light polarization is parallel to the jth axis.

For most of the spectrum, when the size of the particle is small enough the extinction is almost entirely due to absorption. We can see this by taking the ratio of C_{scat} to C_{abs},

$$\frac{C_{scat}}{C_{abs}} = \frac{V}{6\pi} k^3 \frac{(\varepsilon'-\varepsilon'')+\varepsilon''^2}{\varepsilon_m \varepsilon''} \tag{25}$$

where the real and imaginary parts of ε are explicitly shown. Values of this ratio are given in Table 1 using the dielectric constants of Al, with $\varepsilon_m=1.0$.

Since (25) does not depend on the shape of the particle (i.e., there is no L_j dependence), we have assumed a spherical particle with a radius of 50Å. From the table we see that it isn't until well into the UV that the scattering becomes important and, therefore, in general, scattering may be neglected.

Table 1. Ratio of Scattering to Absorption for Al in the Rayleigh Limit

Wavelength (μm)	Frequency (cm^{-1})	C_{scat}/C_{abs}
100	10^2	10^{-7}
10	10^3	10^{-5}
1	10^4	10^{-3}
.33	3×10^4	10^{-2}
.10	10^5	.3

For a collection of randomly oriented identical ellipsoids we can find the average absorption cross section by summing (24) over j and dividing by three,

$$< C_{abs} > = \frac{V}{3} k \sum_{j=1}^{3} \frac{\varepsilon_m \varepsilon''}{L_j\{[\varepsilon'+\varepsilon_m(1/L_j-1)]^2 + \varepsilon''^2\}} \qquad (26)$$

which is now written in real notation. It should be noted that we are assuming single particle absorption, i.e. the particle separation is sufficient that the field seen by one particle is unaffected by the presence of neighboring particles. We expect the absorption to be large whenever the denominator of this expression is close to zero. There will be a resonance whenever the term in square brackets is equal to zero, the strength of the resonance depending on the size of ε". Setting the term in square brackets equal to zero and solving for ε', we get,

$$\varepsilon' = -\varepsilon_m \, (1/L_j - 1) \qquad (27)$$

as the condition for resonance.

For a sphere all of the L_j's are equal, and therefore have the value 1/3, so there will be a maximum in the absorption whenever,

$$\varepsilon' = -2\varepsilon_m.$$

For a distribution of identical, noninteracting, ellipsoids with arbitrary L_j's there will be three peaks in the absorption, corresponding to the three values of L_j. Furthermore, we see that for a system of particles which contains all shapes of ellipsoids (so that L_j can take on any value from 0 to 1) there should be absorption over the entire region where ε' is negative.

To illustrate these three cases we have plotted the absorption/vol for Al particles in air, so that ε_m=1.0. (see Fig. 3.). We have also plotted ε' vs. frequency on the same frequency scale below. For the spheres curve there is a large peak in the absorption at the frequency for which ε'=-2. Physically, this corresponds to collective oscillations of the free electron plasma within the boundaries of the spherical particles. The dashed curve is for ellipsoids with L_1=.01, L_2=.3, and L_3=.69. As expected, there are three peaks. A discussion of how the remaining curve was obtained is left for the next section.

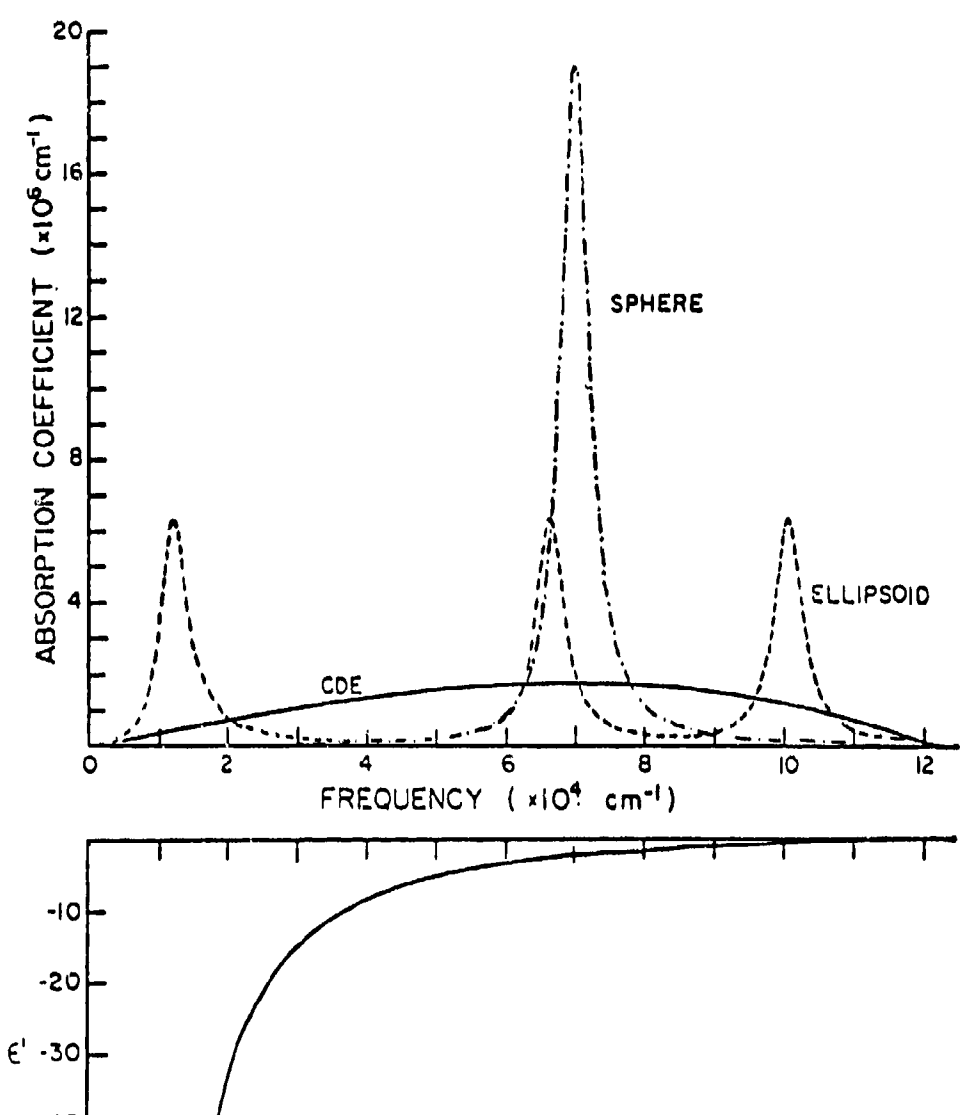

Fig. 3. Calculated Absorption for Al in the Rayleigh Approximation

Top figure: Calculated Absorption for spheres (dot dash), a single ellipsoid with L_1=.01, L_2=.3, and L_3=.59; and for a continuous distribution of ellipsoids (solid line)

Bottom figure: ε' vs. frequency; the cross marks the point where $\varepsilon'=-2$

3.3.1 The Shape Distribution.

The average absorption cross section for a collection of randomly oriented, identical ellipsoids is given by (26). Let us assume that the small particle system under consideration consists of a variety of shapes of ellipsoids. How do we handle this situation? If a mathematical expression for the distribution of shapes is known, then (26) could be integrated over that shape distribution function, i.e.,

$$<< C_{abs} >> = \iint P(L_1, L_2) \; < C_{abs} > \; dL_1 dL_2 \qquad (28)$$

where P is the shape distribution function. The << >> denotes the double averaging that is being done, i.e., over orientation and shapes. Because of the restriction that $L_1+L_2+L_3=1$, we can choose L_3 to be fixed by the condition $L_3=1-L_1-L_2$, so that P is a function only of L_1 and L_2.

The evaluation of this integral is given by Huffman and Bohren (1980). They assumed a uniform shape distribution function (i.e., $P(L_1,L_2)$=a constant). In other words, all shapes of ellipsoids are taken as equally probable. The result of this integration is,

$$<< C_{abs} >> = k \; < V > \; Im \left[\frac{2\varepsilon\varepsilon_m}{\varepsilon-\varepsilon_m} \log(\varepsilon/\varepsilon_m) \right] \qquad (29)$$

In the log term the principal value must be used, i.e., $|\varepsilon|>0$, $-\pi<\theta<\pi$.

Let's return to Fig. 3. The curve labeled CDE (which stands for continuous distribution of ellipsoids) was found by evaluating (29). There is absorption ranging from zero frequency ($\tilde{\nu}$=0), where $\varepsilon' = -\infty$, to $\tilde{\nu} = 1.2\times10^5$ cm^{-1}, where ε' crosses the zero axis. The maximum absorption for the CDE curve is approximately an order of magnitude smaller than the maximum for spheres. The CDE curve has a broader absorption band though, so that away from the peak it has a larger absorption. To make this point clearer we have replotted this graph on a log-log scale (Fig. 4.). At 10μm (1000 cm^{-1}), for example, the absorption calculated using the shape distribution is approximately three orders of magnitude higher than for spheres. The significance of this observation will become clearer in Chapter 5.

3.3.2 An Example using the Shape Distribution.

In this section we will calculate the absorption for αAl_2O_3 (corundum crystal structure) particles using the continuous shape distribution and compare it to experimental results. The αAl_2O_3 used was obtained from the Buehler Co. (alpha micropolish), the particle size given by them is .3μm. Measurements were done using the standard KBr pellet technique (see Chapter 4) in the region of the infrared absorption band. The result of these measurements is shown in Fig. 5. For comparison we have also plotted the calculated absorption/vol for spheres and for a distribution

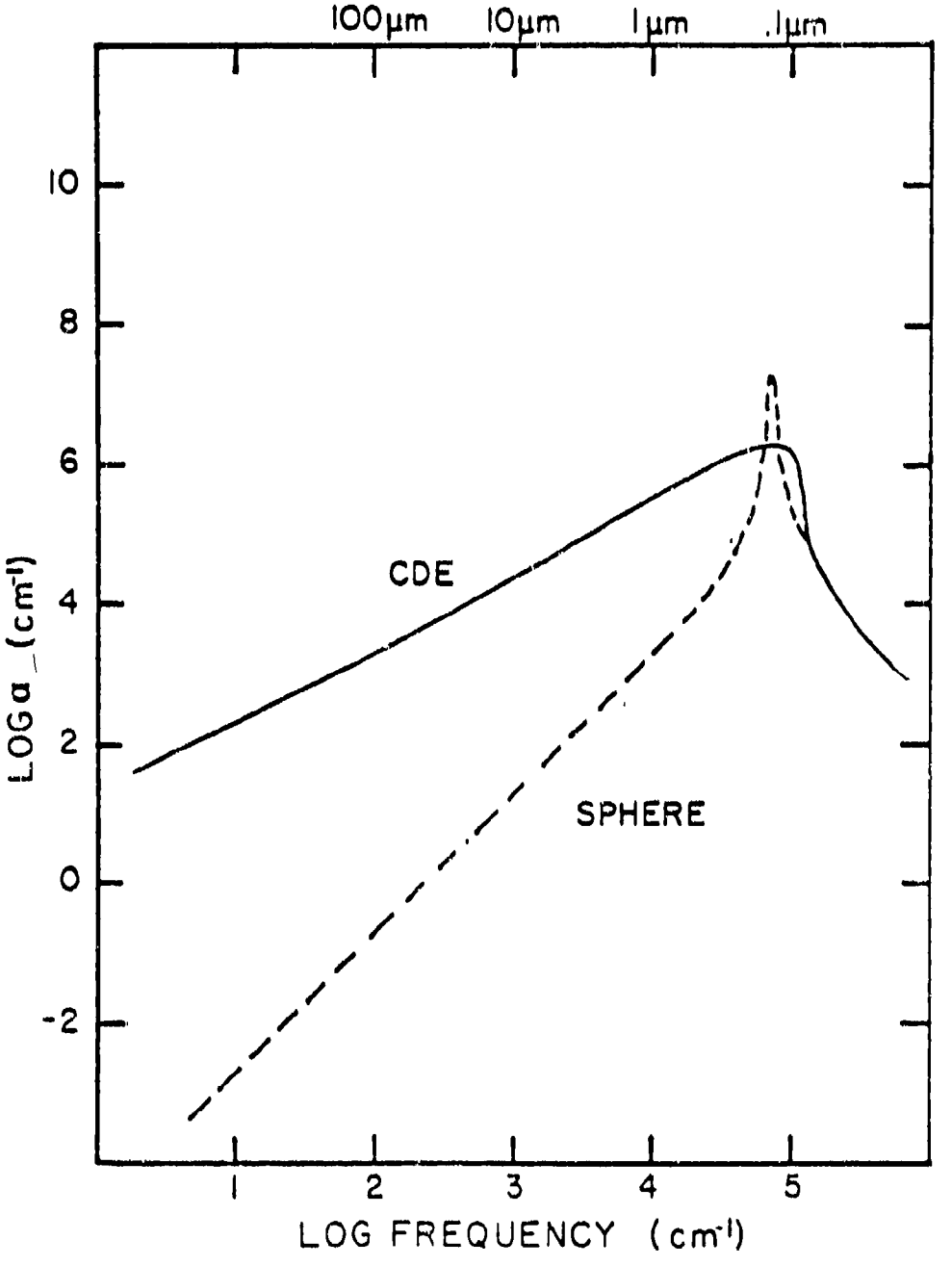

Fig. 4. Log-Log Plot of Calculated Absorption in the Rayleigh Approximation

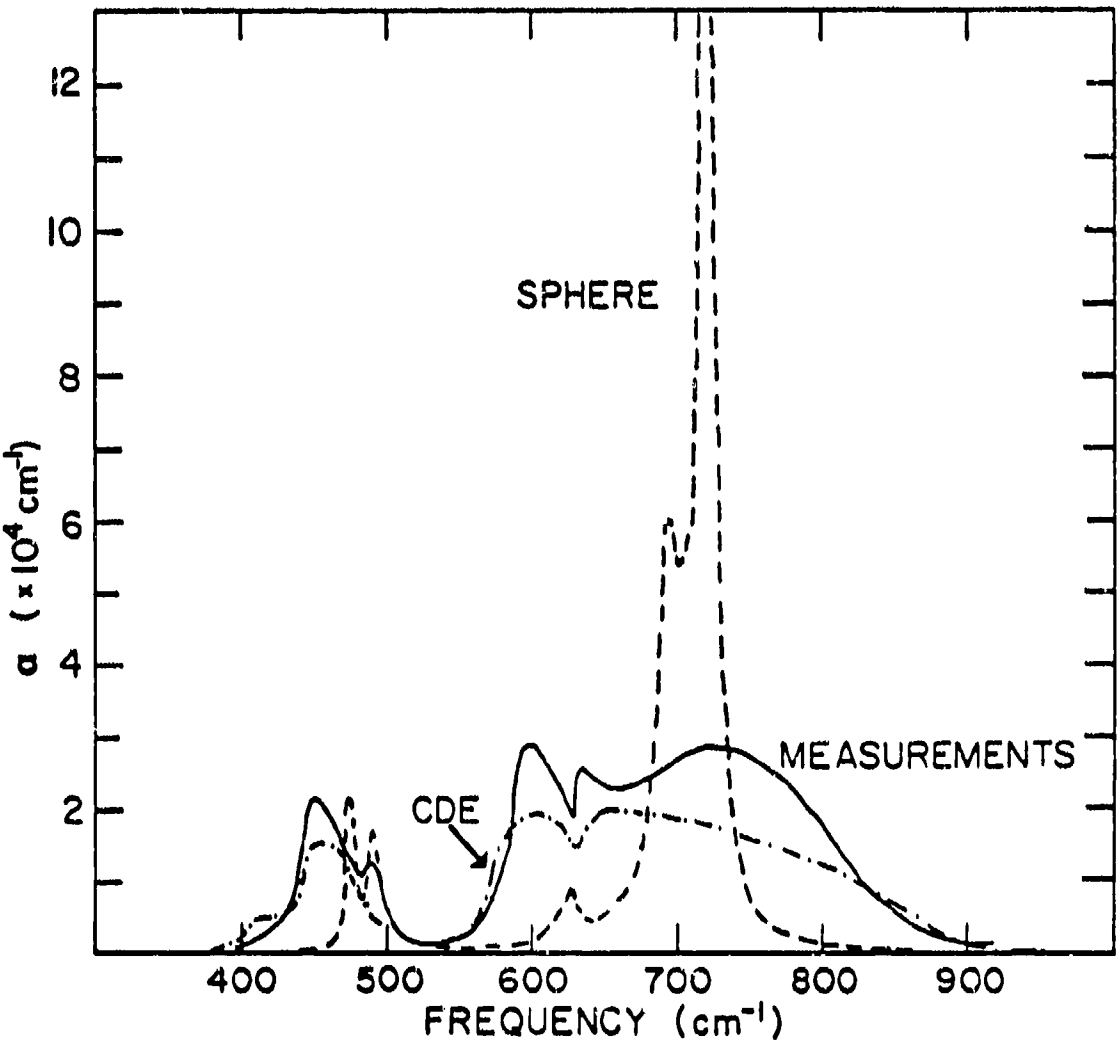

Fig. 5. Extinction of Al_2O_3

Comparison of measured extinction (solid line) of Al_2O_3 in KBr (ε_m=2.3) with calculations for spheres (Note: α_{max} = 2.1 × $10^5 cm^{-1}$) and a distribution of ellipsoidal shapes (CDE) in the Rayleigh Approximation

of ellipsoids using the optical constants of Barker (1963). If we compare the experimental results to the absorption/vol calculated for spheres, the agreement is very poor. The locations, strengths, and widths of the peaks differ substantially. There is much better agreement between the experimental results and the CDE curve. The widths of the calculated and experimental bands are very close and the measured peak magnitude is only about 50% higher than the CDE curve. The experimental curve also exhibits more structure than the CDE curve. Possible reasons for the differences in these two curves are uncertainties in the optical constants used to find the CDE curve and the fact that the actual particle shapes may not correspond exactly to a uniform continuous distribution of ellipsoids. The good agreement between the CDE results and the experimental results gives us reason to believe that small particle systems of other materials may best be described by using a shape distribution.

4. EXPERIMENT

To measure the extinction by small aluminum particles two slightly different sample preparation methods and four measuring instruments are used. In this chapter we will discuss how the Al and Al_2O_3 samples are made and measured. First we will describe the small particle production, followed by a description of how the particles are suspended so that the transmission through them can be measured. In order to determine the extinction from transmission measurements it is necessary to find σ, the mass per unit area of particles. We will describe how σ is determined. Then the instruments which are used to measure the transmission will be discussed. Finally, we will discuss the final step in the sample preparation for far infrared measurements.

4.1 Particle Production.

One of the easiest ways to make very small particles is by using the technique of inert gas evaporation (Kimoto et.al. 1963 and Yatsuya, Kasukabe, and Uyeda 1973). The size of particles that is produced depends on several

factors: the atomic weight of the gas, the pressure of the gas, the evaporation rate of the material, and the distance above the source the particle are collected at. In general, the smallest particles are made by using a low pressure of helium gas at a slow evaporation rate with the collection plate as close as possible to the source.

The procedure for making the small aluminum particles is as follows. First the chamber is evacuated to 2×10^{-5} torr using an oil diffusion pump. Purified aluminum, obtained from the Matheson, Coleman, and Bell Co., is heated in a tungsten wire filament until melted. After the filament has cooled, the system is purged with helium to reduce the partial pressure of oxygen, and then reevacuated. Now the valve between the pump and the bell jar is closed and one torr of helium gas, as measured by a thermocouple gauge, is introduced into the chamber. The current through the filament is slowly raised until the smoke of small aluminum particles begins to be produced. A metal plate with either glass slides, polyethylene or LiF substrates attached to it is positioned 10cm above the filament to collect the particles. When the desired density of particles is achieved, the current through the filament is turned off. After the filament is allowed to cool, air is let into the system and the substrates are removed from the metal plate.

The particles were produced under the same conditions for every sample so that ideally the particle size should be the same for all samples. Extensive studies on the formation of Al particles produced by inert gas evaporation in He have been done by Yatsuya, Kasukabe, and Uyeda (1973). They determined that the particles are almost spherical and measured how the particle size depends on the pressure of the gas (for a given filament temperature and distance from the source to collection plate). By extrapolating their results to the pressure used in our experiment we determined the particle diameter to be approximately 50Å. However, the spherical particles clump together to form chains and clusters which changes their effective size (and shape). For this reason we do not believe it would be useful to do accurate measurements of particle sizes on an electron microscope.

Amorphous aluminum oxide (aAl_2O_3) particles can be made using a similar technique. In this case, 10 torr of air and 50 torr of He were admitted into the system, and the smoke was made in the same manner as for Al. A tantalum boat was used rather than a tungsten filament since tungsten oxidizes to produce WO_3 particles. The aAl_2O_3 smoke was collected on a metal plate and then scraped off and stored in a small vial. An xray powder pattern was taken on the particles. There were two faint and indistinct lines located at the positions where the two brightest lines for

crystalline γAl_2O_3 occur suggesting that the material is mainly amorphous with perhaps some γAl_2O_3 mixed in.

We also did measurements using commercially available Al_2O_3 powder obtained from the Linde Co.. The diameter of the particles is given as .05μm. This material appears to be primarily γAl_2O_3 based on the analysis of the powder xray pattern and also since it has sharper structure in the IR than the smoke.

4.2 Suspension of Particles.

In order to measure the amount of light that is absorbed by a collection of particles they must be suspended in some manner. The easiest way is to collect them on a transparent substrate. For measurements in the ultraviolet this method works well since the particles can be kept reasonably well isolated and there is still a measurable amount of absorption. We use this method for Al particles in the UV (.12μm-.45μm) with LiF as a substrate. Because the absorption is found to decrease with increasing wavelength for Al particles, the density of particles has to be increased. Since we wish to keep the particles isolated, the best way to do this is to stack layers of particles on top of each other with a transparent substrate between each layer. A convenient material to use for measurements in the visible to the far IR is polyethylene. The number of layers of polyethylene used depends on how strong the particle

absorption is. To keep the layers from falling apart, and to ensure that the Al particles are totally surrounded by polyethylene, they are fused together by placing them between microscope slides and applying gentle hand pressure while heating them on a hot plate.

For the Al_2O_3 smoke and powder we use the standard KBr pellet technique (see, for example, Miller 1972) for measurements from the visible to the mid IR. A small amount (.2mg-.3mg) of the Al_2O_3 is mixed with .5gm of IR quality KBr in a small vial which has a steel ball bearing in it and is shaken for 5 minutes in a Crescent "Wig-L-Bug" dental amalgamator. The mixture is then pressed into a 13mm transparent pellet by using a special die and applying 12 tons of force. For measurements on Al_2O_3 in the far IR the polyethylene powder method is used. The material is mixed with .1gm of polythethylene and poured into the KBr die. The die is placed on a hot plate until the powder melts. It is allowed to cool and then the polyethylene disc is carefully removed with the aid of a razor blade.

4.3 Mass Calibration.

The determination of the mass per unit area (σ) for the Al particles is a difficult problem. Since σ is very low ($.5\mu g/cm^2$-$5\mu g/cm^2$) it is not easy to measure directly using an analytical balance. To solve this problem we used the following method to determine the mass of a sample

optically. Al smoke was collected on 20 1"×1" pieces of glass microscope slides (generally with higher densities than will be used in the experiment). The transmission through each smoked slide was measured in the visible using a Cary 14 spectrophotometer. The slides were weighed with the smoke on and reweighed after the smoke had been removed, the difference is the mass of the Al. Then the extinction cross section per unit volume is found, at some wavelength (we chose 5000Å), by using the equation,

$$T = \exp(-\alpha\sigma/\rho)$$

for each of the 20 slides. Since the absorption depends somewhat on the mass per unit area, α vs. σ is plotted and a least squares fit is done. The slope was found to be 10.6 cm^{-3}/gm with a y-intercept of 2.8×10^{5} cm^{-1}. Therefore, we find for the typical masses we will use in the experiment that $\alpha(5000Å)=2.85\times10^{5}cm^{-1}$. Now that α is known at this wavelength, σ can be determined for an arbitrary sample by measuring the transmission through it and inverting (13). This is the method used for the Al particles in both the polyethylene sheet method and the LiF method.

For the Al_2O_3 samples the smoke or powder was weighed directly on an analytical microbalance.

4.4 Measuring Instruments.

Four different measuring instruments were required to measure the absorption by Al particles from .12μm-250μm. The instrument used in each spectral region along with the type of sample used is summarized in Table 2.

In the far infrared (25μm-250μm) measurements were done on a Beckman IR 11 spectrophotometer. It was modified to use a liquid He cooled doped germanium bolometer as a detector with the output sent to a PAR model 28 lock-in amplifier. The output from the lock-in was sent to a digital voltmeter or a chart recorder. Because there are reflectance losses at the polyethylene surfaces a reference blank was made in the same manner as the samples using clean polyethylene. To determine the absorption by the Al particles, the ratio of the transmission through the sample to the transmission through the blank is found.

A Perkin Elmer 398 spectrophotometer is used in the mid IR region. It is a dual beam instrument; the sample is placed in the front beam and the reference blank is placed in the back beam. An optical attenuator, or comb, in the reference path moves to keep the intensities of the two beams equal. The position of the comb indicates the transmittance of the sample and is sent electrically to the recorder. This is useful since polyethylene exhibits several strong sharp absorption bands in this region of the spectrum and the machine can usually compensate for these.

Table 2. Spectral Region, Sample Type, and Instrument

Region	Wavelength (Frequency)	Sample Type	Instrument	Spectral Resolution
Far IR	250μm-20μm ($40-500cm^{-1}$)	poly. stack	Beckman IR11	∿5cm
Mid IR	25μm-2.5μm ($400-4000cm^{-1}$)	poly. stack	Perkin Elmer 398	∿5cm
Near IR to Vis.	2μm-.33μm ($5000-3.3\times10^{4}cm^{-1}$)	poly. stack	Cary 14	∿10Å
Vis. to Far UV	.6μm-.12μm ($2\times10^{4}-8\times10^{4}cm^{-1}$)	LiF substrate	McPherson Seya-Namioka	∿30Å

For the near IR to the visible region we used a Cary 14 spectrophotometer. It is also a dual beam instrument which automatically compensates for variations in the transmission of the reference sample.

A McPherson model 235 Seya Namioka monochromater, with a Bausch and Lomb grating (radius=498.1mm, λ_{blaze}=1500Å, 600 lines/mm), was used for measurements in the UV, with a hydrogen discharge lamp as a light source. The lamp produces a continuum from 5000Å to 1600Å and a multiline spectrum below 1600Å. The detector is a photomultiplier tube that had been coated with the fluorescent material sodium salicylate, with the output signal going to a picoammeter. To compensate for nonuniform light levels produced by the hydrogen lamp, part of the light that exits from the monochromater is deflected to a second identical phototube. The voltage to both tubes is supplied by a single programmable high voltage power supply. A servomechanism keeps the current through the second phototube constant by controlling the voltage of the power supply, thus normalizing the output of the first phototube.

The experimental apparatus was interfaced to an Imsai 8080 microcomputer by Ballart (1980) to facilitate data collection. The output from each phototube is sent to a separate picoammeter. The signals from the two picoammeters are sent through a multiplexer to an analog to digital converter and then to a parallel port of the

microcomputer. When the wavelength is being scanned a pulse is sent from the McPherson to the computer every 5Å so that the computer can keep track of the wavelength. To find the absorption by the aluminum particles alone, first the transmission vs. wavelength of a clean part of the LiF is measured, then we measure the transmission through the smoked part, and finally a zero level scan is done with the first phototube pushed aside so that the light does not hit it. The zero level scan is necessary because the signal from the picoammeter depends on the voltage across the phototube, which causes the zero level to change as the wavelength is scanned. The computer stores the data from each of these three runs and then performs the calculations to find the absorption. The results are then plotted on an X-Y recorder which was interfaced to the computer via two digital to analog converters. A block diagram of the McPherson electronics is given in Fig. 6.

LiF was used as a substrate for measurements in the UV since it is transparent further into the UV than any other readily available material. Measurements were not possible below 1200Å because the LiF became too absorbing.

4.5 Far IR Samples.

Thirty-six samples were produced by the polyethylene sheet method. The mass density per layer of the samples ranged from .5μg/cm²/layer to 4μg/cm²/layer. Transmission

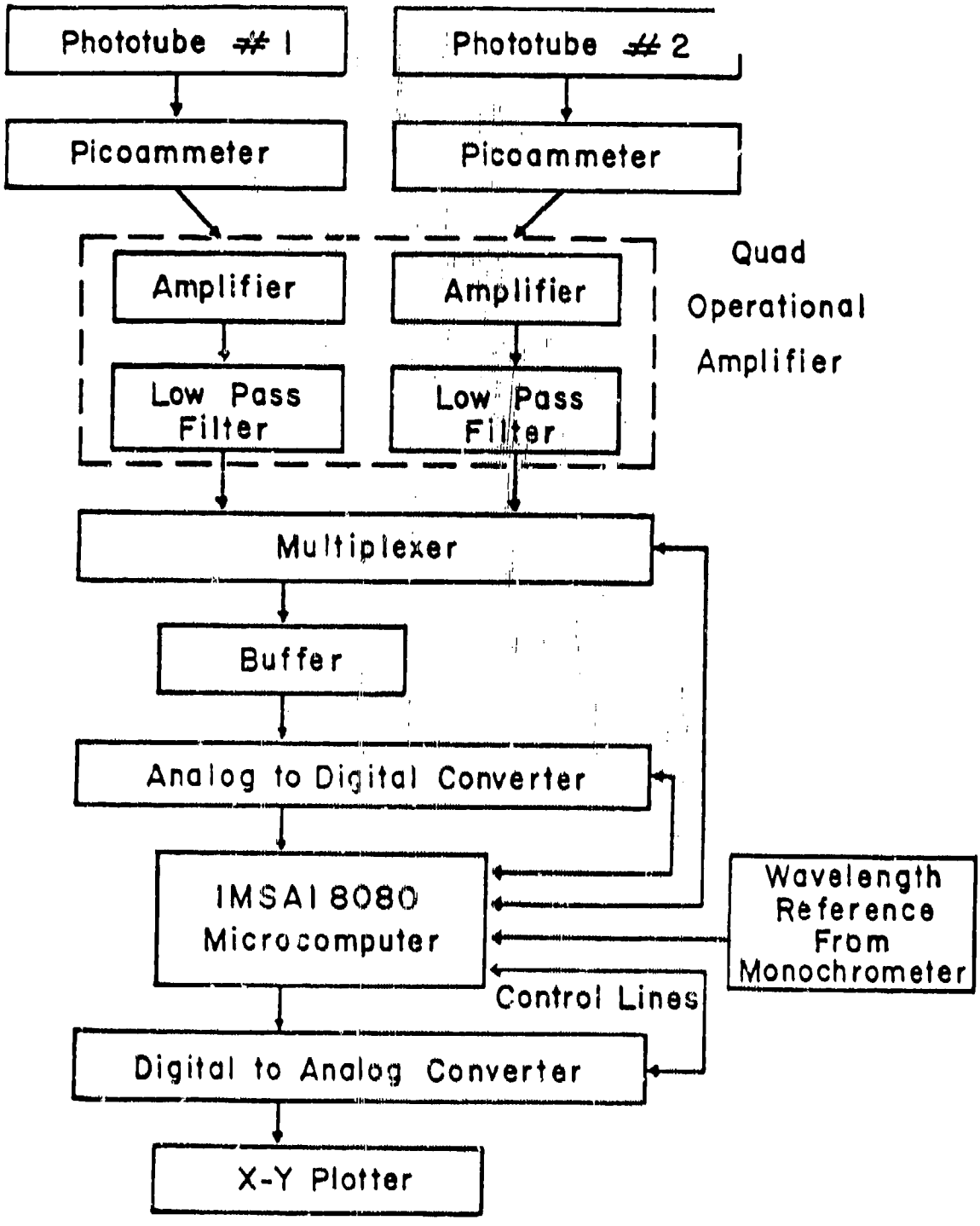

Fig. 6. Microcomputer Interface

measurements were done on each sample from the visible to the mid IR (.4μm-25μm). We used (13) to calculate the absorption and plotted absorption vs frequency on a log-log scale. The curves were then compared to see which ones looked most alike. The reason for this is that there is some difference in the absorption depending on how densely the particles are packed onto the polyethylene. They broke up into four groups (which we call I-IV), the samples with the lowest mass densities (.5μg/cm^2/layer to 1.2μg/cm^2/layer) generally fell into group I and those with the highest generally fell into group IV (2μg/cm^2/layer to 4μg/cm^2/layer). The samples in group I were then fused together using heat and pressure to form sample I. The same thing was also done with groups II-IV. These samples now have a high enough mass density to produce appreciable absorption in the far infrared.

5. RESULTS AND DISCUSSION

5.1 Al Results.

In Fig. 7, we have plotted the result of the extinction measurements for sample I for the wavelength region .4μm-170μm and have compared it to the sphere theory and to the shape distribution calculation (CDE). This sample has an average mass/area/layer of .7μg/cm²/layer. Also plotted on this figure is the average extinction coefficient for five samples with mass densities ranging from 1μg/cm² to 5μg/cm² in the wavelength region of .12μm-.5μm. The statistical uncertainty in the measurements is smaller than the size of the data points for 50μm<λ<.12μm and increases in the far infrared as shown by the error bars. The large error in the far IR is caused by a relatively large electronic noise level. Also in this region the Al is becoming almost transparent so the transmission through the sample is very close to the transmission through the reference. The discontinuity in the data at .5μm is due to the fact that for shorter wavelengths the dielectric constant of the medium is 1 rather than 2.3 (i.e. we switched from the polyethylene

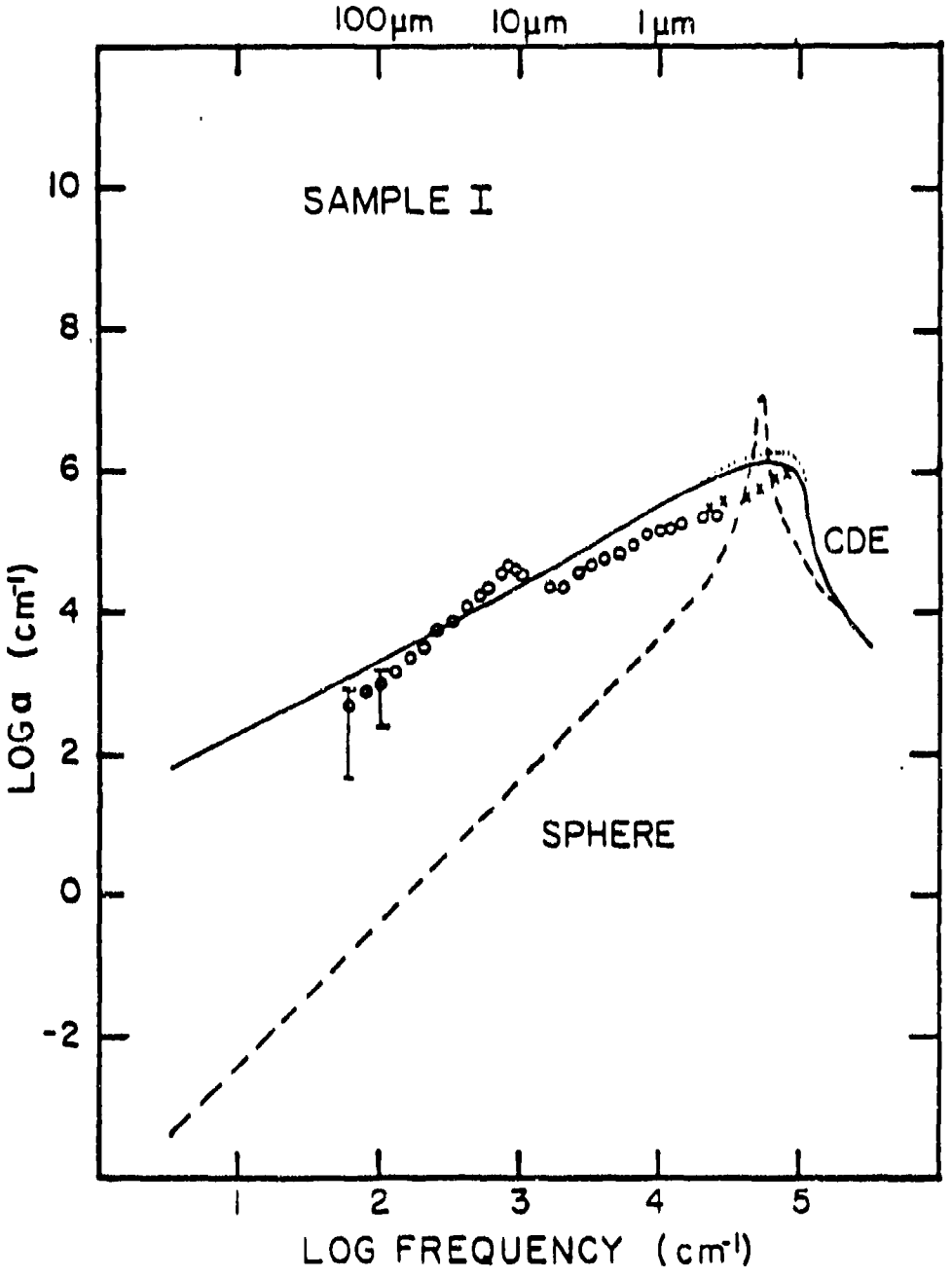

Fig. 7. Measured Extinction for Al (sample I)

Comparison of experimental results (open circles, $\varepsilon_m = 2.3$; x's, $\varepsilon_m = 1$) to sphere theory (dashed line) and CDE theory (solid and dotted lines)

samples to the LiF substrate samples.) The agreement between the data and the CDE curve is quite good and is certainly much better than between the data and the sphere theory, particularly in the far IR where the sphere theory is approximately three orders of magnitude below the other two curves. The most obvious difference between the data and the CDE curve is the bump at 12μm. This is almost certainly due to an amorphous Al_2O_3 layer on the particles since aAl_2O_3 has an absorption band in this region. It is well known that Al surfaces oxidize rapidly and several monolayers of oxide can form on a surface in a short period of time even in a fairly good vacuum.

Fig. 8. shows the measured extinction coefficient for sample IV, which has σ =2.3μg/cm^2/layer, in the wavelength range .33μm-280μm. In general sample IV has a higher extinction coefficient than sample I. The reason for this may be that the density of particles is so high that the independent particle assumption is being violated, i.e., when a particle goes through resonance it affects its neighbors. Another possible explanation is that since the particles are so packed together they effectively form particles of a larger size so the use of Rayleigh theory is no longer valid.

In future discussions in this work we will only consider sample I since it has the lowest particle density

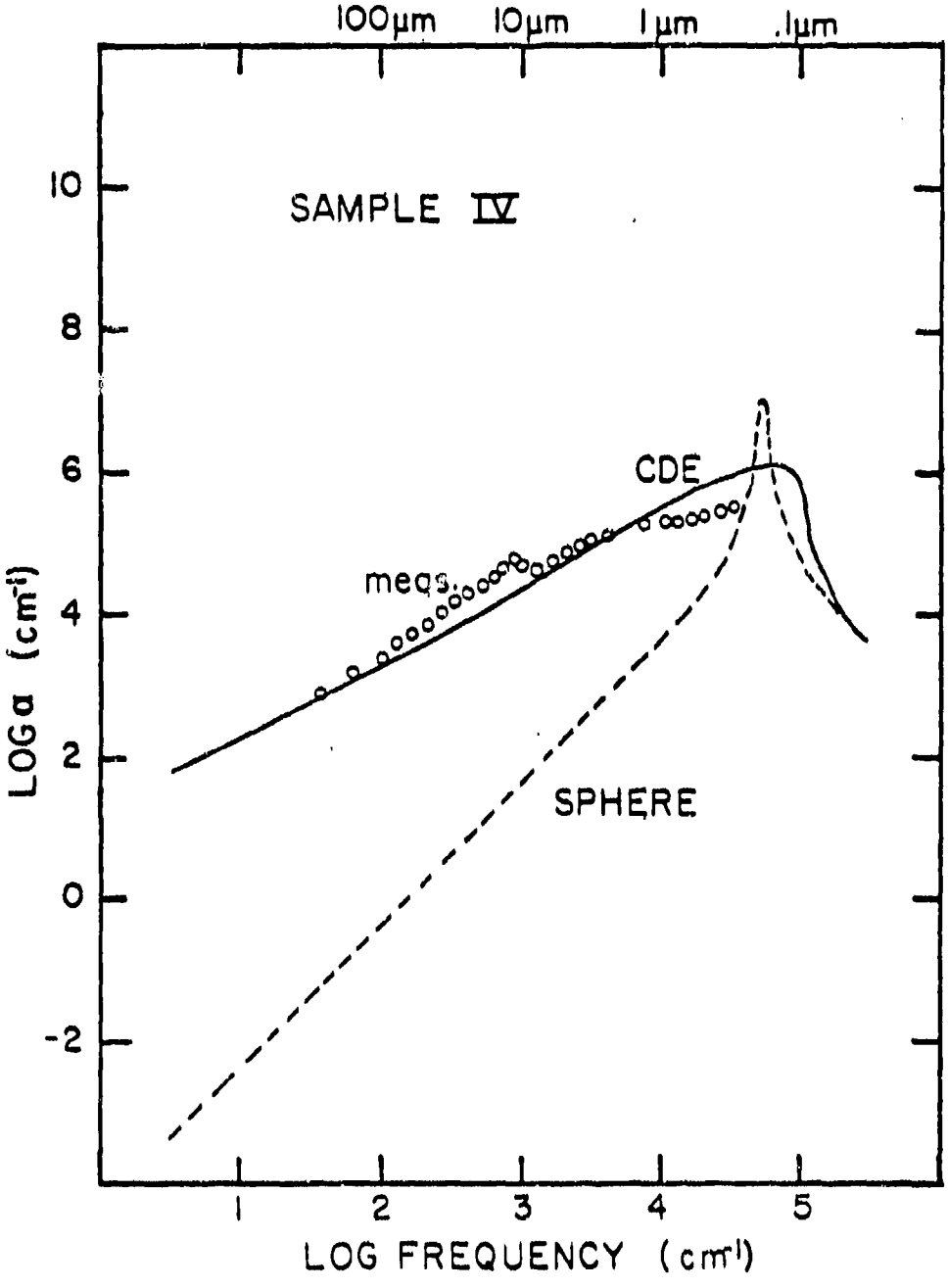

Fig. 8. Measured Extinction for Al (sample IV)

and, therefore, will be most likely to fulfill the Rayleigh conditions and the noninteracting particle assumption.

5.2 Al_2O_3 Results.

The measured extinction cross section/volume for aAl_2O_3 is plotted in Fig. 9. For comparison we have also plotted the measured extinction coefficient for γAl_2O_3. The two curves are almost identical from .6μm to 25μm and begin to differ in the far IR, with the amorphous material having a higher extinction than the γAl_2O_3. This is consistent with the results of Strom et.al. (1974). They observed that amorphous materials tend to have larger extinction in the far IR than their crystalline counterparts; even orders of magnitude larger. The extinction spectrum for aAl_2O_3 is a composite of measurements for several different samples. For the region of the IR absorption band of aAl_2O_3 (10μm-25μm), measurements were done on three samples with masses ranging from .207mg-.345mg with KBr as a medium. Since the extinction decreases significantly on both sides of this band it is necessary to use a higher mass of particles to produce a measurable amount of extinction. For measurements in the wavelength regions 25μm-160μm and .6μm-10μm we used two samples, both with 4.4mg of aAl_2O_3, in a polyethylene medium.

From Fig. 9. we see that the extinction has a minimum at approximately 4μm and increases for shorter wavelengths. Calculations of the absorption coefficient for

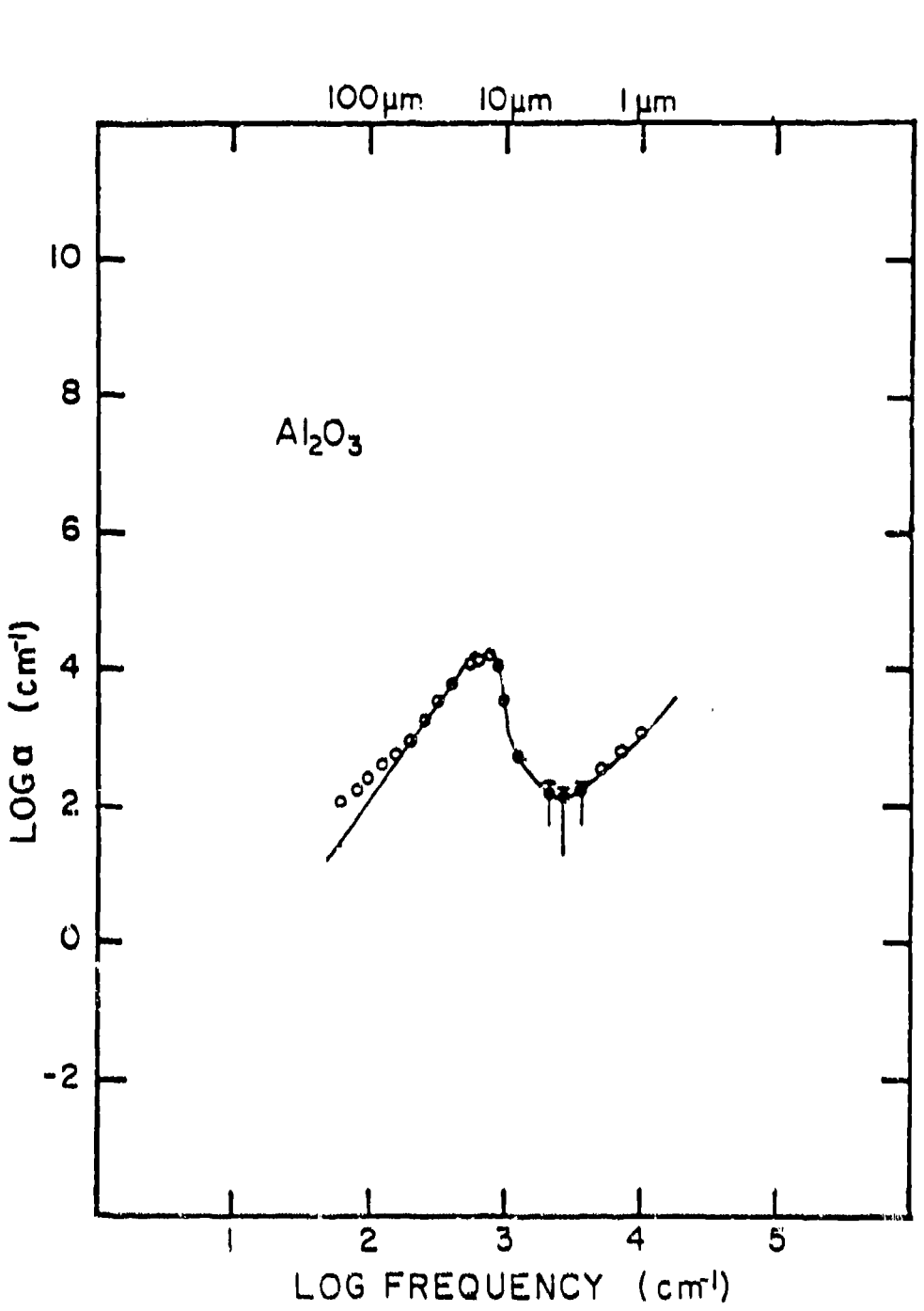

Fig. 9. Measured Extinction of Al_2O_3

γAl_2O_3 (solid line) and αAl_2O_3 (open circles)

aAl_2O_3 (for particles of any shape) show that the absorption should continue to decrease, so that the increase is probably attributable to scattering. From calculations of single particle scattering it is found that the scattering coefficient begins to increase at about 5μm, but is several orders of magnitude lower than the measurements. This difference in magnitude may be due to multiple scattering since there is a fairly high concentration of particles (4.2% by mass). In the region of the minimum the total extinction is smaller than the uncertainty in the measurements, as shown by the error bars.

5.3 Two Layer Particles.

As discussed earlier, the major difference between the experimental results and the CDE curve is the oxide bump at 12μm. Since it is not possible to avoid the oxide coating we have decided to take this into account in the shape distribution calculation. It should be noted that the absorption of a coated particle is not simply the sum of the absorptions by the core and the coating, since the electric field seen by the core is affected by the presence of the coating. Therefore, we consider the problem of a coated ellipsoid, i.e., an ellipsoid of material 1 surrounded by a layer of material 2. The absorption cross section/volume for a collection of randomly oriented, noninteracting, identical ellipsoids is (Bohren and Huffman, to be

published),

$$\langle \alpha_{abs} \rangle = \frac{k}{3} \sum_{j=1}^{3} \mathrm{Im} \left\{ \frac{(\varepsilon_2 - \varepsilon_m)[\varepsilon_2 + (\varepsilon_1 - \varepsilon_2)(1-f)L_j] + f\varepsilon_2(\varepsilon_1 - \varepsilon_2)}{[\varepsilon_2 + (\varepsilon_1 - \varepsilon_2)L_j(1-f)][\varepsilon_m + (\varepsilon_2 - \varepsilon_m)L_j + fL_j\varepsilon_2(\varepsilon_1 - \varepsilon_2)]} \right\} \quad (30)$$

where

k is the wavenumber ($k=2\pi/\lambda$),

ε_1 is the complex dielectric constant of the inner material,

ε_2 is the complex dielectric constant of the outer material,

ε_m is the dielectric constant of the medium, and

f is the volume fraction occupied by the inner ellipsoid.

To find the absorption coefficient for a collection of randomly shaped ellipsoids we follow the same procedure used in Chap. 3 , i.e., we integrate (30) over a shape distribution function. Again it is assumed that the shape distribution function is a constant, and the integration is done over L_1 and L_2 (with L_3 fixed by the condition $L_3=1-L_1-L_2$). Because of the complexity of (30) it was necessary to do the integration numerically. The domain of integration is shown in Fig. 10a. Although all shapes of ellipsoids are contained in any of the regions 1-6, for ease of computation we integrate over the whole triangle (with proper normalization). The double integral over L_1 and L_2 is replaced by the double sum,

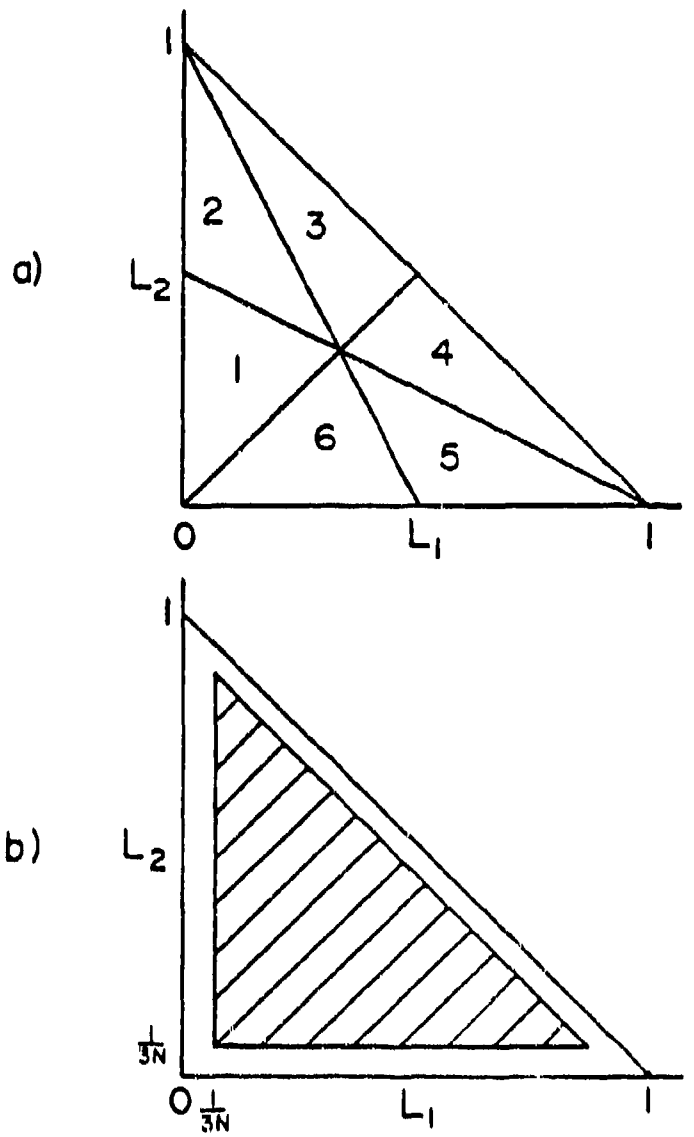

Fig. 10. Region of Integration

a) All shapes of ellipsoids are contained in each of the six regions
b) The shaded area is the domain of integration

$$<<\alpha_{abs}>> = \sum_{L_1=\frac{1}{3N}}^{1-\frac{2}{3N}} \sum_{L_2=\frac{1}{3N}}^{1-\frac{1}{3N}-L_1} <\alpha_{abs}> \qquad (31)$$

with increments of 1/N, where N is the number of steps that L_1 (or L_2 or L_3) is divided into.

Optical constants for the amorphous oxide coating and the aluminum core are required for the computations. For Al, a Drude free electron model is fitted to experimental data tabulated by Hagemann et.al. (1974). The Drude expression for the complex dielectric constant is (see, for example, Wooten 1972),

$$\varepsilon_1 = 1 - \frac{\omega_p^2}{\omega(\omega+i\Gamma_b)} \qquad (32)$$

where ω_p and Γ_b are the plasma frequency and the damping constant, respectively. We achieved a good fit to the measured reflectance of Al over a broad energy range from 0 to 15 eV by choosing ω_p=15eV and Γ_b=.6eV.

For the aAl_2O_3 coating, the dielectric constants tabulated by Hagemann et.al. (1974) are used for wavelengths less than .3μm. Experimentally determined dielectric constants for aAl_2O_3 do not appear to be available in the infrared. Since bulk samples of aAl_2O_3 are not available for optical constants determinations by the usual techniques of reflection and/or transmission spectroscopy, we were forced to use the small particle samples described in Chap. 4. Details of how the optical constants were determined are given in Appendix A.

We use these optical constants for aAl_2O_3 and Al in (30) and (31) in order to do a numerical calculation for the absorption by a shape distribution of coated ellipsoids, with N and f as adjustable parameters. In Fig. 11. we see the effect changing N has on the calculated absorption for Al (f=1.0). In general, the numerical result follows the analytic curve (Fig. 11.a) until some critical frequency where the slope changes, so that the absorption is quadratic in the frequency rather than linear. Also plotted in this figure are the results of Granqvist et.al. (1976). It is seen that their measured far IR extinction has quadratic frequency dependence. Initially, N is chosen large enough so that the cutoff occurs past the oxide absorption band. f is then varied until the best fit to our experimental results in the region of the oxide peak is obtained. In this way it was determined that f=.5, i.e., half of the total particle volume is occupied by aAl_2O_3. Finally, N is adjusted until the numerical result closely fits our far IR data for oxide coated Al particles, and is found to be about 800.

The limitation on the size of N that was used may have a physical interpretation. Since very small values of L are cut out (see Fig. 10.b) this effectively eliminates extremely elongated ellipsoids (as well as very large flat ellipsoids). In fact we can get an idea of the maximum

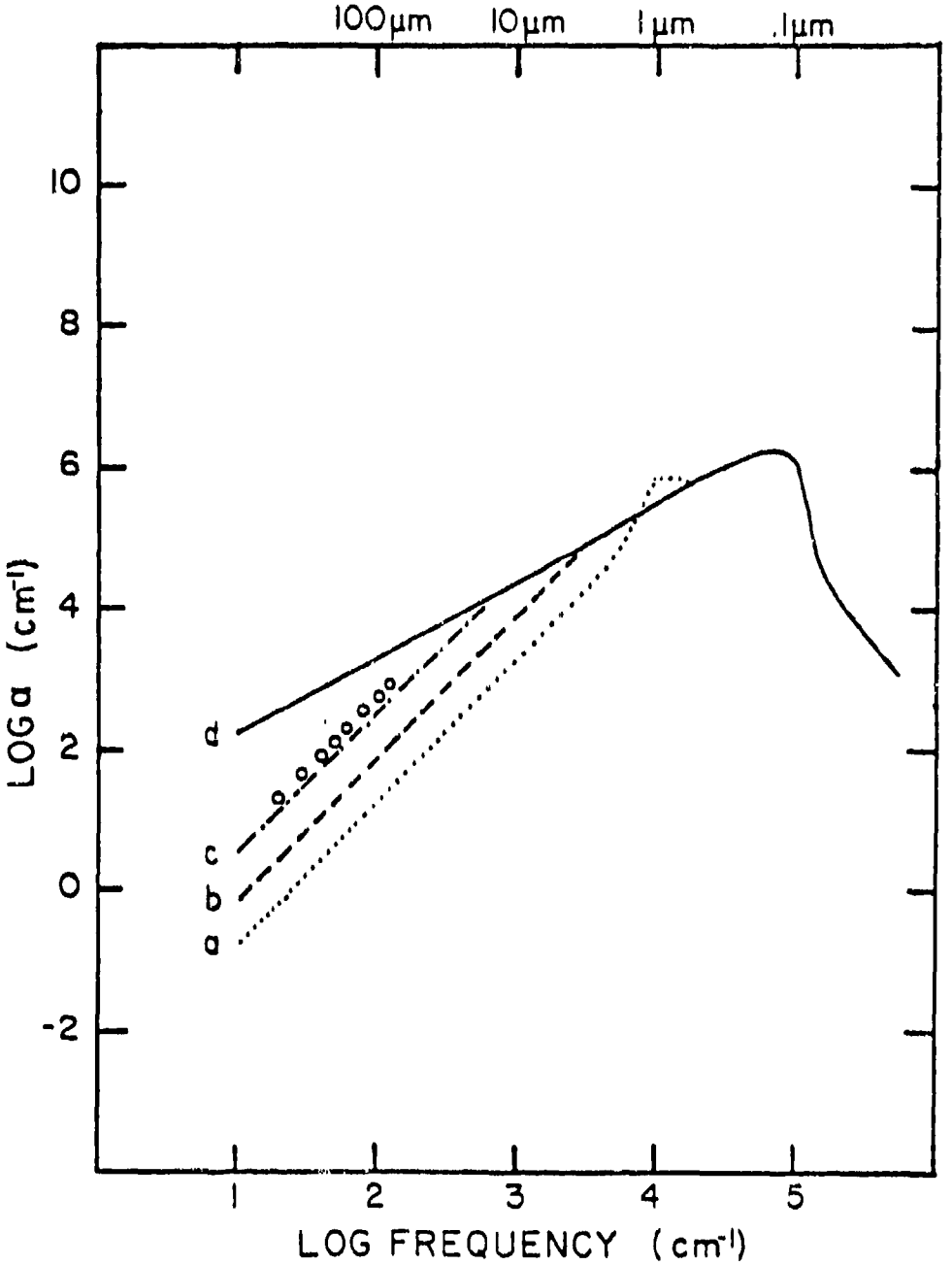

Fig. 11. Effect of Changing N on Calculated Absorption

a) N=50 (dotted line)
b) N=200 (dashed line)
c) N=800 (dot dash line)
d) analytic result

Also shown is the measured extinction of Granqvist et al. (1976) (open circles)

length of ellipsoid that is possible. As a special case let's consider a prolate spheroid with b=c a where a,b, and c are the semi-axes of the ellipsoid. From van de Hulst (1957), the expression for the depolarization factor, L_1, is

$$L_1 = \frac{1-e^2}{e^2}\left[-1+\frac{1}{2e}\ln\left(\frac{1+e}{1-e}\right)\right]; \qquad e^2 = 1-(b/a)^2.$$

For L_1 we will use the minimum value possible 1/2400. By trial and error we find a=100b. Therefore, the maximum length of ellipsoid possible in our model is one in which the longest axis is 100 times the smallest axis.

Fig. 12. shows the final fit of the distribution of coated ellipsoids to the experimental results. This is, in a sense, a comprehensive summary of this work from which we can draw reasonable insights concerning the long standing problem of anomalous far IR absorption by Al particles. The agreement between the data and the numerical fit is seen to be very good. The largest discrepancy occurs in the UV with a maximum relative error of about a factor of 2 (when compared to the CDE curve with ϵ_m=1), but at these short wavelengths we expect the assumptions of the Rayleigh approximation to be violated (Fig. 2.) leading to an expected decrease of volume normalized extinction compared to the small particle limit (Huffman 1977). In addition the calculation ignores scattering which becomes important in the UV. This leads to an increase in the extinction. The combination of these two effects probably explains the

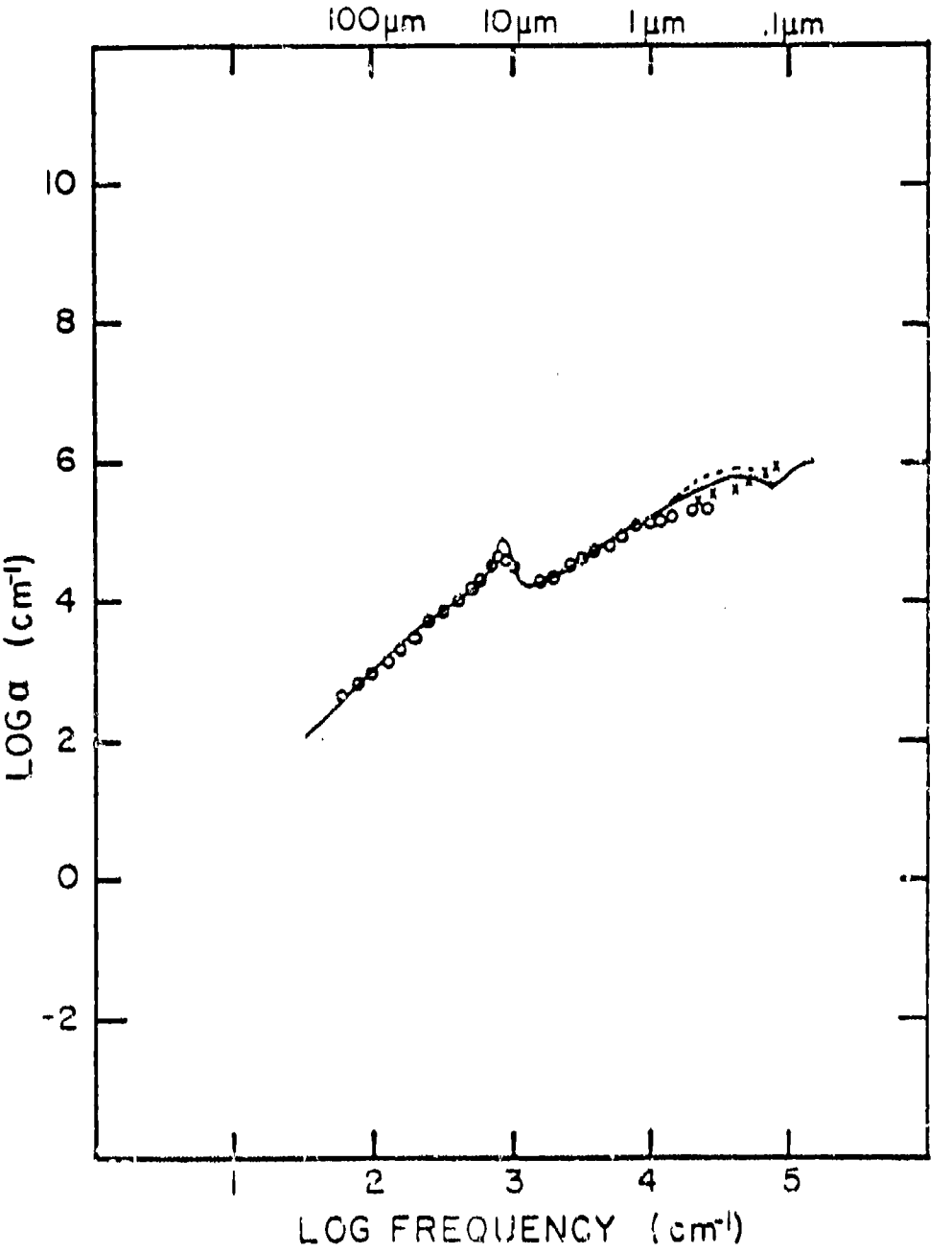

Fig. 12. Comparison of Measured Extinction to Numerical Fit

Experimental results (open circles for $\lambda > .5$ m and x's for $\lambda < .5$ m) compared to numerical fit with N=800 and f=.5 (ε_m=2.3 solid line, ε_m=1 dotted line)

absence of the predicted dip in the UV. In the middle IR the aqreement is quite good. The far infrared anomaly is resolved without the need for anything other than a classical shape distribution calculation. There was no evidence of periodic structure in the far IR caused by quantum size effects. Of course we would expect any such structure to be masked by the large absorption due to shape effects.

Some objections can be raised to this simple explanation, however. After all, we have used a rather simplified model, i.e. real particles are not ideal ellipsoids. However, there is independent evidence that the absorption determined by integration over a wide range of ellipsoidal shapes closely approximates the absorption by a collection of irregularly shaped particles. The measurements on Al_2O_3 given in Chap. 3 , as well as measurements on crystalline quartz (Huffman and Bohren 1980) agree well with the CDE model. Another possible shortcoming of our model is that we treat all possible shapes of ellipsoids as being equally likely. This works well for Al, αAl_2O_3, and SiO_2, but it may be that a nonuniform shape distribution function will have to be used for some other materials.

One thing that has not been included in our model is the effect on the absorption due to a size limited mean free path, since the electron mean free path is larger than the

size of the particle (see Kreibig 1974). This can be taken into account by replacing the bulk damping constant Γ_b in (32) by,

$$\Gamma_o = \Gamma_b + v_F/(Lc) \tag{33}$$

where v_F is the Fermi velocity, c is the speed of light, and L is a geometrical factor proportional to the size of the particle (L=4/3a for a sphere of radius a). The complex dielectric constant now becomes,

$$\varepsilon_1(\omega) = 1 - \frac{\omega_p^2}{\omega[\omega + i(\Gamma_b + v_F/(Lc))]} \tag{34}$$

To find the effect of the size limited mean free path on the absorption we substitute (34) into (31) for ε_1. To estimate the magnitude of this effect we assume a spherical particle of radius 25Å. The Fermi velocity for Al is 2×10^8 cm/sec so that $\Gamma_o = 5\Gamma_b$. With this value of Γ_b the absorption coefficient at 100μm is about a factor of 2 larger and decreases at shorter wavelengths. Since the original discrepancy is over 3 orders of magnitude, this factor can be ignored.

The mean free path limitation introduces a size dependence into the expression for the absorption. For spherical particles small enough to satisfy the Rayleigh criteria, Granqvist (1978) calculates that the size dependence of Γ leads to the absorption being inversely proportional to the size. In contrast, the absorption

coefficient for pure Al particles calculated using the shape distribution is very insensitive to the size of Γ. In fact changing Γ by a factor of 5 produces virtually no change in the absorption coefficient. It may be concluded that the absorption coefficient for a distribution of shapes is relatively size independent. This, of course, assumes that the particles are small enough that Rayleigh theory holds so that eddy current losses are negligible.

5.4 Other Explanations of "Anomalous Absorption.

As pointed out in Chap. 2 there have been a number of theories proposed to account for the anomalously high far IR absorption observed by Granqvist et.al. (1976). We will now discuss these in further detail to see how well they agree with the extension of the measurements to shorter wavelengths that we have done. Since the theories all assume the dielectric constant of the medium to be 1, we will compare their results to the experimental fit curve with $\epsilon_m=1$ (rather than 2.3).

1) In Simanek's (1977) first theory he proposed that the absorption was taking place mainly in the oxide coating of the particles. He modeled the particle system as a collection of long randomly oriented aAl_2O_3 cylinders with spherical Al particles embedded within. For the absorption coefficient he finds,

$$\alpha(\omega) = \frac{k}{3}\left[1+\frac{8}{(\mathrm{Re}\ \varepsilon_{MG}+1)^2+(\mathrm{Im}\ \varepsilon_{MG})^2}\right]\mathrm{Im}\ \varepsilon_{MG} \qquad (35)$$

where ε_{MG} is the complex dielectric constant of the composite using the Maxwell-Garnett theory. ε_{MG} is given by,

$$\varepsilon_{MG} = \varepsilon_2 \frac{\varepsilon_1(1+2f)+2\ \ (1-f)}{\varepsilon_1(1-f)+\varepsilon_2(2+f)} \qquad (36)$$

where f is the fraction of the total volume of the cylinder occupied by the metallic cores. In the far infrared $|\varepsilon_1| >> |\varepsilon_2|$ (ε_1 is the complex dielectric constant of Al and ε_2 the complex dielectric constant of aAl_2O_3) and ε_{MG} can be simplified,

$$\varepsilon_{MG} = \varepsilon_2\left(\frac{1+2f}{1-f}\right) = \varepsilon_2 R \qquad (37)$$

Because we do not want to limit the calculation to the far IR we do not make this assumption, but rather, use the full Maxwell Garnett dielectric constant. For ε_2 the dielectric constants that were determined experimentally were used (Appendix A) instead of the approximate far IR dielectric constant used by Simanek,

$$\varepsilon_2 = 10+i2\times10^{-14}\omega \qquad (38)$$

The result of this calculation is shown in Fig. 13. For comparison we have also plotted the result of the numerical fit with $\varepsilon_m=1$. In the far IR the agreement is good but for shorter wavelengths it is very poor. We can conclude that

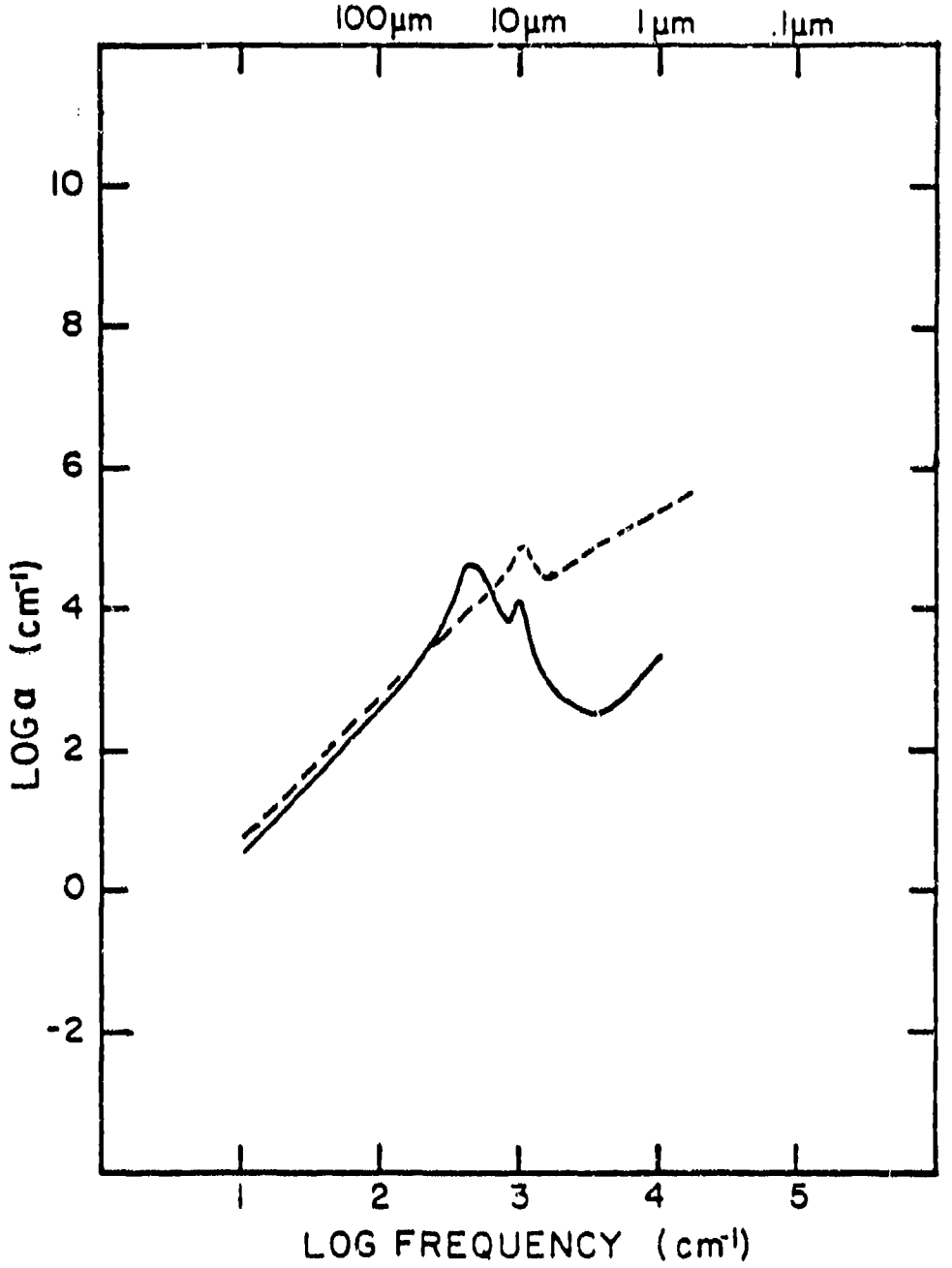

Fig. 13. Simanek's (1977) Results

Simanek's results (solid line) compared to experimental fit with $\epsilon_m = 1$ (dashed line)

the oxide coating is not the major contributor to the absorption.

2) Glick and Yorke (1977) did a calculation to determine the lattice contribution to the absorption for small Al particles since they believed the electronic component to be small. Their results showed that the lattice absorption should mirror the phonon density of states for Al. In Fig. 14.a the density of states for Al is plotted. We have plotted their calculated absorption (as far as it extends) in Fig. 14.b and have compared it to our experimental fit curve. Their result is about a factor of 6 higher than the experimental data and does not have quite the same frequency dependence. They suggest that further measurements be done to see if there is a leveling off in the absorption that they predict since the data of Granqvist et.al. stops just short of this point. We have extended the measurements to shorter wavelengths and do not see a leveling off. Furthermore, it would seem that if Glick and Yorke extended their calculations the absorption should begin to decrease significantly. This was also not observed experimentally (compare Fig. 7.). Due to this discrepancy it appears that the theory of Glick and Yorke does not adequately represent the absorption by small Al particles.

There are some theoretical reasons to question Glick and Yorke's result. For one thing they used the bulk density of states rather than the actual small particle mode

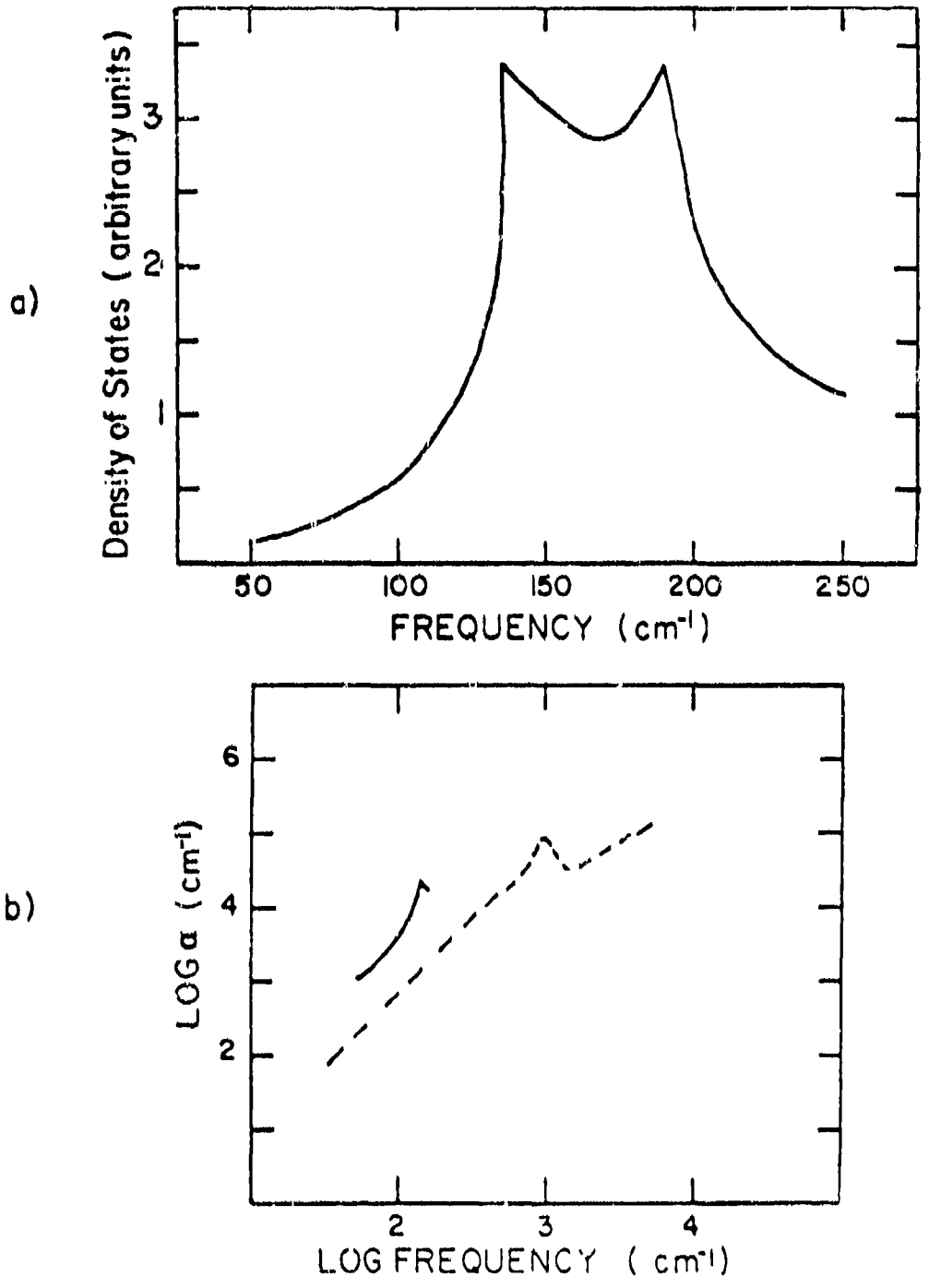

Fig. 14. The Theoretical Results of Glick and Yorke

a) Density of states for Al
b) Glick and Yorke's results (solid line) compared to our experimental fit with τ_m=1 (dashed line)

density in their calculation. Simanek (1980) has pointed out that for very small particles there is another term in the vibrational mode density due to surface modes. He concludes that for particles with a diameter of 50Å the surface term is five times as great as the volume term considered by Glick and Yorke. Also this surface term is linear in frequency which implies a strong deviation from the quadratic dependence seen experimentally.

Another apparent problem with Glick and Yorke's calculation is that they assumed the electric field penetrates only a few angstroms into the particle. This assumption is based on a paper by Rice, Schneider, and Strassler. They calculated the effect of reducing the particle size on the polarizability and found that reducing the size decreases the polarizability, thus allowing the electric field to penetrate the particle. Their calculation, however, assumes a perfect conductor. Therefore, it is questionable whether the penetration depth calculated in this manner can be properly used for Al.

3) Lushnikov et. al. (1978) calculated the absorption by small particles of Al by taking into account the Coulomb interactions between conduction electrons. Their calculation gives quadratic frequency dependence of the absorption but is two orders of magnitude smaller than the experimental results. They admit that the model they use can not be expected to give good quantitative agreement

with experimental data. They say that this is because their model assumes spherical pure Al particles of a definite size, whereas real particles have an oxide coating and tend to clump together into clusters and chains.

4) Ruppin (1979) extends the theory of Simanek (1977) to various metal-oxide configurations by considering the particles to cluster in the shapes of prolate spheroids. Two models are used for the topology. In the first, the metal particles are embedded in an amorphous oxide matrix (Maxwell-Garnett theory). The second model consists of metal and oxide particles forming clusters (Bruggeman theory). To calculate the absorption he uses (26), with $\alpha_{abs} = \langle C_{abs} \rangle / v$,

$$\alpha_{abs} = \frac{k}{3} \operatorname{Im} \sum_{j=1}^{3} \left\{ \frac{\varepsilon_a - 1}{1 + L_j(\varepsilon_a - 1)} \right\}$$

where ε_m has been taken to be 1. ε_a is the complex dielectric constant of the aggregate which for the Maxwell-Garnett theory is equal to ε_{MG} and is given by (36). For the Bruggeman theory $\varepsilon_a = \varepsilon_b$ and is determined by the equation,

$$\frac{3f}{2+\varepsilon_1/\varepsilon_b} + \frac{3(1-f)}{2+\varepsilon_2/\varepsilon_b} = 1$$

where, as usual, ε_1 and ε_2 are the complex dielectric constants of the metal and oxide respectively. Since the dielectic constants of aAl_2O_3 were not known, Ruppin used the approximate dielectric constant from Simanek (1977),

given in (38). He suggests, however, that this dielectric constant is a possible source of error in his calculation. The results of Ruppin's calculations are given in Fig. 15. (with the ratio of the major to the minor axis equal to 6) where we have used the dielectric constants that we determined experimentally for aAl_2O_3. For comparison the experimental fit curve to our data with $\varepsilon_m = 1.0$ is also given. In the far IR there is reasonable agreement but for shorter wavelengths both of his curves differ significantly from the experimental results. From this we conclude that the absorption calculated assuming a collection of identical ellipsoids modeled by either the Maxwell-Garnett or the Bruggeman theories does not adequately explain the experimental results.

5) In Simanek's second theory (1980) the absorption is calculated using Mott's (1970) a.c. conductivity formulation. He abandons his previous theory because preliminary measurements by Sievers (1978) suggest that the absorption by pure aAl_2O_3 particles is far too low. Our measurements show, however, that aAl_2O_3 particles have an absorption coefficient comparable to that of the oxide coated Al particles in the far IR. In Simanek's new model the mechanism for absorption involves electrons which are localized at defects of the oxide coating. These defects are due to excess aluminum and oxygen vacancies which arise because of nonstoichiometry of the aAl_2O_3 at the metal-oxide

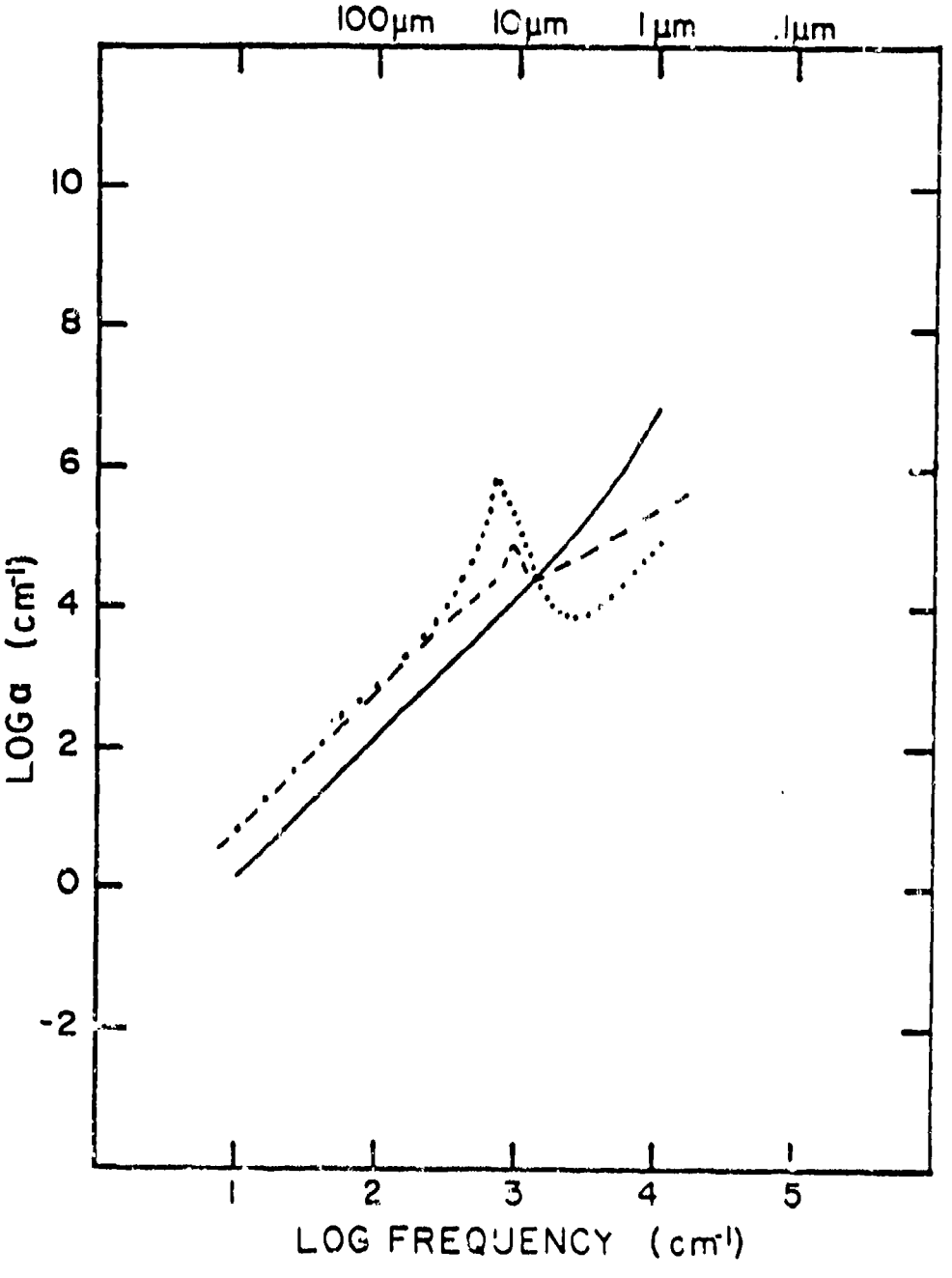

Fig. 15. Ruppin's Theoretical Results

Ruppin's calculated absorption using Maxwell-Garnett theory (dotted line) and Bruggeman theory (solid line) as compared to our experimental fit (dashed line) with $\varepsilon_m = 1$

interface. The absorption is caused by electrons executing resonant transfer between trap states localized at the defect sites. The a.c. conductivity for this mechanism has been found by Mott to be,

$$\text{Re } \sigma(\omega) = 8\pi e^2/\hbar\, [N(E_F)\hbar\omega]^2 \alpha^{-5} [\ln(\tfrac{2I_o}{\hbar\omega})]^4 \qquad (39)$$

where

$1/\alpha$ is the range of the electron wave function,

I_o is related to the overlap of localized electron wave functions,

$N(E_F)$ is the density of trap states at the Fermi energy and is assumed to be constant.

The absorption coefficient is given by (35), where for ε_{MG} we have used (37) which is valid for wavelengths less than 5um.

$$\alpha(\omega) = \frac{k}{3} R \text{ Im } \varepsilon_2 \left[1 + \frac{8}{(R \text{ Re } \varepsilon_2 + 1)^2 + (\text{Im } \varepsilon_2)^2 R^2}\right] . \qquad (40)$$

Simanek used (35) to calculate the far IR absorption with $\text{Im}\,\varepsilon_2$ replaced by $4\pi\sigma/\omega$, and the following assumptions,

1) $1/\alpha = 2\text{Å}$,

2) R=1.7, which corresponds to f=.2,

3) $(R \text{ Im } \varepsilon_2)^2$ in the denominator of the bracketed expression is small and $\text{Re } \varepsilon_2$ is taken to be 10,

4) I_o=10 eV.

He then determined $N(E_F)$ to be $2\times10^{21}\text{cm}^{-3}\text{eV}^{-1}$ by requiring

agreement with the data of Granqvist et.al. (1976). He states that this value is typical for metal-oxide interfaces, citing the work of Halbritter (1974) who considered Nb-Nb_2O_5 interfaces. We have found, however, that by using Simanek's values 1)-4) that $N(E_F)$ should be $3\times10^{20}cm^{-3}eV^{-1}$ to fit Granqvist's data at 100μm.

To extend Simanek's (1980) theory to shorter wavelengths the Im ε_2 must include a term to account for the dielectric constant of the pure aAl_2O_3, ε_2^{pure}, i.e.,

$$\text{Im } \varepsilon_2 = \text{Im } \varepsilon_2^{pure} + 4\pi\sigma/\omega,$$

With this expression for Im ε_2 in (40) we calculated the absorption, which is plotted in Fig. 16 . We took $N(E_F)$ to be $3\times10^{20}cm^{-3}eV^{-1}$ and used our experimentally determined dielectric constants for Re ε_2 and Im ε_2^{pure}, along with Simanek's values for $1/\alpha$ and I_o and R. For comparison our experimental fit curve with $\varepsilon_m=1$ is also shown. We see that there is reasonably good agreement, the primary difference being the location of the oxide bump. A more serious problem with this model is its strong dependence on the parameters $1/\alpha$, $N(E_F)$, and I_o, while Simanek gives no real justification for the values he uses. Before more definite conclusions can be reached on this model, accurate determinations of these parameters must be made.

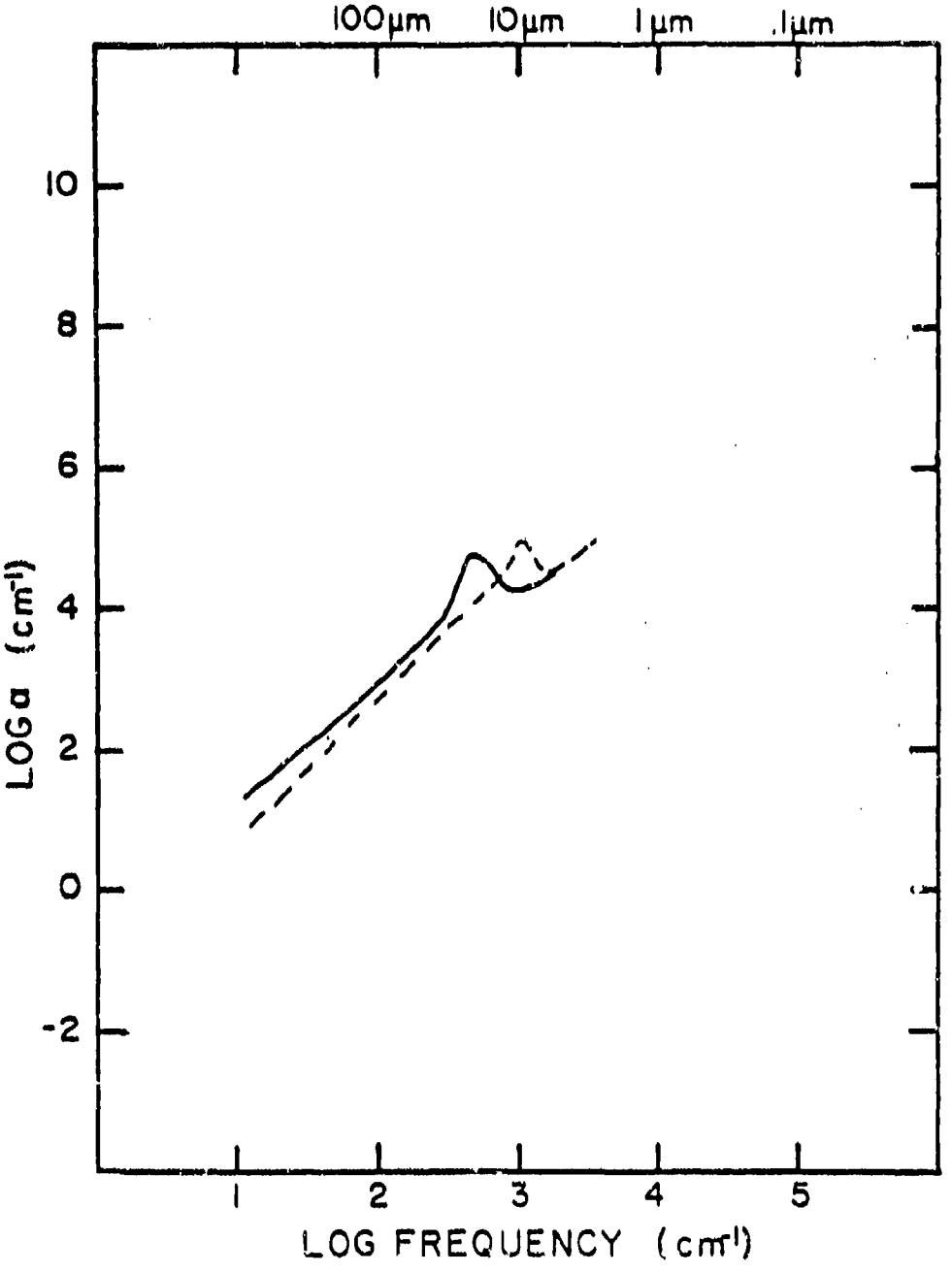

Fig. 16. Simanek's (1980) Theoretical Results

Simanek's results compared to our experimental fit curve with $\epsilon_m=1$

6. CONCLUSION

We have measured the extinction by small particles of Al from the far IR to the far UV. This was done because experimental results by Granqvist et.al. (1976) disagreed by over three orders of magnitude with both the quantum mechanical Gor'kov Eliashberg (1966) theory and the classical Drude theory. Our measurements served to confirm those of Granqvist et. al. in the far IR and extend the data to the UV. Several authors had proposed theories to account for Granqvist's observed "anomalous" absorption. We have extended their calculations to shorter wavelengths to compare them to our data. Although these theories show reasonable agreement in the far IR, they differ markedly from our experimental data at shorter wavelengths. Simanek's (1980) second paper is a possible exception. It shows good agreement with the experimental data but depends crucially on several parameters which are not accurately known.

In this work we have performed a shape distribution calculation, which includes the effects of an oxide coating on the particles, in order to explain the experimental data.

This calculation is based on the classical Drude theory and does not consider quantum size effects. The shape distribution in our model is a uniform continuous distribution of ellipsoids. This model shows excellent agreement with the experimental results over the entire wavelength region measured. In order to determine whether the enhanced absorption is due primarily to shape effects or to the oxide coating, measurements were done on pure aAl_2O_3. In the far IR these measurements were similar to those of the coated Al particles; however, for wavelengths shorter than 10μm, the absorption by the pure aAl_2O_3 particles is orders of magnitude lower than for coated particles. This would imply that the enhancement is due to shape effects. On the other hand, it is possible that the Mott (1970) a.c. conductivity mechanism, which considers the effect of defects at the metal-oxide interface, enhances the absorption by an oxide coating as compared to pure aAl_2O_3 particles. This is the basis for Simanek's (1980) second paper. The measurements on Al_2O_3 and quartz (Huffman and Bohren 1980) indicate that shape effects as calculated in the CDE model are sufficient to account for the observed absorption. Our measurements suggest that shape effects are also the major contributing factor in the absorption by oxide coated Al particles, but further measurements should be done on non-oxidizing metals to ascertain the exact role played by the oxide coating.

BLANK

APPENDIX A

DETERMINATION OF DIELECTRIC CONSTANTS FOR POWDERED MATERIALS

In Chap. 3 it was shown that the shape distribution model (CDE) agrees well with the experimental results for αAl_2O_3, thus suggesting the validity of the CDE model. Assuming this model works equally well for other materials, we have developed a method (developed under Naval contract number N00019-78-C-0479) for determining IR dielectric constants of small particle systems by inverting the CDE calculation with the aid of the Lorentz oscillator theory. In our method we use (29),

$$\alpha = C_{abs}/V = k\ \mathrm{Im}\left[\frac{2\varepsilon\varepsilon_m}{\varepsilon-\varepsilon_m}\log(\varepsilon/\varepsilon_m)\right]$$

along with the expression for the complex dielectric constant from the Lorentz theory,

$$\varepsilon = \varepsilon_\infty + \sum_{j=1}^{N} \frac{\omega_{pij}^2}{(\omega_j^2-\omega^2)-i\Gamma_j\omega} \qquad (A.1)$$

ε_∞, ω_{pij}, Γ_j, and ω_j are fitting parameters in this method. N is the number of oscillators necessary to describe the system; usually it is equal to the number of peaks in the absorption spectrum. ε_∞ is the real part of the dielectric constant at infinite energy, and normally can be taken to be

the square of the handbook value for the index of refraction for visible light. To determine the dielectric constants for the material, the fitting parameters, ω_j, Γ_j, and $\omega_{p,j}$ are adjusted via an interactive computer program until the calculated absorption (α_{CDE}) is in good agreement with the absorption measured experimentally (α_{exp}).

This technique was used to determine the dielectric constants of amorphous Al_2O_3 (aAl_2O_3). For amorphous materials it is generally not obvious what value of N to use since the absorption peaks are not sharp but tend to be broad and unresolved. In this case, N is chosen large enough to obtain a reasonable fit. For aAl_2O_3 we used N=2. Fig. A.1 illustrates the fit to the data obtained with this method. The values of the fitting parameters are given under the figure. The dielectric constants are found using (A.1) and are plotted in Fig. A.2.

Our method of determining dielectric constants for small particle systems is very similar to one of the standard methods for the determination of optical constants from reflectivity measurements on bulk solids. For this case, Fresnel's equation is used rather than the CDE equation and is coupled with the Lorentz oscillator theory. Although the dielectric constants obtained by our method may not be as accurate as those determined from reflectivity measurements on bulk materials, it is the best method currently available for materials which are only available in powder form.

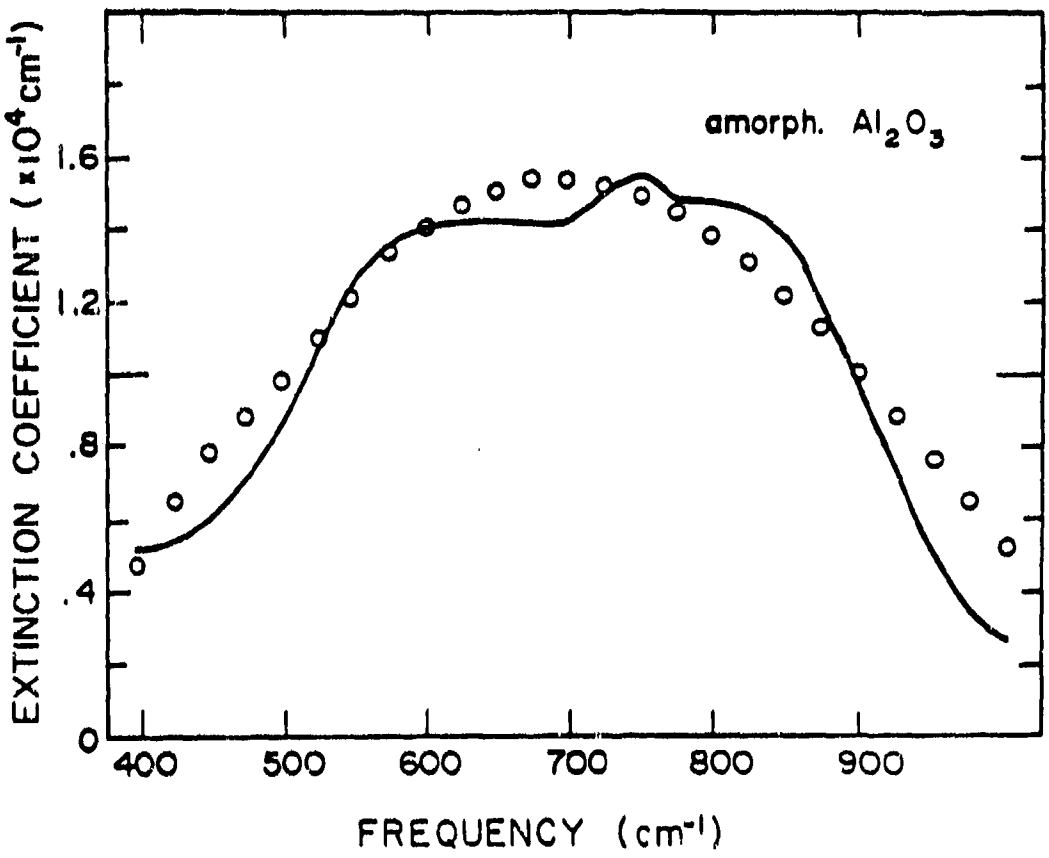

Fig. A-1 Extinction Coefficient of aAl_2O_3

Oscillator fit (open circles) compared to measurements (solid line). The oscillator parameters used are:
$\varepsilon_\infty = 3.0$,
$\omega_1 = 420 cm^{-1}$, $\Gamma_1 = 150 cm^{-1}$, $\omega_{p_1}^2 = 10\ \omega_1^2$,
$\omega_2 = 530 cm^{-1}$, $\Gamma_2 = 160 cm^{-1}$, $\omega_{p_2}^2 = 2.5\ \omega_2^2$

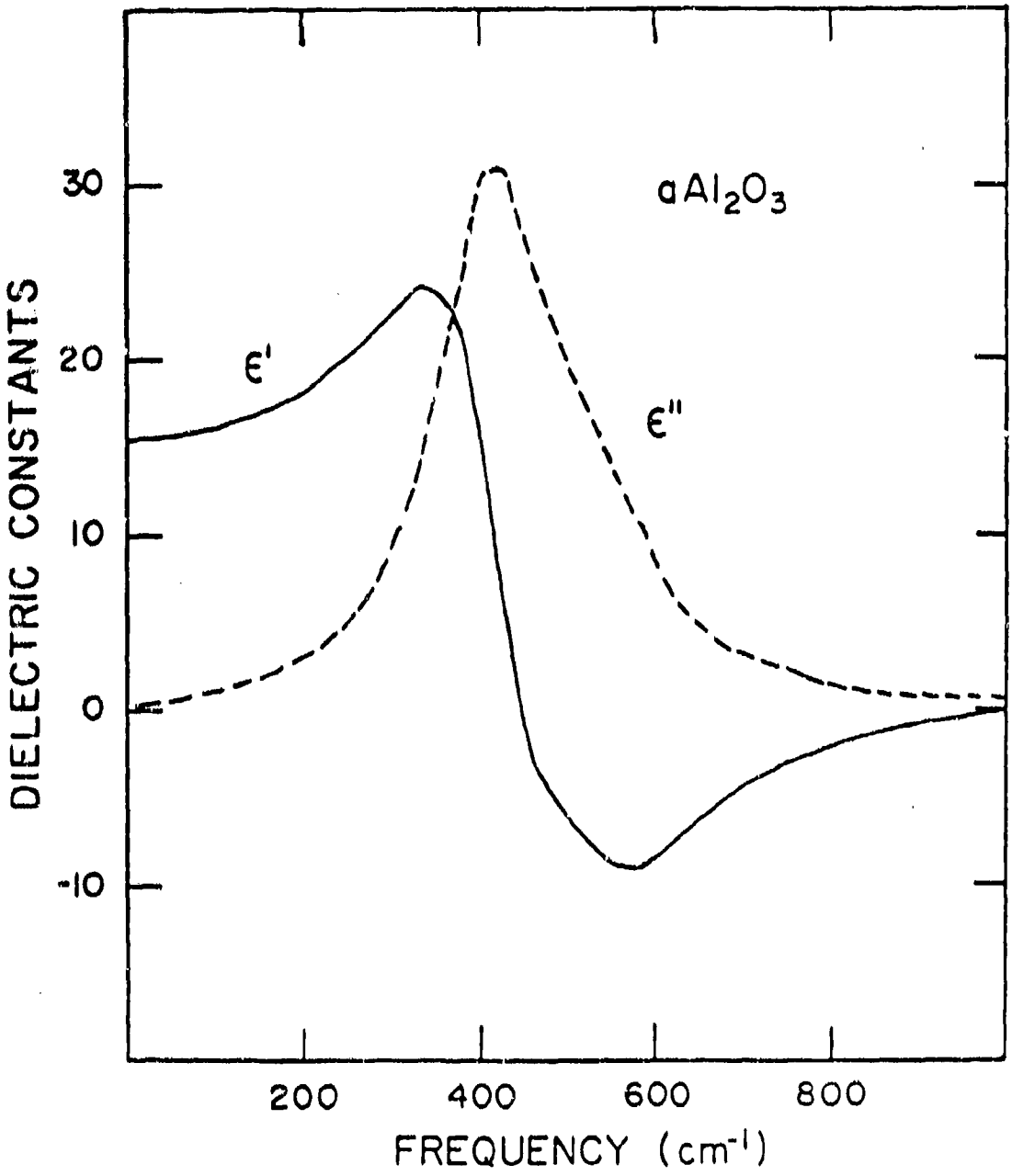

Fig. A-2 Dielectric Constants for αAl_2O_3

Dielectric constants determined using the Lorentz oscillator theory coupled with the CDE theory

8. LIST OF REFERENCES

Ballart, R., PhD Dissertation, Dept. of Physics, University of Arizona (1980).

Barker, A. S., Phys. Rev., 132, 1474 (1963).

Bohren, C. F., and D. R. Huffman, Absorption and Scattering of Light by Small Particles, Wiley, New York (to be published).

Devaty, R. P., and A. J. Sievers, Phys. Rev. B, 22, 2123 (1980).

Glick, A. J., and E. D. Yorke, Phys. Rev. B, 18, 2490 (1978).

Gor'kov, L. P., and G. M. Eliashberg, Sov. Phys. JETP, 21, 940 (1965).

Granqvist, C. G., Z. Physik B, 30, 29 (1978).

Granqvist, C. G., and R. A. Buhrman, J. Appl. Phys., 47, 2200 (1976).

Granqvist, C. G., R. A. Buhrman, J. Wyns, and A. J. Sievers, Phys. Rev. Lett., 37, 625 (1976).

Hagemann, H. J., W. Gudat, and C. Kunz, Deutsches Elektronen-Synchrotron DESY, SR-74/7 (1974).

Halbritter, J., Phys. Lett., 49A, 379 (1974).

Huffman, D. R., Adv. in Phys., 26, 129 (1977).

Huffman, D. R., and C. F. Bohren, in Light Scattering by Irregularly Shaped Particles, D. W. Schuerman Ed., Plenum Press, New York (1980).

van de Hulst, H. C., Light Scattering by Small Particles, Wiley, London (1957).

Jackson, J. D., Classical Electrodynamics, Wiley, New York (1962).

Kimoto, K., Y. Kamiya, M. Nonoyama and R. Uyeda, Jap. J. Appl. Phys., 2, 702 (1963).

Kreibig, U., J. Phys. F, 4, 999 (1974).

Lushnikov, A. A., V. V. Maksimenko, and A. J. Simonov, Sov. Phys. Sol. St., 20, 292 (1978).

Maksimenko, V. V., A. J. Simonov, and A. A. Lushnikov, Phys. Stat. Sol. B, 83, 377 (1977).

Miller, R. G., Laboratory Methods in Infrared Spectroscopy, Heyden, London (1972).

Mott, N. F., Phil. Mag., 22, 7 (1970).

Rice, M. J., W. R. Schneider, and S. Strassler, Phys. Rev. B, 8, 474 (1973).

Ruppin, R., Phys. Rev. B, 19, 1318 (1979).

Sievers, A. J., Dept. of Physics, Cornell Univ., unpublished (1978).

Simanek, E., Phys. Rev. Lett., 38, 1161 (1977).

Simanek, E., in Topical Meeting on Optical Phenomena Peculiar to Matter of Small Dimensions, Optical Society of America (1980).

Stratton, J. A., Electromagnetic Theory, McGraw-Hill, New York (1941).

Strom, U., J. R. Hendrickson, R. J. Wagner and P. C. Taylor, Sol. St. Comm., 15, 1871 (1974).

Tanner, D. B., A. J. Sievers, R. A. Buhrman, Phys. Rev. B, 11, 1330 (1975).

Wooten, F., Optical Properties of Solids, Academic Press, New York (1972).

Yatsuya, S., S. Kasukabe, and R. Uyeda, Jap. J. Appl. Phys., 12, 1675 (1973).

Part II

THE OPTICAL PROPERTIES OF CARBON

Written by Otto Edoh

9. ABSTRACT

Optical properties of carbon are studied in bulk state from $\lambda \sim 0.05$ to 100 μm for graphite, and from $\lambda \sim 0.05$ to 1000 μm for glassy carbon; in small particle state, the optical studies cover the spectral range going from $\lambda \sim 0.1$ to 100 μm for all the materials.

A Kramers-Kronig analysis of near normal reflectance data and/or a reflectance data fit to a Drude-Lorentz model gave bulk optical constants. These optical constants are used in theoretical calculations of extinction and the results compared with experimental results obtained from measurements of a variety of carbon particles. It is inferred that the high experimentally observed extinction is mainly due to a shape effect.

10. INTRODUCTION

Optical properties of small particles have become important for a variety of reasons. For example, atmospheric scientists are concerned with the effects of small particles on weather. It is known that the role of atmospheric aerosols in the earth's heat balance depends on their absorptivity and scattering properties (National Academy of Sciences, 1975). In order to predict accurately whether the warming tendency due to absorption and the cooling tendency due to backscattering in the earth's atmosphere will dominate, it is necessary to understand the optical properties of aerosol particulates (Twomey and Huffman, 1982).

The optical properties of small particles are important in astrophysics. The astrophysicist needs to understand the extinction by small particles in order to infer the nature of the solid grains responsible for the observed interstellar absorptions (Huffman, 1977).

Two further examples demonstrate the great diversity of applications of small particles. For military applications, it is desirable to understand the optical properties of particles which are to be used to generate smoke clouds for obscuration of laser weapons and surveillance devices;

for certain solar energy collector types, it has been shown that the energy collection is enhanced by doping the working fluid with very small absorbing particles (Hunt, 1980).

In applications of the later kinds, it is necessary to maximize the absorption by small particles. Thus carbon is a prime candidate material. For example, Abdelrahman, Fumeaux, and Suter (1979) have chosen graphite particles as ideal for suspension in the gas of a solar receiver. Hunt (1978, 1979) has designed a collector-heat exchanger which will utilize carbon particles suspended in air.

The extinction by small particles can be calculated for certain shapes if the optical constants as a function of wavelength are known. Although the literature on optical constants of carbon is abundant, the information is disparate and confined to limited spectral regions. Workers rarely agree with one another in their results. (See Twitty and Weiman, 1971 for a review.)

In this study, two carbonaceous materials, graphite and glassy carbon, chosen because they are well defined (and thus reproducible), are discussed. Graphite is the crystal form, and glassy carbon appears to be the best defined carbon variety close to ideally amorphous carbon.

Definitions and concepts which are dealt with in this work are covered in Chapter 11. In Chapter 12, optical constants of graphite and glassy carbon are surveyed; reflectance data of these materials are compiled from the

literature and augmented by our own measurements and/or extrapolations. The data are analyzed to yield optical constants over a broad spectral range. In Chapter 13 extinction by fine particles and smoke of carbon is experimentally measured, and results compared to theoretical calculations done with the use of the measured optical constants.

11. REVIEW OF CONCEPTS AND DEFINITIONS

This chapter establishes the notation, defines the optical constants and summarizes the theories which will be used in this work.

After defining the optical constants of solids and showing their relation to the dielectric constant, the classical dispersion relations and the Kramers-Kronig relations are reviewed. The extinction by small particles are introduced through the Mie theory for spheres which leads to the Rayleigh approximations. Rayleigh theory for ellipsoids, and its generalization to the distributions of ellipsoidal shape, are then discussed. Finally, a sum rule for small particle extinction is introduced.

11.1 Complex Index of Refraction; Relation to the Complex Dielectric Constant.*

Optical properties of solids deal with the interaction of electromagnetic radiation with solid matter. This interaction is described by wavelength dependent complex index of refraction:

$$m(\lambda) = n + i\,k \quad , \qquad (1)$$

*For a detailed treatment, see any E & M text, Jackson 1975 for example.

where n is the real index of refraction and k the index of absorption. n and k are related to the complex dielectric function ε through the relation:

$$m^2 = (n + ik)^2 = \varepsilon \quad .$$

From $\varepsilon = \varepsilon_1 + i\varepsilon_2$ it follows that:

$$\varepsilon_1 = n^2 - k^2 \tag{2}$$

$$\varepsilon_2 = 2nk \quad . \tag{3}$$

The (n,k) or $(\varepsilon_1, \varepsilon_2)$ pair describes completely the optical properties of a material, but they cannot be directly measured by experiment. The experimental connection is made through the reflectance:

$$R = \left|\frac{E_r}{E_i}\right|^2 = |r|^2$$

where r, the reflectivity coefficient, is a complex function, defined at the surface of a solid, as the ratio of the reflected electric field E_r to the incident electric field E_i. At normal incidence:

$$r = \frac{(n-1) + ik}{(n+1) + ik} \tag{4}$$

and

$$R = \frac{(n-1)^2 + k^2}{(n+1)^2 + k^2} \quad . \tag{5}$$

11.2 Dispersion Relations.

Classical Dispersion Relations*

The classical theory of absorption was developed by Lorentz (for insulators) and Drude (for free electron metals). The combined use of the two models yields:

$$\varepsilon = 1 - \frac{\omega_p^2}{\omega^2 + i\gamma\omega} + \sum_j \frac{\omega_{pj}^2}{\omega_j^2 - \omega^2 - i\gamma_j\omega}$$

which is equivalent to

$$\varepsilon_1 = 1 - \frac{\omega_p^2}{\omega^2 + \gamma^2} + \sum_j \frac{\omega_{pj}^2(\omega_j^2-\omega^2)}{(\omega_j^2-\omega^2)^2 + \gamma_j^2\omega^2} \qquad (6)$$

$$\varepsilon_2 = \frac{\gamma\omega_p^2}{\omega(\omega^2 + \gamma^2)} + \sum_j \frac{\omega_{pj}^2\,\omega\gamma_j}{(\omega_j^2-\omega^2)^2 + \gamma_j^2\omega^2} \quad , \qquad (7)$$

where ω_j, γ_j and ω_{pj} are respectively the resonance frequency, the damping constant and the plasma frequency of the j^{th} oscillator. They determine the position, the width and the strength of the j^{th} oscillator. The terms out of the summation signs are the Drude terms. The summation is over the number of oscillators. In more compact form (6) and (7) become:

$$\varepsilon_1 = 1 + \sum_j \frac{\omega_{pj}^2(\omega_j^2-\omega^2)}{(\omega_j^2-\omega^2)^2 + \gamma_j^2\omega^2} \quad , \qquad (8)$$

---

*For more information, see for example Wooten (1972, Ch. 3).

$$\varepsilon_2 = \sum_j \frac{\omega_{pj}^2 \, \omega\gamma_j}{(\omega_j^2-\omega^2)^2 + \gamma_j^2\omega^2} \quad . \tag{9}$$

The Drude terms are obtained from (8) and (9) by assuming that the resonance peak of the first oscillator is at zero frequency ($\omega_{j=1} = 0$).

This multiple oscillator model is used in the determination of optical constants of solids. From a reflectance curve, the first values of the parameters ω_j, γ_i and ω_{pj} are found for each peak by locating its position, and determining its width and its strength. They are used in equations (8) and (9) to calculate $\varepsilon_1(\lambda)$ and $\varepsilon_2(\lambda)$ which, by the use of equations (2) and (3) yield $n(\lambda)$ and $k(\lambda)$; the n and k obtained are used in (5) to yield the reflectance. The parameters are varied until the calculated reflectance fits the measured reflectance as well as desired, giving the corresponding $\varepsilon_1(\lambda)$ and $\varepsilon_2(\lambda)$ or $n(\lambda)$ and $k(\lambda)$.

This technique is still valid even if the solid is anisotropic. In this case, the sample has to be well oriented and polarized light must be used.

The Kramers-Kronig Relations*

The reflectivity coefficient can be written as:

$$r(\omega) = \rho(\omega) \, e^{i\theta} \tag{10}$$

(10)

*See for example Wooten (1972, Ch. 6 and Appendix G).

Equating the real parts and the imaginary parts of (4) and (6) leads to:

$$n = \frac{1 - \rho^2}{1 + \rho^2 - 2\rho \cos \theta} \quad . \tag{11}$$

$$k = \frac{2\rho \sin \theta}{1 + \rho^2 - 2\rho \cos \theta} \quad . \tag{12}$$

The knowledge of the phase θ will allow the calculation of n and k. The determination of θ can be done through the use of the Kramers-Kronig relations, which connect the real and imaginary parts of the response function of a linear system. The response function must have the following characteristics:

It has to be frequency dependent.

It has to be causal.

It has to be analytic in the upper half of the complex ω plane.

It can be shown that the reflectivity coefficient is a response function between the incident and reflected wave at the surface of a solid. It can also be shown that

$$\ln r(\omega) = \ln \rho(\omega) + i\theta(\omega)$$

satisfies the requirements for the application of the Kramers-Kronig relations.

The relation between $\theta(\omega)$ and $\rho(\omega)$ which is of interest in this treatment is:

$$\theta(\omega) = -\frac{2\omega}{\pi} P \int_0^\infty \frac{\ln \rho(\omega')}{\omega'^2 - \omega^2} d\omega' \quad ,$$

where P is a principal part. The removal of the principal part and the replacement of $\rho(\omega')$ by $|R(\omega')|^{\frac{1}{2}}$ gives:

$$\theta(\omega) = \frac{\omega}{\pi} \int_0^\infty \frac{\ln [R(\omega')/R(\omega)]}{\omega^2 - \omega'^2} d\omega' \quad .$$

In terms of wavelength, the substitution of $\omega = 2\pi c/\lambda$ can be made to yield:

$$\theta(\lambda) = \frac{2\lambda}{\pi} \int_0^\infty \frac{\ln [R(\lambda')/R(\lambda)]}{\lambda'^2 - \lambda^2} d\lambda' \quad . \qquad (13)$$

Relation (13) suggests that the reflectance has to be measured from zero to infinite wavelength. This is impossible in practice; in general, the reflectance is measured for λ such that:

$$\lambda_{min} \leq \lambda \leq \lambda_{max} \quad .$$

Thus, (13) can be rewritten:

$$\theta(\lambda) = \frac{2\lambda}{\pi} \int_0^{\lambda_{min}} \frac{\ln [R(\lambda')/R(\lambda)]}{\lambda'^2 - \lambda^2} d\lambda'$$

$$+ \frac{2\lambda}{\pi} \int_{\lambda_{min}}^{\lambda_{max}} \frac{\ln [R(\lambda')/R(\lambda)]}{\lambda'^2 - \lambda^2} d\lambda' + \frac{2\lambda}{\pi} \int_{\lambda_{max}}^\infty \frac{\ln [R(\lambda')/R(\lambda)]}{\lambda'^2 - \lambda^2} d\lambda'$$

$$= \theta_1(\lambda) + \theta_2(\lambda) + \theta_3(\lambda) \quad .$$

θ_2 is calculated with the actual experimental data. For $\theta_1(\lambda)$ and $\theta_3(\lambda)$, some sort of extrapolation has to be done. For metal and metal-like materials, the Drude model can be used to find $R(\lambda')$ and compute $\theta_3(\lambda)$. For other kinds of materials, Steyer (1974) derived a relation based on the classical dispersion theory.

The short wavelength spectral range is more difficult to treat. To include all the interband transitions, the reflectance is approximated by:

$$R(\lambda) = R_{le} \times (\lambda/\lambda_{le})^{s} \quad , \tag{14}$$

where $\lambda < \lambda_{le}$ and $s > 0$. R_{le} and λ_{le} are the reflectance and the wavelength at the last experimental point. At lower wavelengths, the reflectance is approximated by:

$$R(\lambda) = R_f \times (\lambda/\lambda_f)^{s} \quad . \tag{15}$$

R_f is calculated by the use of (14) at the point where the second extrapolation starts.

With this extrapolation, it is assumed that the wavelength is low enough to allow a free-electron description of the electrons.

These extrapolations are used in the integration of $\theta_1(\lambda)$ to yield (Wooten, 1972, p. 249):

$$\theta_1(\lambda) = \frac{1}{2\pi} \ln \left[\frac{R_f}{R(\lambda)}\right] \ln \left[\frac{|\lambda-\lambda_{1e}|}{\lambda+\lambda_{1e}}\right]$$

$$+ \frac{1}{\pi} \sum \left[s \frac{(\lambda_{1e}/\lambda)^{2n+1}}{(2n+1)^2} + (4-s) \frac{(\lambda_f/\lambda)^{2n+1}}{(2n+1)^2} \right] . \quad (16)$$

The parameter s and the wavelength λ_f are chosen such that the calculated optical constants are in agreement with those obtained from an independent measurement in a limited spectral range.

The actual reflectance data and the extrapolations are used in the numerical integration which is done by the use of Simpson's rule of integration.

11.3 Extinction by Small Particles.

Introduction to Mie Theory

A beam of light which passes through a collection of particles is attenuated. This attenuation, due to scattering and absorption by the particles, is called extinction which is defined to be:

$$\text{Extinction} = \text{Scattering} + \text{Absorption} .$$

A way for inferring the extinction is to calculate the transmission T of the beam through a path length ℓ of the distribution of particles. For N spherical particles per unit volume, each of radius a:

$$T = I/I_o = \exp(-NQ_{ext}\pi a^2)\ell \quad , \tag{17}$$

where:

$$Q_{ext} = Q_{sca} + Q_{abs} \quad .$$

The Q's are called efficiency factors for spheres, and are related to the following quantities:

$C_{sca} = Q_{sca}\,\pi\,a^2$ is the cross section for removal of energy from the incident beam by scattering,

$C_{abs} = Q_{abs}\,\pi\,a^2$ is the cross section for removal of energy from the incident beam by absorption,

$$C_{ext} = C_{sca} + C_{abs} \quad . \tag{18}$$

Mie (1908) and Debye (1909) developed a theory for calculating the efficiency factors for spheres of arbitrary sizes. This theory, usually referred to as the Mie theory is presented in books by van de Hulst (1957), Kerker (1969) and Bohren and Huffman (1983).

From the theory:

$$Q_{sca} = \frac{2}{x^2} \sum_{n=1}^{\infty} (2n+1)\,[|a_n|^2 + |b_n|^2] \quad , \tag{19}$$

$$Q_{abs} = \frac{2}{x^2} \sum_{n=1}^{\infty} (2n+1)\,\mathrm{Re}(a_n + b_n) \quad , \tag{20}$$

where $x = 2\pi a/\lambda$ is the size parameter. The coefficients a_n and b_n are complex expressions involving spherical Bessel and Hankel functions and their derivatives. They can be computed for given values of the complex index of refraction

n and the size parameter x. The computation procedure is given by Wichramasinghe (1973) and related computer programs are in the book by Bohren and Huffman (1983).

Theory and experiment are connected as follows. If we define:

$$N = n/V \quad ,$$

where n is the total number of particles in the volume V,

$$C = m/V = \frac{n}{V} \frac{4}{3} \pi a^3 \rho \quad ,$$

where m is the total mass of particles and ρ the mass density of the particle material, (17) becomes:

$$I/I_o = \exp\left(-\alpha \frac{C\ell}{\rho}\right)$$

$$= \exp\left(-\alpha \frac{\sigma}{\rho}\right) \quad , \tag{21a}$$

$$\alpha = \frac{\rho}{\sigma} \ln\left(I_o/I\right) \quad . \tag{21b}$$

If the optical density (O.D.) defined as: $O.D. = \frac{1}{2.3} \ln \frac{I_o}{I}$ is used, then $\alpha = 2.3 \frac{\rho}{\sigma} (O.D.)$, where σ is the mass/area of particles. Also

$$\alpha = \frac{Q_{ext} \pi a^2}{4/3 \pi a^3} = \frac{3}{4} \frac{Q_{ext}}{a} \quad . \tag{22}$$

α is the volume normalized extinction coefficient and is related to the mass extinction coefficient α_p by:

$$\alpha_p = \frac{\alpha}{\rho} \quad . \tag{23}$$

In the case of a size distribution of spheres:

$$\alpha = \frac{\int N(a) Q(a) \pi a^3 da}{\int N(a) \frac{4}{3} \pi a^3 da} ,$$

where N(a) is the number of particles per unit volume with radii varying between a and a + da.

From (21), α can be determined experimentally by measuring the transmission and σ. The use of (22) leads to an experimental value of Q_{ext}.

If the particles are very small compared to the wavelength ($a << \lambda$) and when the phase shift of light in the particle is negligible ($|m|x << 1$) (Rayleigh approximation), then the Mie efficiency factors can be expanded in power series as functions of the size parameter x; the lowest power terms of importance in a first approximation are:

$$Q_{sca} = \frac{8}{3} x^4 \left| \left(\frac{m^2-1}{m^2+2} \right) \right|^2 , \qquad (24)$$

$$Q_{abs} = 4 x \, Im \left\{ \frac{m^2-1}{m^2+2} \right\} . \qquad (25)$$

Relations (24) and (25) apply when the particles are in a medium with complex index of refraction $m'^2 = 1$. They can be generalized to give:

$$Q_{sca} = \frac{8}{3} x^4 \left| \left(\frac{\varepsilon-\varepsilon_m}{\varepsilon+2\varepsilon_m} \right) \right|^2 , \qquad (26)$$

$$Q_{abs} = 4 x \, Im \left\{ \frac{\varepsilon-\varepsilon_m}{\varepsilon+2\varepsilon_m} \right\} , \qquad (27)$$

where ε is the dielectric constant of the particles and ε_m is the dielectric constant of the medium in which they are embedded.

The Rayleigh approximations have introduced two main simplifications in the treatment of extinction by small particles. First of all, there is no shape effect in volume normalized extinction, as illustrated in Fig. 17 . At small radii, the extinction is a constant. However, for radii above 0.012 μm, the extinction is extremely radius dependent. One notices a decrease in extinction for radius larger than 0.1 μm. This decrease is due to saturation effect; when absorption is very effective, the inner parts of the sphere do not participate in the absorption process. With larger spheres, more of the inner volume is ineffective, which results in a decrease of the extinction per unit volume.

From an experimental point of view, one does not have to worry about the size distribution of particles if they are small enough compared to the wavelength. This occurs easily in the IR spectral range.

The second simplification introduced by the Rayleigh approximations is that the shape effects can be more easily treated theoretically, as will be shown in the next section.

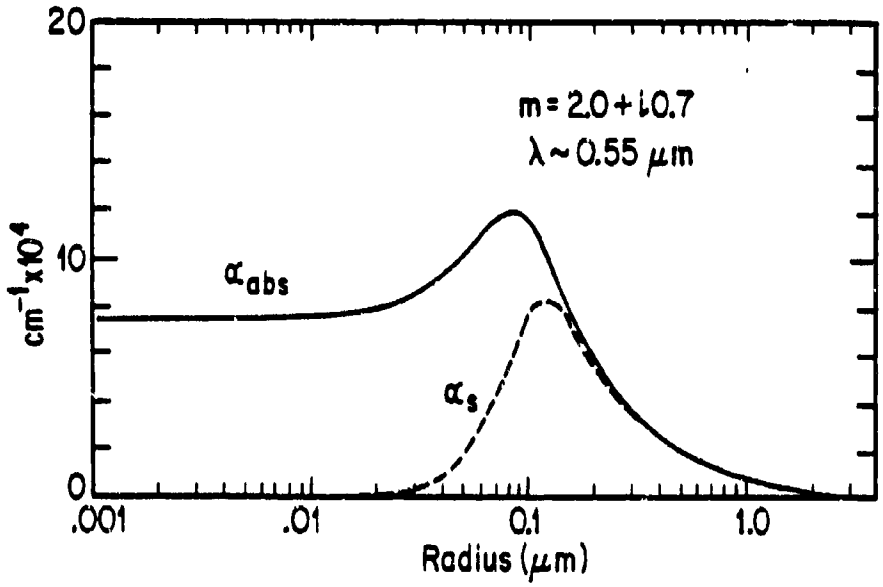

Fig. 17. Absorption and scattering cross sections normalized per unit volume of solid for carbon in the visible, calculated using Mie theory

11.4 Rayleigh Theory for Ellipsoids; The Shape Distribution.

Small particles have been discussed with the assumption that they are spherical. Although this is not very often true, the spherical hypothesis allowed the use of the Mie theory which can be generalized to infinite cylinders only. A more realistic shape for particles is the ellipsoid, for which polarizability in an electric field can be determined and used in the derivation of an approximate expression for the absorption and scattering cross-sections, if the Rayleigh conditions are valid. The derivation of the polarizability can be found in the bibliography given for the Mie theory.

For an ellipsoidal particle with semi-axes a, b and c in an electric field parallel to the j^{th} axis ($j = 1,2,3$), polarizability is given by:

$$\alpha_j = \frac{V}{4\pi} \frac{\varepsilon - \varepsilon_m}{\varepsilon_m + L_j(\varepsilon - \varepsilon_m)} \quad , \tag{28}$$

where $V = (4/3)\pi$ abc is the volume of the ellipsoid. The depolarization factors L_j are given by:

$$L_1 = \frac{abc}{2} \int \frac{ds}{(s+a^2)\ \{(a^2+s)(b^2+s)(c^2+s)\}^{\frac{1}{2}}} \quad , \tag{29}$$

where:

$$s = a + b + c \quad .$$

L_2 and L_3 are computed the same way, with the right substitution in (29). Using the integrals by which the L_j's are calculated, it can be shown that:

$$\sum_{j=1}^{3} L_j = 1 \quad . \tag{30}$$

In the Rayleigh approximations, C_{sca} and C_{abs} for a single ellipsoid of abitrary L_j are:

$$C_{sca}^{j} = \frac{k^4}{6\pi} V^2 \left| \frac{\varepsilon-\varepsilon_m}{\varepsilon_m + L_j(\varepsilon-\varepsilon_m)} \right|^2 \quad , \tag{31}$$

$$C_{abs}^{j} = kV \, \mathrm{Im} \left\{ \frac{\varepsilon-\varepsilon_m}{\varepsilon_m + L_j(\varepsilon-\varepsilon_m)} \right\} \quad . \tag{32}$$

The superscript j shows that E field is parallel to the j^{th} axis; $k = 2\pi/\lambda$. For a collection of ellipsoids randomly oriented, an average value is taken; the absorption case is given:

$$\langle C_{abs} \rangle = \frac{V}{3} k \sum_{j=1}^{3} \frac{\varepsilon_m \varepsilon_2}{L_j\{[\varepsilon_1+\varepsilon_m(1/L_j-1)]^2 + \varepsilon_2^2\}} \quad . \tag{33}$$

From (33) it can be seen that resonance occurs when:

$$L_j\varepsilon_1 + \varepsilon_m(1-L_j) = 0$$

or

$$\varepsilon_1 = -\varepsilon_m(1/L_j - 1) \quad . \tag{34}$$

Since $0 \leq L_j \leq 1$, the resonance occurs only for negative values of ε_1. For spheres, $L_j = 1/3$ for all directions, and the resonance is obtained for:

$$\varepsilon_1 = -2\varepsilon_m \quad .$$

A distribution of identical ellipsoids with arbitrary L_j's will give three absorption peaks because of the three values of L_j.

A more general treatment of the preceding case is done by considering a variety of shapes of ellipsoids.

Given a shape distribution expression $P(L_1,L_2)$, it is possible to compute:

$$\langle\langle C_{abs} \rangle\rangle = \iint P(L_1,L_2) \langle C_{abs} \rangle \, dL_1 \, dL_2 \quad . \tag{35}$$

The integration is done over L_1 and L_2 only since from (30) it is seen that only two L_j's are independent.

Assuming that all shapes of ellipsoids are equally probable, which mathematically means that $P(L_1,L_2)$ is a constant, Huffman and Bohren (1980) found (35) to be:

$$\langle\langle C_{abs} \rangle\rangle = k\langle V \rangle \, \mathrm{Im}\left[\frac{2\varepsilon\varepsilon_m}{\varepsilon-\varepsilon_m} \log\,(\varepsilon/\varepsilon_m)\right] \quad . \tag{36}$$

(For the log calculation, use $|\varepsilon|$ and $-\pi < \theta < \pi$.) For this treatment, a system of particles with all shapes of ellipsoids should produce absorption over the whole spectral range where ε_1 is negative. Rathmann (1981, p. 18) calculated aluminum absorption coefficients for spheres, single ellipsoids and a continuous distribution of ellipsoids.

Relation (36) is used in our theoretical calculations, and the corresponding curves are labeled CDE (continuous distribution of ellipsoids).

Sum Rule for Extinction

Bohren and Huffman (1983) have derived a sum rule for extinction by spherical particles:

$$\int_0^\infty C_{ext}(\lambda)\, d\lambda = 4\pi^3 a^3 \frac{\varepsilon(\lambda=\infty)+1}{\varepsilon(\lambda=\infty)+2} \quad . \tag{37}$$

For conducting materials, $\varepsilon(\lambda=\infty)$ is large; thus (37) has an upper limit such that:

$$\int_0^\infty C_{ext}(\lambda)\, d\lambda \leq 4\pi^3 a^3 \quad . \tag{38}$$

Using (22) in conjunction with $C_{ext} = Q_{ext}\, \pi^2 a^2$ gives:

$$C_{ext}(\lambda) = \frac{4}{3}\, \pi a^3\, \alpha(\lambda) \quad . \tag{39}$$

A substitution of (39) in (38) leads to:

$$\int_0^\infty \alpha(\lambda)\, d\lambda \leq 3\pi^2 \quad . \tag{40}$$

This relation will be used to check the sphericity of experimentally produced particles.

The sum rule (37) was first derived by Purcell (1969) for spheroidal particles.

12. BULK OPTICAL CONSTANTS

Carbon is the generic designation of a large variety of carbonaceous materials including graphite and amorphous carbon. Graphite and amorphous carbon are well defined, but many types of coal and soot differ in composition and structure. According to Dalzell and Sarofin (1969), soots are randomly mixed graphitic particles in a matrix of amorphous carbon; they differ from one another by their hydrogen/carbon ratio. The actual difference in the composition of carbonaceous materials, and apparent differences resulting from the use of inappropriate experimental technique in the determination of the optical constants, have led to results, which in some cases, are hardly comparable. Disagreements in results are shown through the review of some previous work presented below. The large variation in published optical constants can be seen in Fig. 18.

Stull and Plass (1960) derived dispersion relations for carbon, which they used to fit some other workers' reflectance data between $\lambda \sim 0.436$ μm and 13 μm. The same method has been used by Dalzell and Sarofin (1969) to fit soot pellet reflectance data in about the same spectral

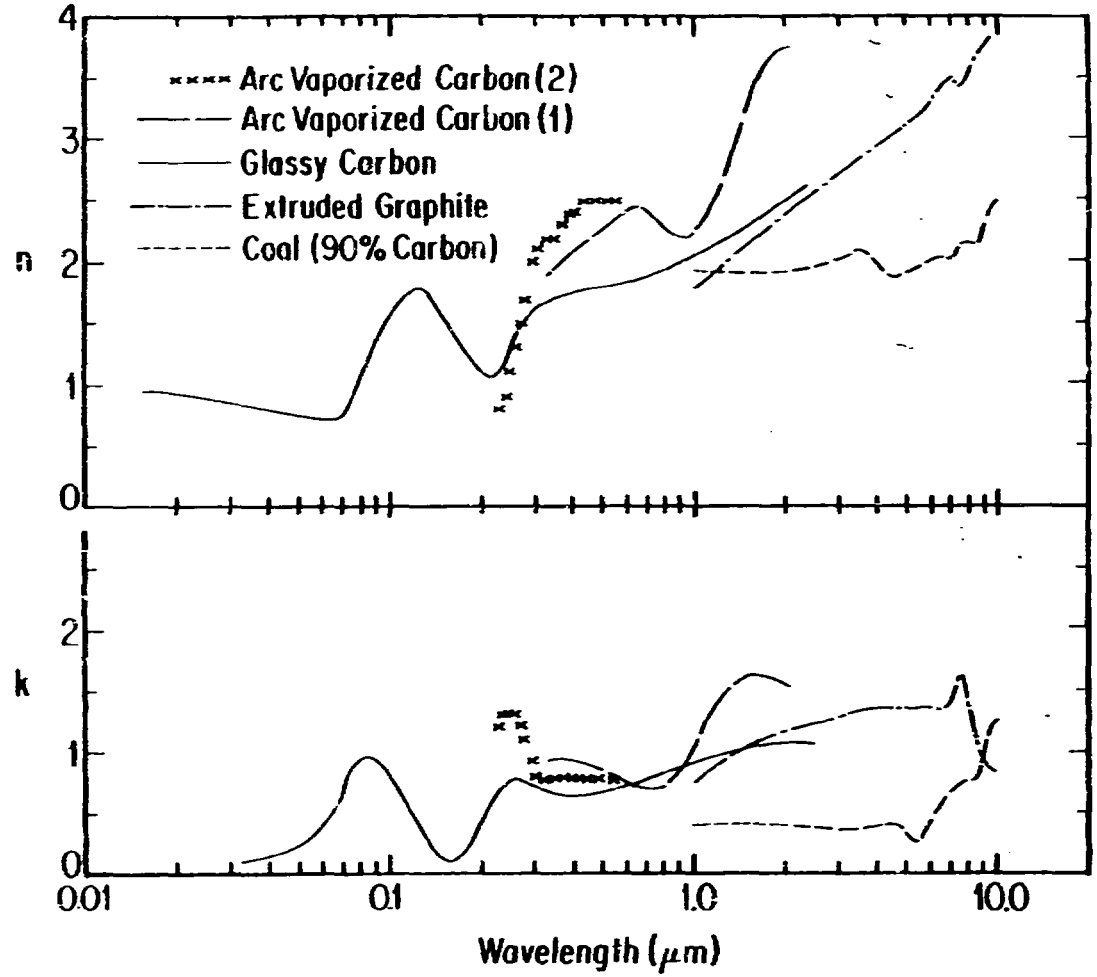

Fig. 18. Optical constants n and k for amorphous carbon

Glassy carbon (Williams and Arakawa, 1972), arc vaporized carbon (Arakawa et al., 1977 for (1) and DiNardo and Goland, 1971 for (2)), extruded graphite and coal (Foster and Howarth, 1968)

range. The results of the two groups do not agree with one another. More recently, Lee and Tien (1981) derived a dispersion model based on electronic band structure considerations. The dispersion constants were determined from the transmission data of soot flame. They questioned their predecessors' methods and results. Tomaselli et al. (1981) measured reflectance of pressed pellets of various carbonaceous materials. They graphically analyzed data by plotting iso-reflectance curves and reading n and k from published tables. None of their results came close to published results for similar materials. DiNardo and Goland (1971) derived optical constants of arc evaporated carbon film by matching the transition radiation theory to experiments from $\lambda \sim 0.23$ μm to 0.56 μm. Arakawa, Williams, and Inagaki (1977) studied a similar material from $\lambda \sim 0.33$ μm to 2.1 μm. A comparison of the two results shows a clear disagreement (see Fig.18.). According to Arakawa et al. (1977), the optical properties of arc evaporated carbon vary with the conditions of preparation of the film. Pluchino et al. (1980) isolated a single micro-sized particle of carbon; they electrostatically suspended and irradiated it with a laser beam. The scattered radiation intensity was measured as a function of angle. Electron-microscopy showed that the particle was spherical. Data were then analyzed with the Mie theory. At $\lambda \sim 0.48$ μm and for a particle radius $a \cong 3.06$ μm, n and k are found to be 1.7 and 0.8 respectively.

This review along with Fig. 18 has shown that there is no general consensus on optical constants of carbon; it has shown also that available optical constants are confined to a limited spectral range.

In this section, we survey the optical constants of graphite and glassy carbon, and gather existing reflectance data on these materials. In order to calculate the optical constants over a wide spectral range, the reflectance information gathered is completed by our measurements and/or extrapolations wherever it is necessary, to yield a reflectance curve over a wide spectral range, for use in the Kramers-Kronig analysis. A fit of the reflectance data, based on the combined use of Drude and Lorentz dispersion relations has also been done.

Techniques for the determination of optical constants are given; then graphite and glassy carbon are studied in turn.

12.1 Techniques for Measuring Optical Constants

Optical properties of solids are due to the wavelength dependence of n and k (ε_1 and ε_2) which cannot be measured directly experimentally. The techniques used to collect information leading to optical constants are summarized in Table [3].

Table 3. Techniques for determining optical constants of solids

From Huffman (1977)

Technique	Comments
Transmission methods	
(1) n from minimum deviation; k from transmission and n	High accuracy for n
(2) n and k from transmission and normal incidence reflectance measurements	Easy but useful only in relatively transparent regions
Reflection methods	
(1) Two polarized reflectance measurements at one oblique incidence angle	Larger sample sizes required
(2) Two reflectance measurements at different angles	
(3) Determination of special angles (i.e., Brewster's angle) and reflectance there	
(4) Determination of ellipsometric parameters	Sensitive to surface films
(5) Reflectance in a broad wavelength range and Kramers-Kronig analysis	Extrapolation to 0 and to ∞ necessary
(6) Reflectance vs. wavelength and oscillator model fit to the data	Compact presentation of results as oscillator parameters
Other methods	
(1) Electron energy loss measurements	Does not require polished surfaces

12.2 Graphite.

Perfect graphite crystals are rare. Figure 19. represents the ideal natural graphitic structure. The basal planes are such that every other plane fits exactly over the first; this is the ABAB arrangement. Another one is such that the basal planes are in the ABCABC sequence.

The atoms of carbon are associated in hexagonal rings. Each atom has four electrons on its outer shell; three of them (σ-electrons) participate in holding together the hexagonal ring by covalent bonds; the fourth one (π-electron) moves in the ring and contributes to the bonding between planes. Many properties of graphite, including its optical properties, are highly anisotropic. The anisotropy of the optical properties is due to the ease with which the π-electrons move in the layer planes; higher energy is needed to jump from plane to plane.

Forms most closely approaching the ideal structure of the material graphite are pyrolytic graphite and annealed pyrolytic graphite. Pyrolytic graphite is produced by a decomposition of a hydrocarbon on a hot surface. Although it is not a true graphite, its properties are extremely anisotropic. It can be converted into almost perfect single crystals by heating at temperatures above 2900°C for several hours. It is then called (stress) annealed pyrolytic graphite (Shobert, 1964).

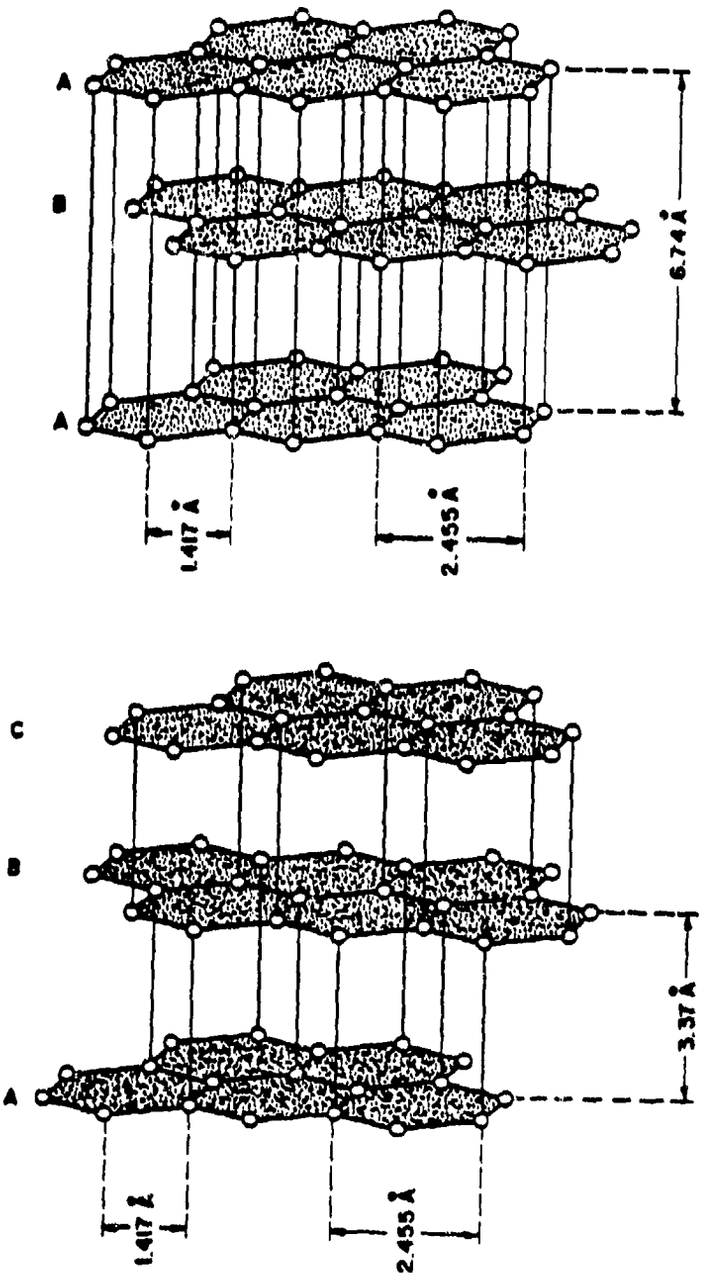

19. Crystal structures of graphite
From Shobert (1964)

The optical properties of graphite depend on the direction of the E-field with respect to its optical c-axis, $E \perp C$ and $E \parallel C$ leading to $\varepsilon_\perp$ and $\varepsilon_\parallel$ respectively. Because samples can easily be prepared by cleavage of the crystal in the basal plane, many optical constants for the $E \perp C$ direction are available in the literature. Fewer measurements have been done for $E \parallel C$ since the sample preparation is considerably more difficult in this case. $E \perp C$ and $E \parallel C$ optical constants of graphite will be reviewed in turn.

Survey of Optical Constants of Graphite

Many workers measured reflectance on natural graphite, pyrolytic graphite or annealed pyrolytic graphite. They analyzed their data by the Kramers-Kronig method (Taft and Philipp, 1965; Philipp, 1977), by fitting (Greenaway et al., 1969; Klucker, Skibowski, and Steinman, 1974) or by the use of Fresnel's equations (Carter et al., 1965).

Zeppenfeld (1967) was the first to use the electron energy loss method for deriving optical constants of graphite. This method consists of determining the properties of bulk materials by measuring the transmission of electron beams through thin films. ε_1 and ε_2 are obtained by the Kramers-Kronig analysis of the energy loss function $f(\omega)$ which is related to the dielectric function by (Daniels et al., 1970):

$$f(\omega) = - \mathrm{Im}\ (1/\varepsilon) \quad .$$

The survey of optical constants is summarized in Table 4.

Comparison of results for E ⊥ C is seen in Fig. 20.a which shows ε_2 in a spectral range which contains a strong peak. Good agreement exists in the shape of the curve, but the discrepancy in the magnitude of the peak is obvious.

For E // C, Fig. 20.b shows complete disagreement between the results of the reflectance techniques and those of the electron energy-loss method. Because of the severity of the discrepancy, Venghaus (1975) repeated the electron energy-loss measurements on graphite. His results were in agreement with the measurements done with the same technique by other workers (Zeppenfeld, Tosatti & Bassani), but still in disagreement with reflectance method results. Wessjohan (Venghaus, 1975) computed reflectance using Venghaus (1975) and Klucker et al. (1974) ε data; Venghaus's results compared favorably with experiments, but those from Klucker et al. failed to do so. Although Klucker (1971), who noticed the discrepancy between his experimental results and calculations, assigned this failure to scattered light, Venghaus concluded that the electron energy-loss method gives better results.

In IR ($\lambda \sim 2.5$ μm to 100 μm), Venghaus measured the reflectance on graphite in the E//C direction and analyzed the data by the Kramers-Kronig method.

Table 4 Survey of optical properties of graphite

Reference	Range (μm)	Technique	Polarization	Comments
Carter et al. (1965)	0.11 - 0.30	Reflectance	E ⊥ C	Agreement with Taft and Philipp
Ergun (1967)	0.55	Reflectance	E ⊥ C, E // C	High values of n
Foster & Howarth (1968)	1 - 9.2	Reflectance	E // C	High IR results
Greenaway et al. (1969)	0.25 - 0.62	Multi-angle reflectance	E ⊥ C, E // C	Compares well with this work
Klucker et al. (1974)	0.03 - 0.41	Multi-angle reflectance	E ⊥ C, E // C	Very low values of ε_2
Lenham & Treherne (1966)	0.4 - 19	Reflectance	E ⊥ C, E // C	
Philipp (1977)	1 - 1239	Reflectance	E ⊥ C	Sato reflectance results used
Sato (1968)	41 - 206	Reflectance	E ⊥ C	Did not take free electron behavior into consideration in his analysis
Venghaus (1975)	0.03 - 1.2	Energy-loss	E ⊥ C, E // C	Agreement with Zeppenfeld
Venghaus (1977)	2.5 - 83	Reflectance	E // C	Published results

Table 4 --Continued

Reference	Range (μm)	Technique	Polarization	Comments
Taft & Philipp (1965)	0.05 - 41	Reflectance	$E \perp C$	Commonly accepted results
Zeppenfeld (1967)	0.03 - 1.2	Energy-loss	$E \perp C$, $E \parallel C$	First to use energy-loss techniques on graphite

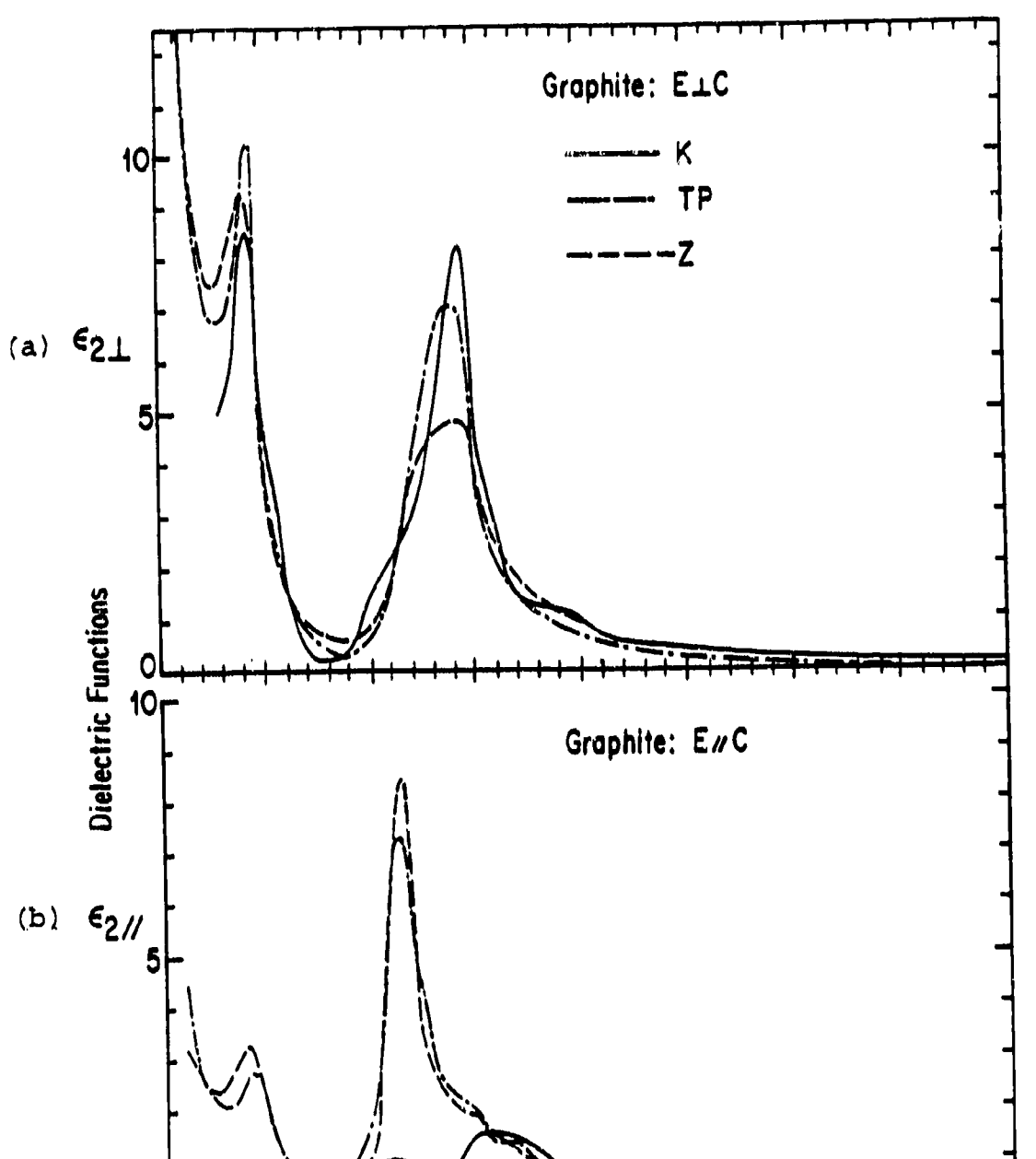

Fig. 20. Imaginary part of the dielectric function for the E ⊥ C (a) and E // C (b) polarizations of graphite

As computed by Klucker et al. (1974), Taft and Philipps (1965), and Zeppenfeld (1967)

This Study's Investigation on Graphite

In order to have a coherent set of optical constants in a broad spectral range for the E $\perp$ C direction of graphite, and also to investigate the discrepancy of the ε_2 peak at $\lambda \sim 0.088$ μm, Philipp's (1977) extended reflectance data (see Fig. 21.) have been analyzed by the Kramers-Kronig method. Philipp obtained his extended reflectance data by combining previously published results (Taft and Philipp, 1965), measurements between $\lambda \sim 12.4$ μm and 41 μm, and Sato's (1968) data.

It is known that the Kramers-Kronig analysis results depend strongly on the extrapolation at low wavelengths (Wooten, 1972). To satisfy the requirements of the extrapolation, which is explained in Chapter11, some guide values of n and k found from an independent experiment are needed. Huffman (1979), in work done at the University of Wisconsin monochromatic radiation facility, measured the transmission of a 0.27 μm thick cleaved graphite sample from $\lambda \sim 1.25$ μm to 0.15 μm. The values of n and k found from this experiment have been used as tests for the choice of the parameter s and the wavelength λ. These values are s = 2, $\lambda_f \sim 0.0258$ μm. Taft and Philipp used the results of the transmission of a 400Å thick sample from $\lambda \sim 0.113$ μm to 0.177 μm as guiding values in their calculations. Results of our calculations are shown in Figs. 22., 23., and 24. and in Appendix B.

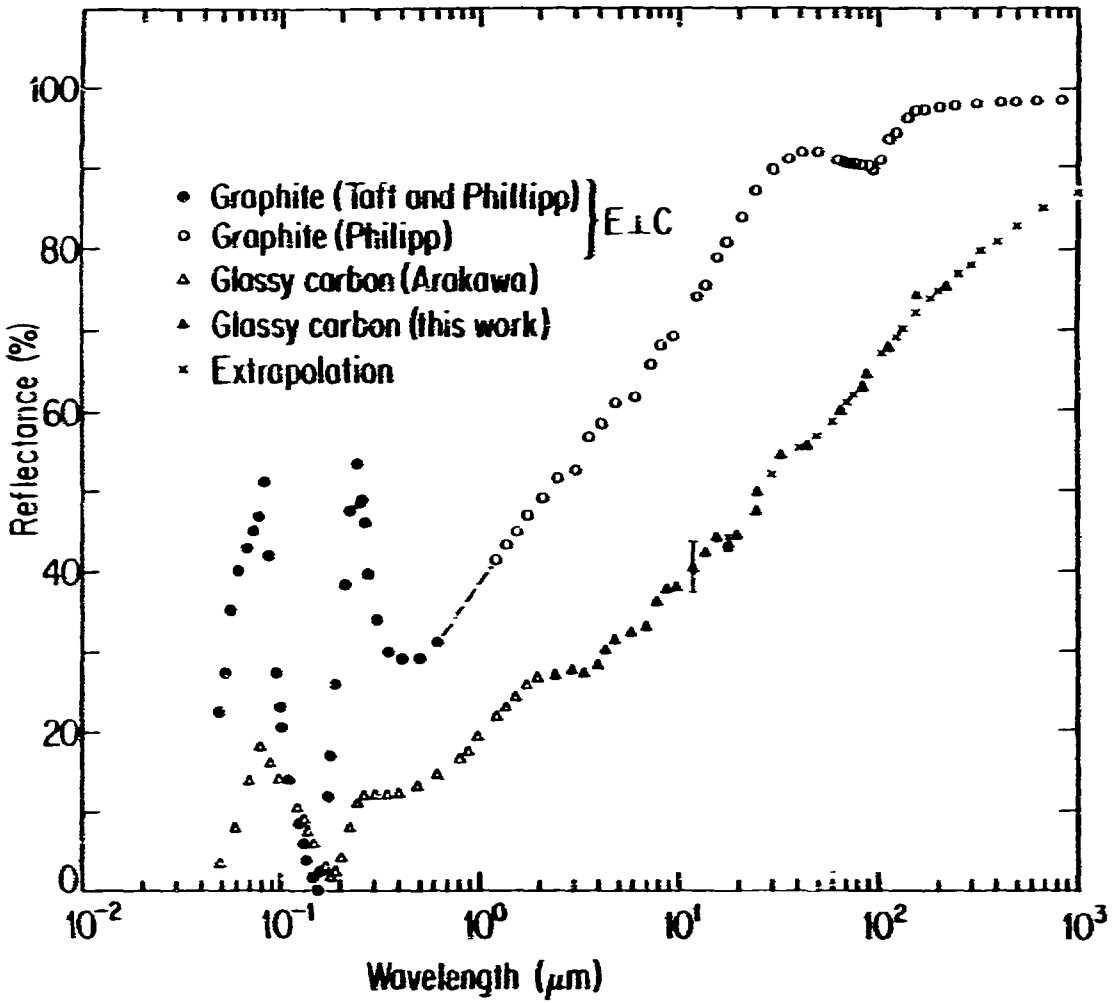

Fig. 21. Reflectance of graphite and glassy carbon

Graphite (Taft and Philipp, 1965; Philipp, 1977), glassy carbon (Williams and Arakawa, 1972 and this work)

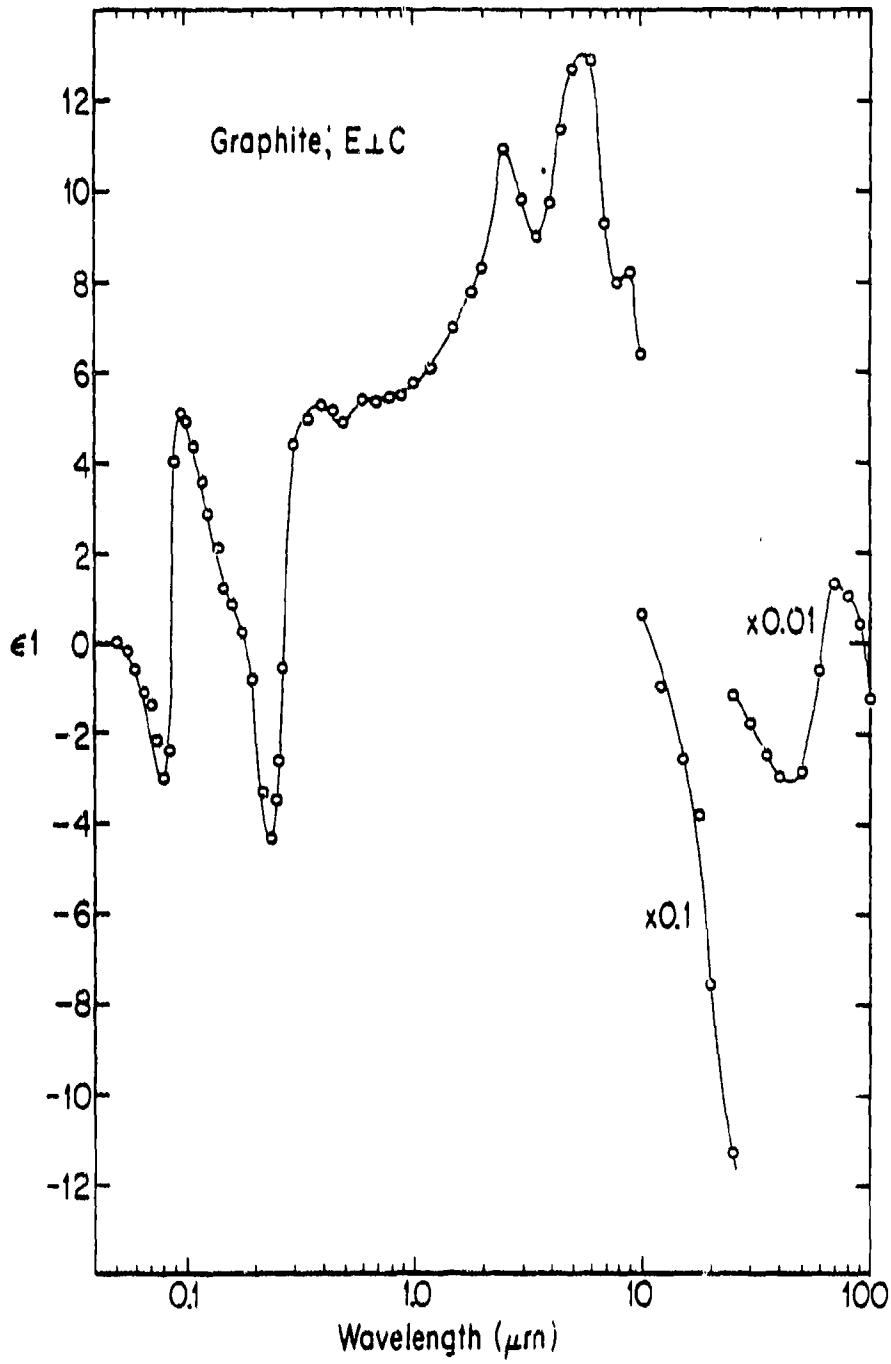

Fig. 22. Real part of the E ⊥ C polarization of graphite as computed by the Kramers-Kronig method

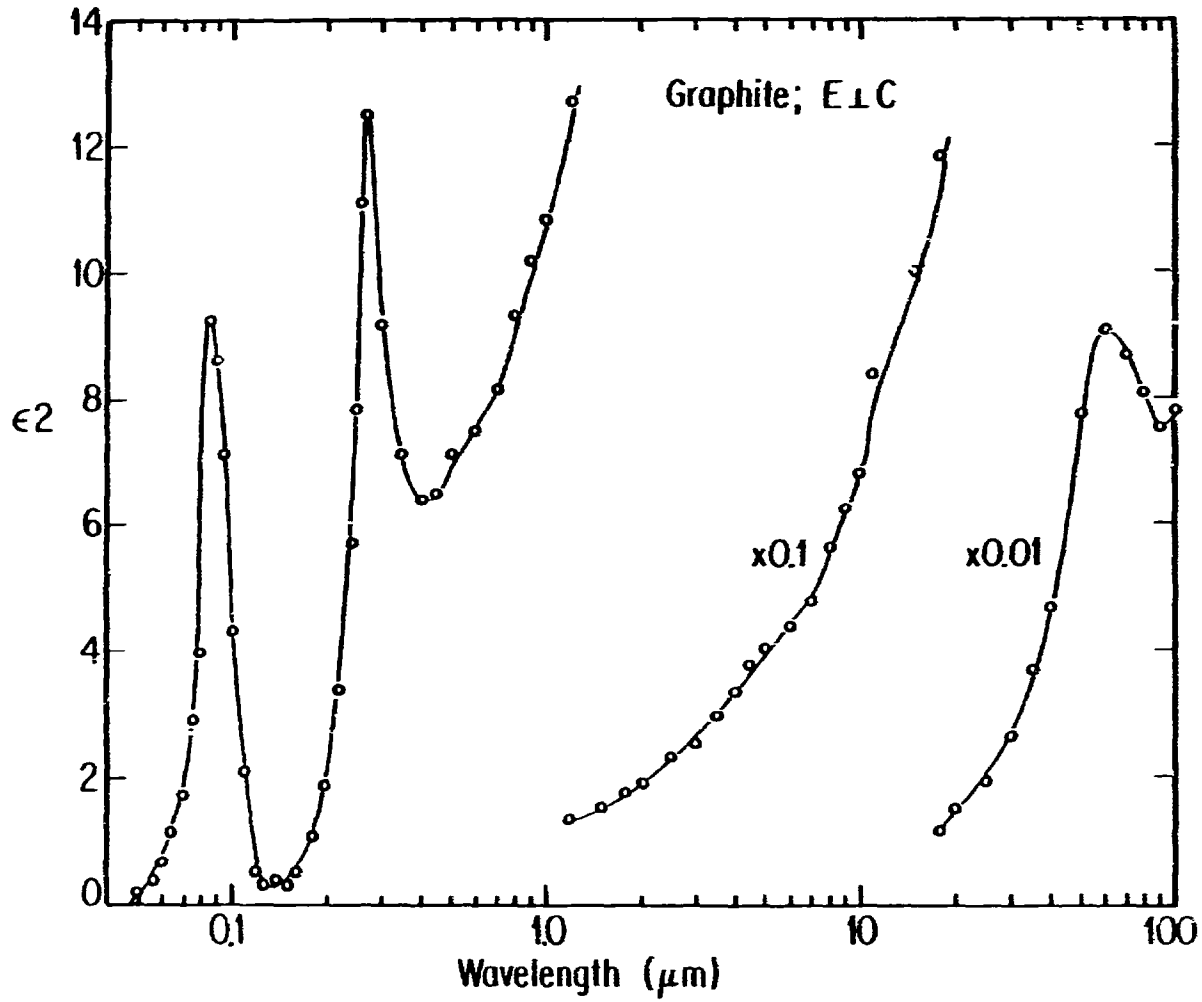

Fig. 23. Imaginary part of the E ⊥ C polarization of graphite as computed by the Kramers-Kronig method

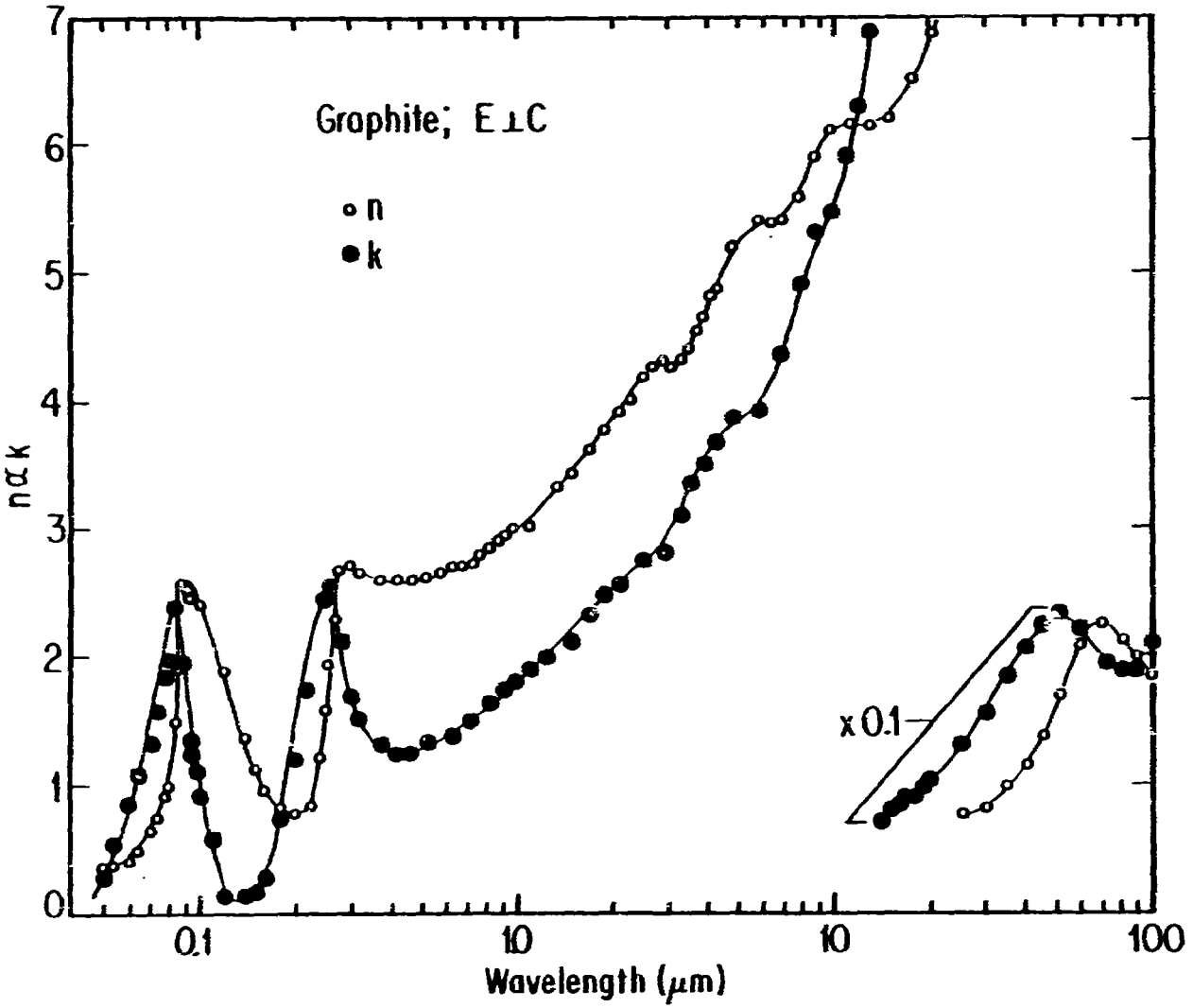

Fig. 24. Optical constants n and k for the E ⊥ C polarization of graphite computed by the Kramers-Kronig method

The reflectance data fit result is shown in Fig. 25. A discussion of the discrepancy observed between the data and the fit from λ = 0.3 to 15 μm is given in the "Discussion of Results" section of this chapter. The oscillator parameters used are presented in Table 5.

Representative values of ε_1 and ε_2 for the E // C direction of graphite derived from the reflectance and the electron energy-loss measurements have been converted to n and k and plotted (Fig. 26.). Venghaus's results below $\lambda \sim 2.5$ m were obtained privately. Venghaus (1977) argued that reflectance measurements are not seriously affected by the roughness of the reflectance surface in the IR wavelength range; n and k obtained by optical methods are thus reliable from 2.5 μm to 100 μm. In the short wavelength range ($\lambda \sim 0.03$ to about 0.22 μm), the increasing dependence on the reflectance on the state of the surface as the wavelength decreases makes the results of the optical method less reliable than those obtained with the electron energy-loss technique. Since above $\lambda \sim 0.25$ μm, the Cerenkov radiation gives the dominant contribution to the electron energy-loss for E // C (Tossati and Bassani, 1970), the electron energy-loss results have been disregarded from $\lambda \sim$ 0.25 μm to 2.5 μm. From 0.15 μm to 0.25 μm, geometrical considerations have been used. The slope of the electron energy-loss n curve at short $\lambda \sim 0.15$ μm is the same as the slope of the reflectance n curve from $\lambda \sim 0.21$ μm to 0.25 μm.

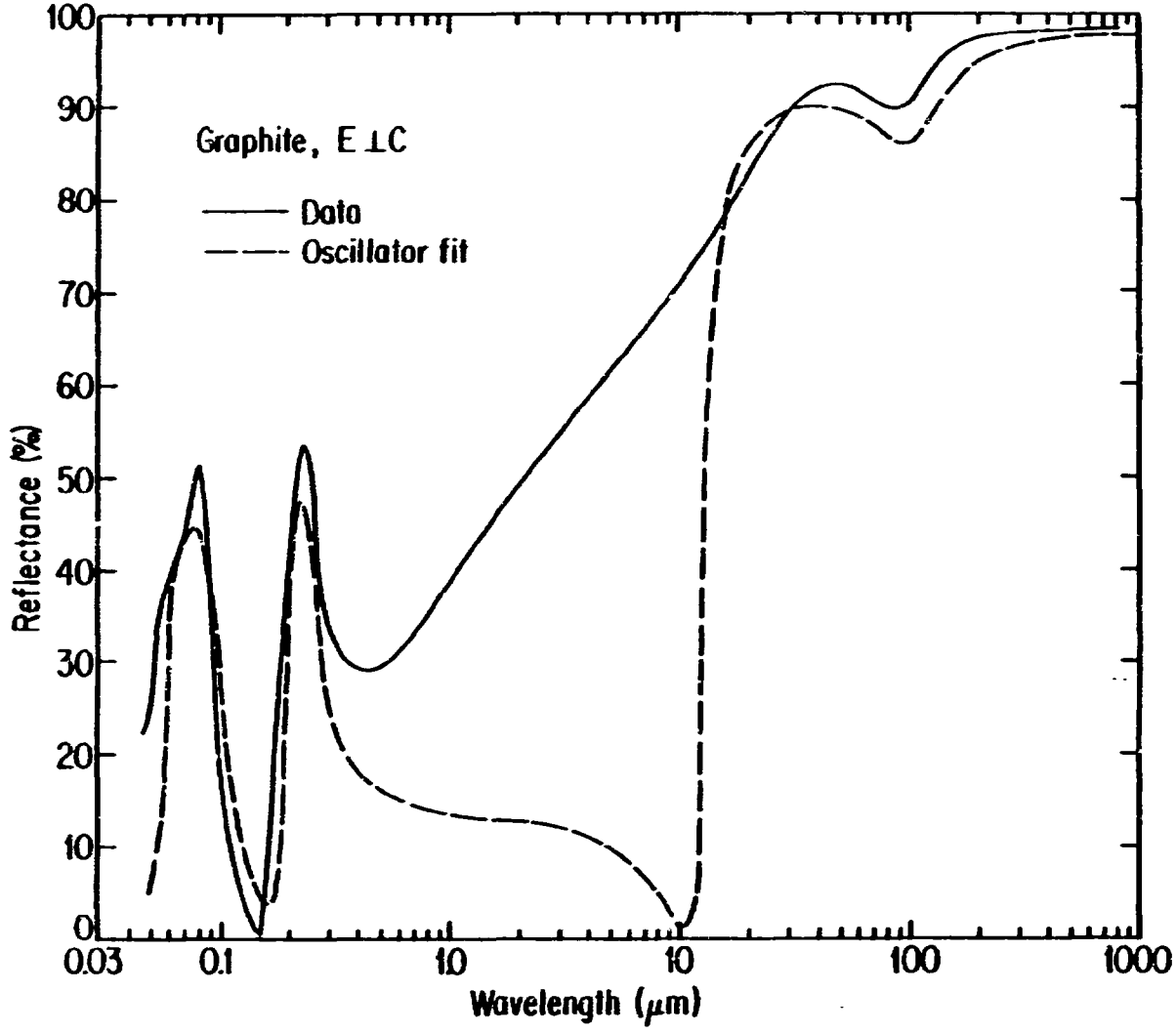

Fig. 25. Oscillator fit of the reflectance of graphite (E ⊥ C polarization)

Table 5. Oscillator parameters for the fit of the reflectance curve for the $E \perp C$ direction of graphite

	Parameter	Value (cm^{-1})
Oscillator 1	ω_{P1}	1200
	ω_1	0.00
	γ_1	15.00
Oscillator 2	ω_{P2}	1300
	ω_2	120
	γ_2	120
Oscillator 3	ω_{P3}	6×10^3
	ω_3	4×10^3
	γ_3	7.5×10^3
Oscillator 4	ω_{P4}	110×10^3
	ω_4	98×10^3
	γ_4	25×10^3

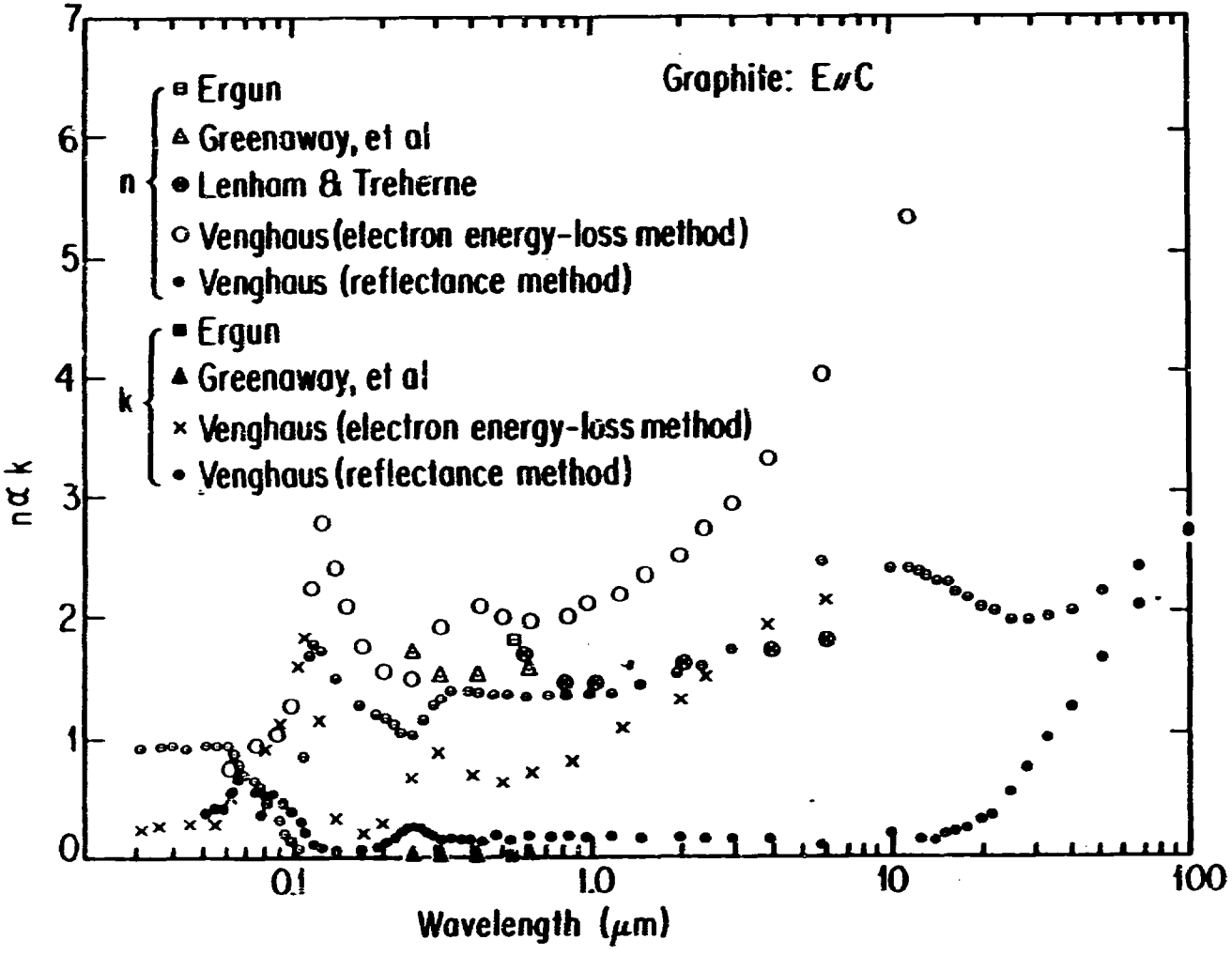

Fig. 26. Optical constants n and k of the E // C polarization of graphite

Based on that consideration, a connecting curve has been drawn between the two n curves from $\lambda \sim 0.15$ μm to 0.21 μm. From this combination of optical method results and electron energy-loss measurements, a set of n and k data for E // C has been put together from $\lambda \sim 0.025$ μm to 100 μm. (See Figs. 27. and 28. and Appendix B.)

For the E // C direction of graphite, the reflectance computed from n and k extracted from the literature has been fitted using a Drude-Lorentz oscillator model; the result is shown in Fig. 29. The oscillator parameters used are presented in Table 6.

12.3 Glassy Carbon.

Glassy carbon, also known as vitreous carbon, is produced by the slow pyrolysis of polymers such as cellusen and aromatic resins. It looks like black glass, has a low density (1.4 - 1.5 g/cm^3) and also a low porosity and permeability to water. It has about the same hardness as glass; it withstands high temperature in absence of oxygen. X-ray studies have shown that glassy carbon has randomly oriented crystals which are not very much altered by heat treatment. At 3273°K, glassy carbon crystallite size is 6 mm; they are smaller at lower temperatures (Halpin and Jenkins, 1969).

Taft and Philipp (1965) published near normal incidence reflectance data of glassy carbon up to 26 eV. Williams and Arakawa (1972) published plots of n and k

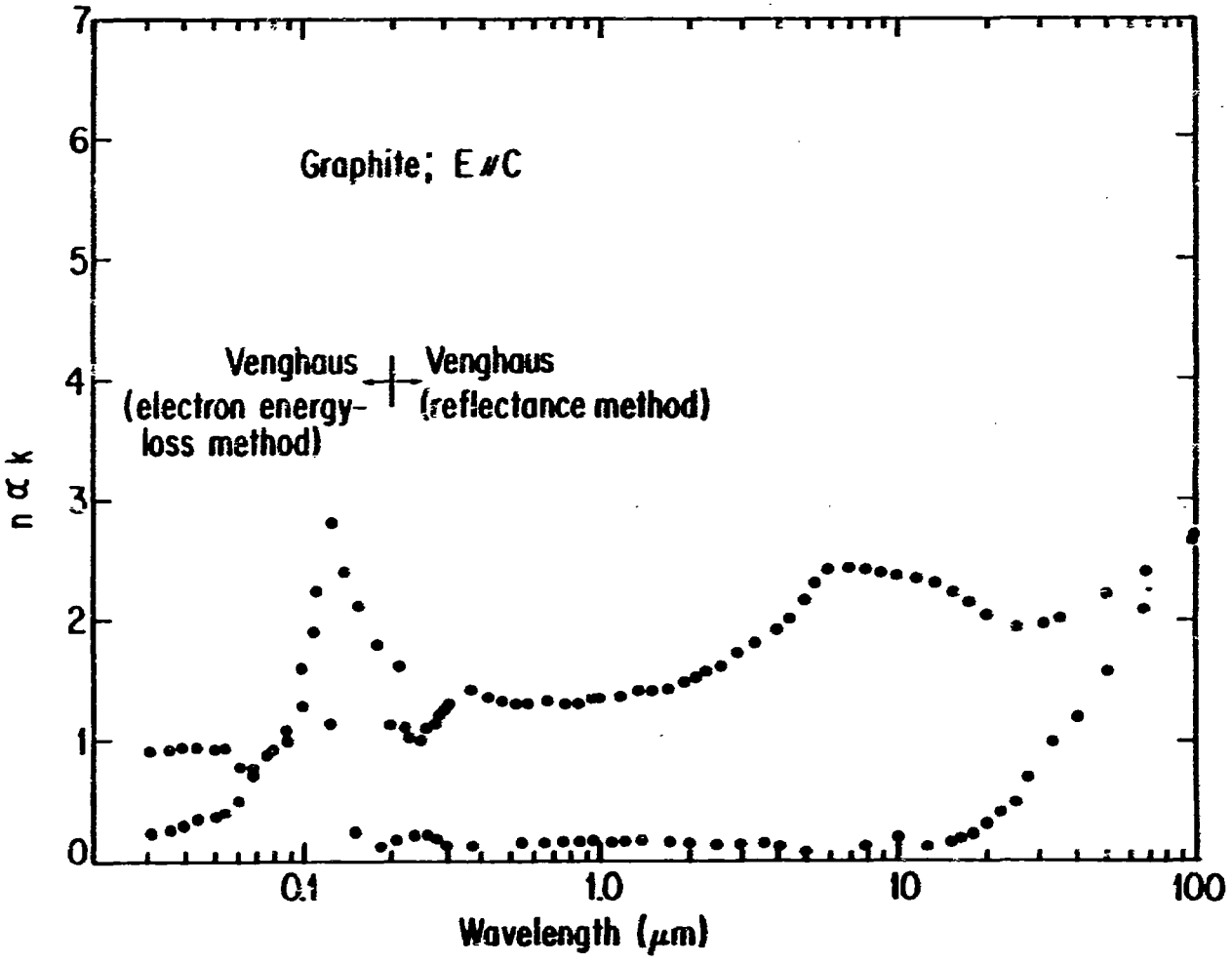

Fig. 27. Adjusted optical constants n and k of the E // C polarization of graphite

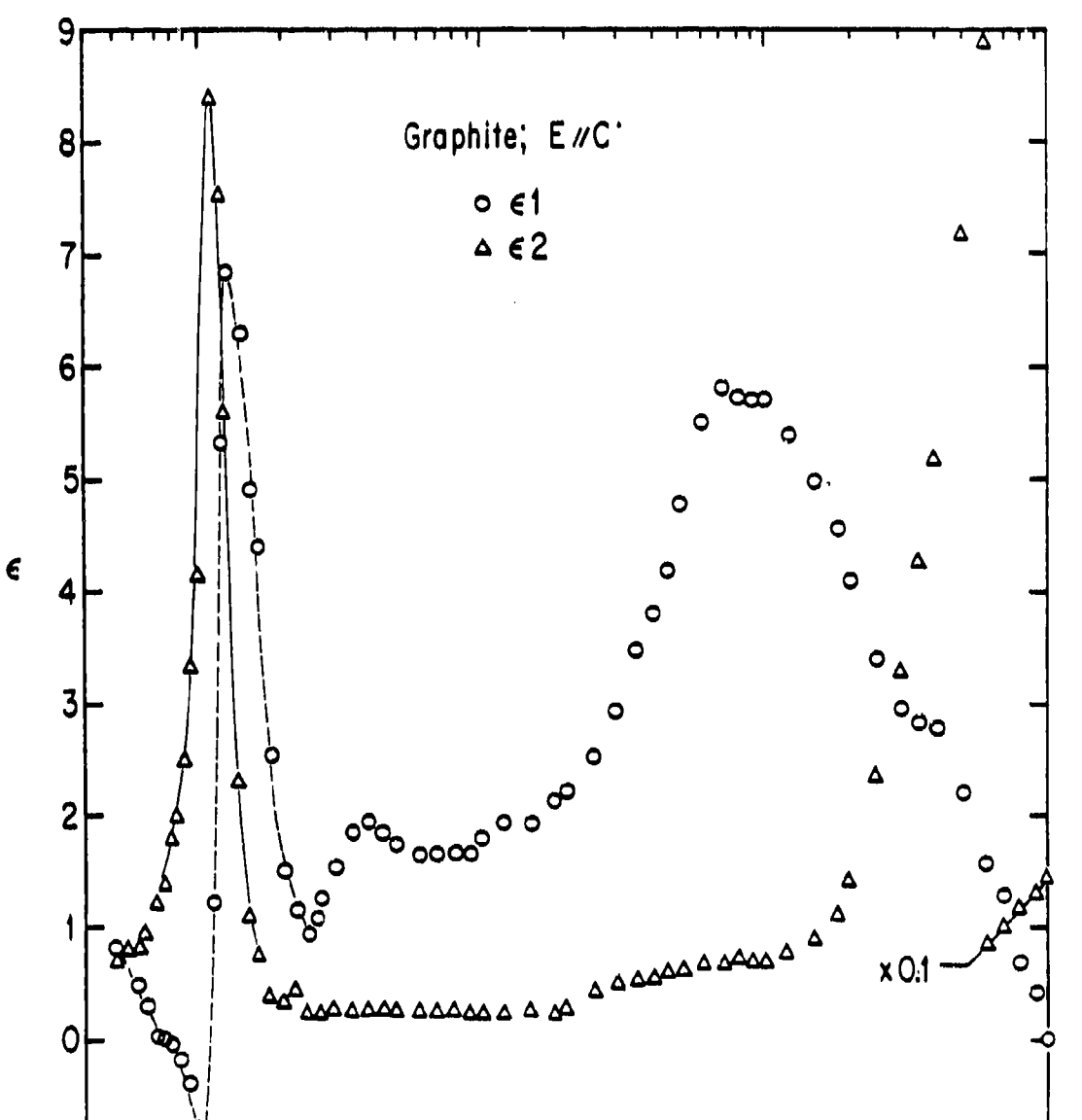

Fig. 28. Real and imaginary parts of the dielectric function of the E // C polarization of graphite

As computed with the use of the adjusted optical constants of Fig. 27

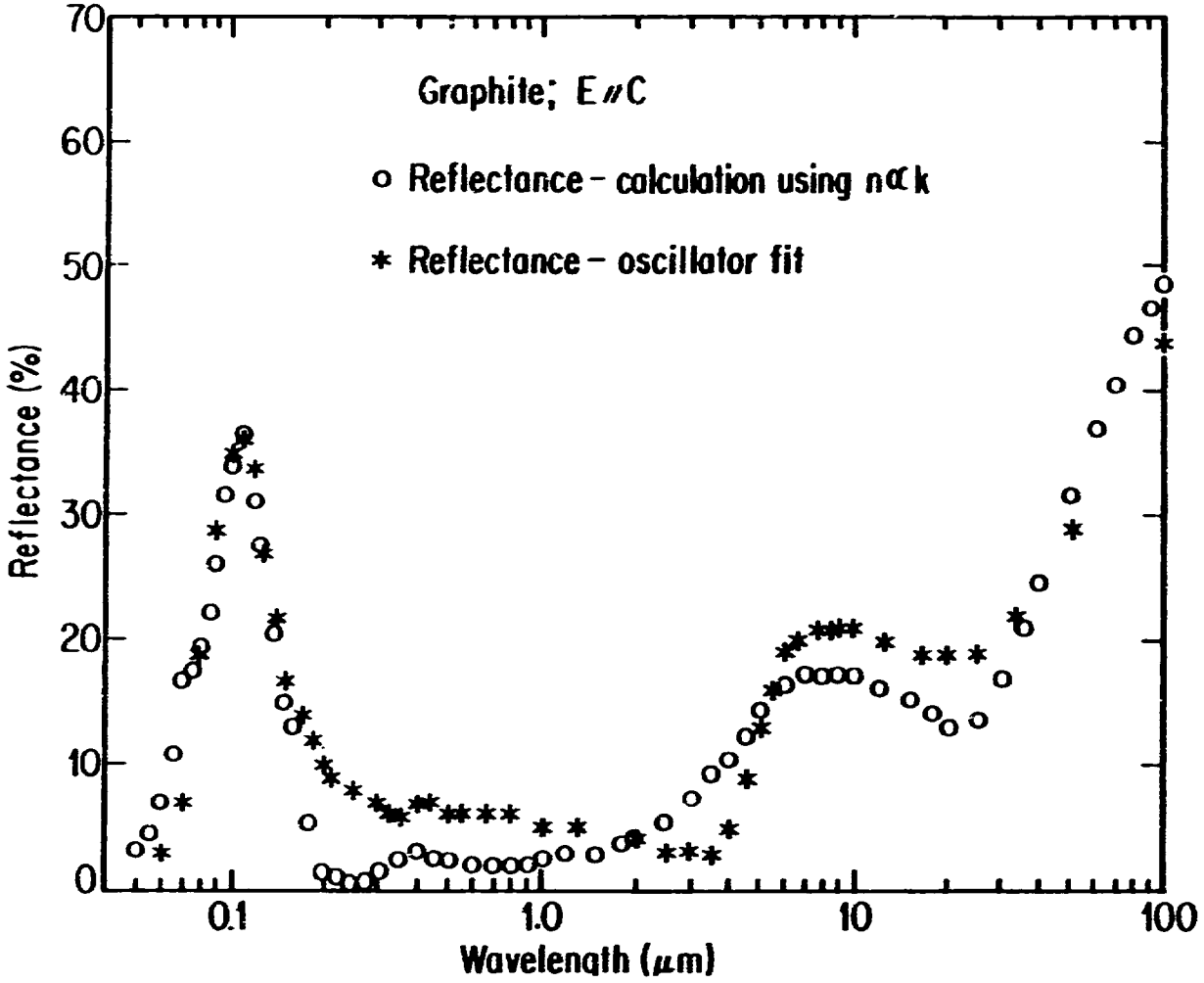

Fig. 29. Reflectance of the E // C polarization of graphite

Table 6. Oscillator parameters for the fit of the reflectance curve for the E // C direction of graphite

	Parameter	Value (cm^{-1})
Oscillator 1	ω_{P1}	8500
	ω_1	0.00
	γ_1	900
Oscillator 2	ω_{P2}	2950
	ω_2	1500
	γ_2	1500
Oscillator 3	ω_{P3}	5,000
	ω_3	25,000
	γ_3	3,000
Oscillator 4	ω_{P4}	95,000
	ω_4	75,000
	γ_4	25,000

of glassy carbon from 0 to 82 eV, but it is practically impossible to obtain any detailed information below about 0.2 eV. It was therefore necessary to complete the available information.

In this study, optical constants based on the analysis of reflectance measurements extending to 225 μm and a Drude fit to reflectance extending to 1000 μm have been derived. The instruments used in the experiment, along with the near normal reflectance measurements will be presented; then the data analysis will be discussed.

Instrumentation and Measurements

Spectrophotometers to which suitable reflectometers (Steyer, 1974) have been attached were used for the measurements. A Cary 14 was used in the visible and in the near IR, a Perkin Elmer 398 in the IR, and a Beckman IR 11 for the far IR (see Table 7).

The Cary 14 and the Perkin Elmer 398 were used in a double beam mode, and the Beckman 11 in a single beam mode. The Beckman 11 was modified to use a liquid He cooled, doped germanium bolometer as a detector. The signal obtained was amplified by a PAR model 28 lock-in amplifier and then sent to a digital voltmeter or chart recorder (Rathmann, 1981).

The reflectometers were designed to give a near normal incidence reflectance. The one used on the Cary 14

Table 7. Spectral region and instrument

From Rathmann (1981)

Region	Wavelength (Frequency)	Instrument	Spectral Resolution
Far IR	250 μm - 20 μm (40 - 500 cm^{-1})	Beckman IR 11	∿ 5 cm
Mid IR	25 μm - 2.5 μm (400 - 4000 cm^{-1})	Perkin Elmer 398	∿ 5 cm
Near IR to Visible	2 μm - 0.33 μm (5000 - 3.3 x 10^4 cm^{-1})	Cary 14	∿ 10 Å

and the Perkin Elmer 398 is built by Barnes Engineering Company; the far IR one was designed and built in our lab.

An aluminized glass reference was used. Good alignment was always checked before any measurement; the aluminum standard or the sample was positioned and the mirrors of the reflectometer rotated until a maximum signal was obtained.

The measurement procedure was as follows:

1. Run the 100% reflectance line, say R_{100}, with the aluminum standard in place.
2. Run the zero reflectance line, say R_0, without any sample.
3. Run the reflectance of a well-polished sample, say R_S.

From the spectrum obtained, it is easy to find:

$$R'(\lambda) = \frac{R_S - R_0}{R_{100} - R_0} \quad ,$$

where $R'(\lambda)$ is a relative reflectance; this data can be used in the Kramers-Kronig analysis computer program where it is converted into an absolute reflectance.

Reflectance from $\lambda \sim 0.35$ μm up to 220 μm has been measured and good agreement obtained with Arakawa's published results in the 0.[illegible] μm to 2.5 μm wavelength range which the experiments have in common. It was thus not

necessary to pursue measurements toward wavelengths shorter than 0.35 μm.

Data Analysis and Results

For use in the Kramers-Kronig analysis, reflectance was extended toward long wavelengths by curve fitting. Free electron behavior was assumed for glassy carbon at larger wavelengths than the last experimental point, and the Drude model used in the fitting. The parameters used were: $\omega_p = 2000\ cm^{-1}$; $\omega_j(1) = 0$, and $\gamma = 900\ cm^{-1}$. Reflectance data going from $\lambda \sim 0.02$ μm to about 10^6 μm were constructed by combining Williams and Arakawa's (1972) results, experimental results of this study, and extrapolated results, for use in the Kramers-Kronig analysis (see Fig. 21.). The results of the analysis are presented in Figs. 30. to 32. and in Appendix B.

We then proceed to use the Drude-Lorentz model and fit the reflectance data obtained for the Kramers-Kronig study; the result is shown in Fig. 33 , and the parameters used are presented in Table 8.

12.4 Discussion of Results.

The reflectance data for graphite in the E ⊥ C orientation and that of glassy carbon have been analyzed by the Kramers-Kronig method and by fitting a Drude-Lorentz model to the reflectance curves. The reflectance data for graphite in the E // C orientation has only been fitted

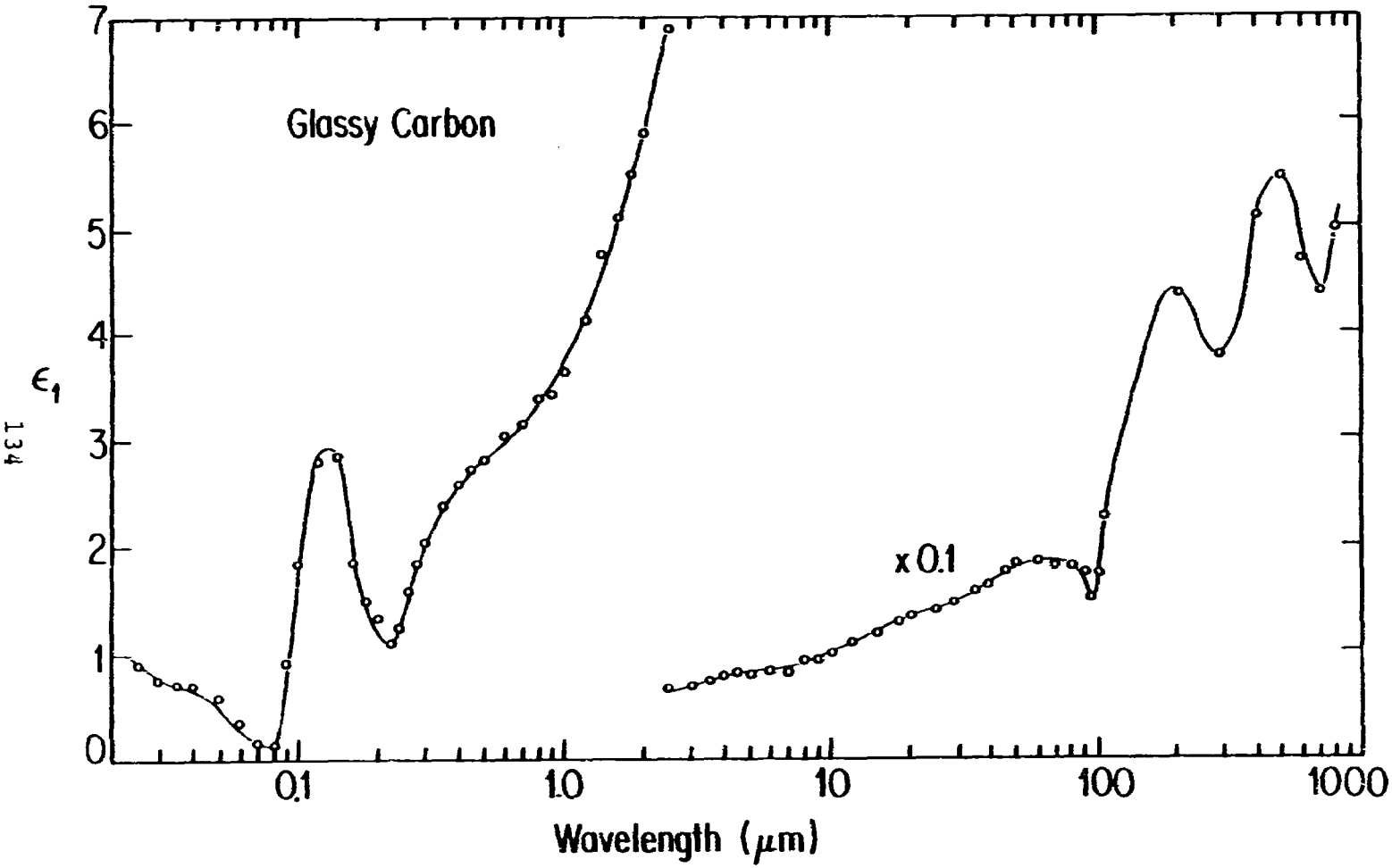

Fig. 30. Real part of the dielectric function of glassy carbon, as computed by the Kramers-Kronig method

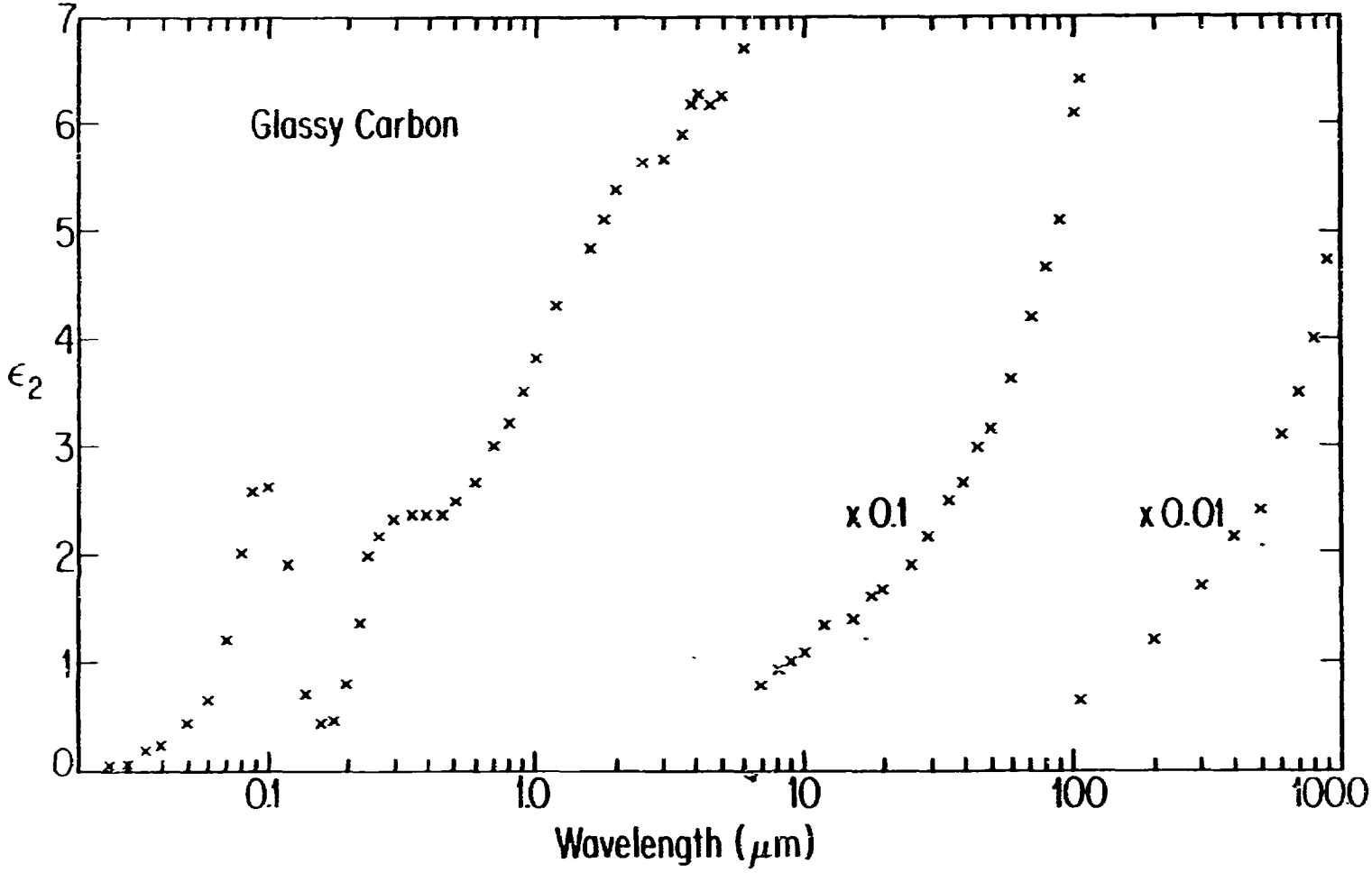

Fig. 31. Imaginary part of the dielectric function of glassy carbon, as computed by the Kramers-Kronig method

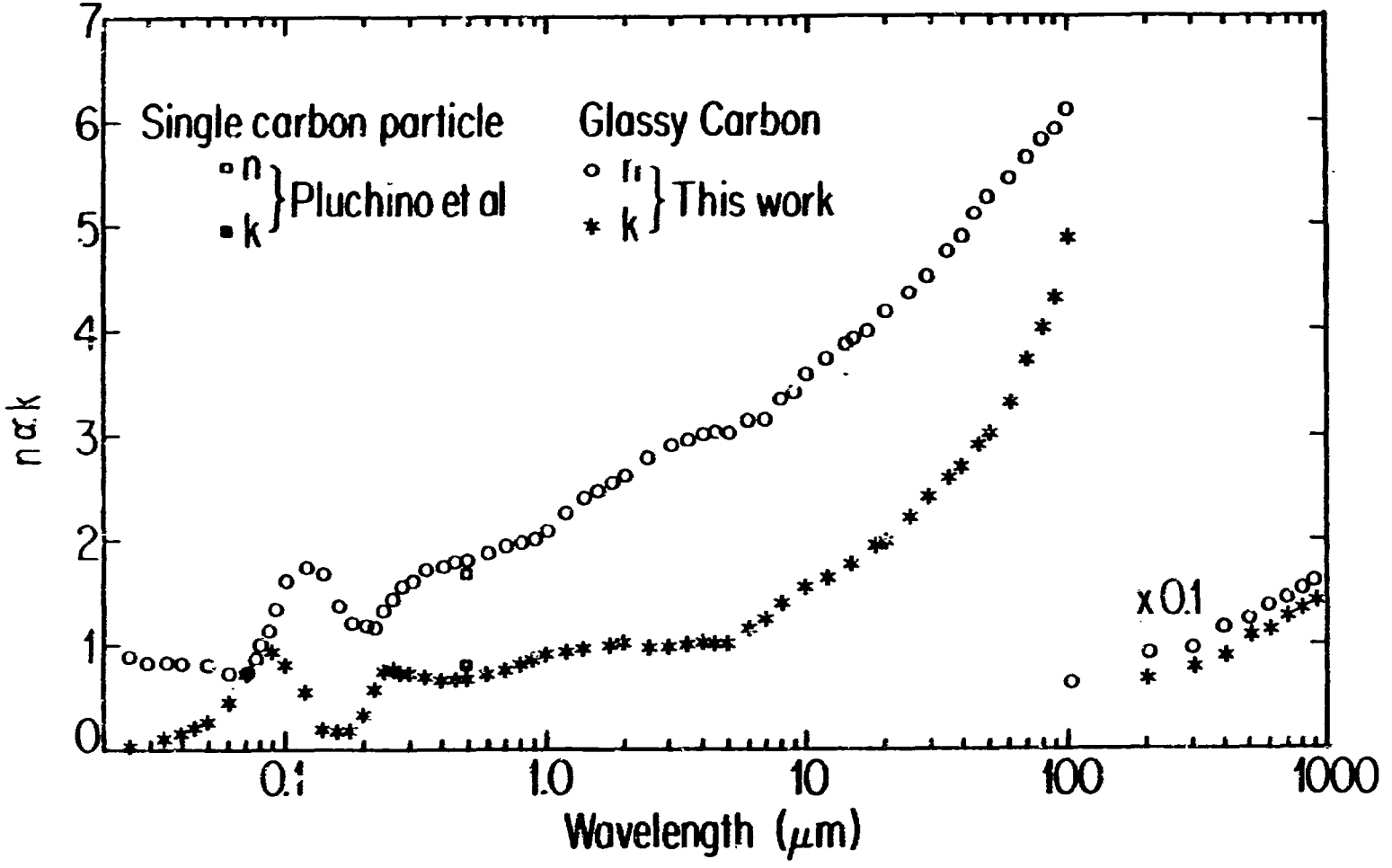

Fig. 32. Optical constants n and k of glassy carbon as computed by the Kramers-Kronig method and comparison to Pluchino et al. (1980) results

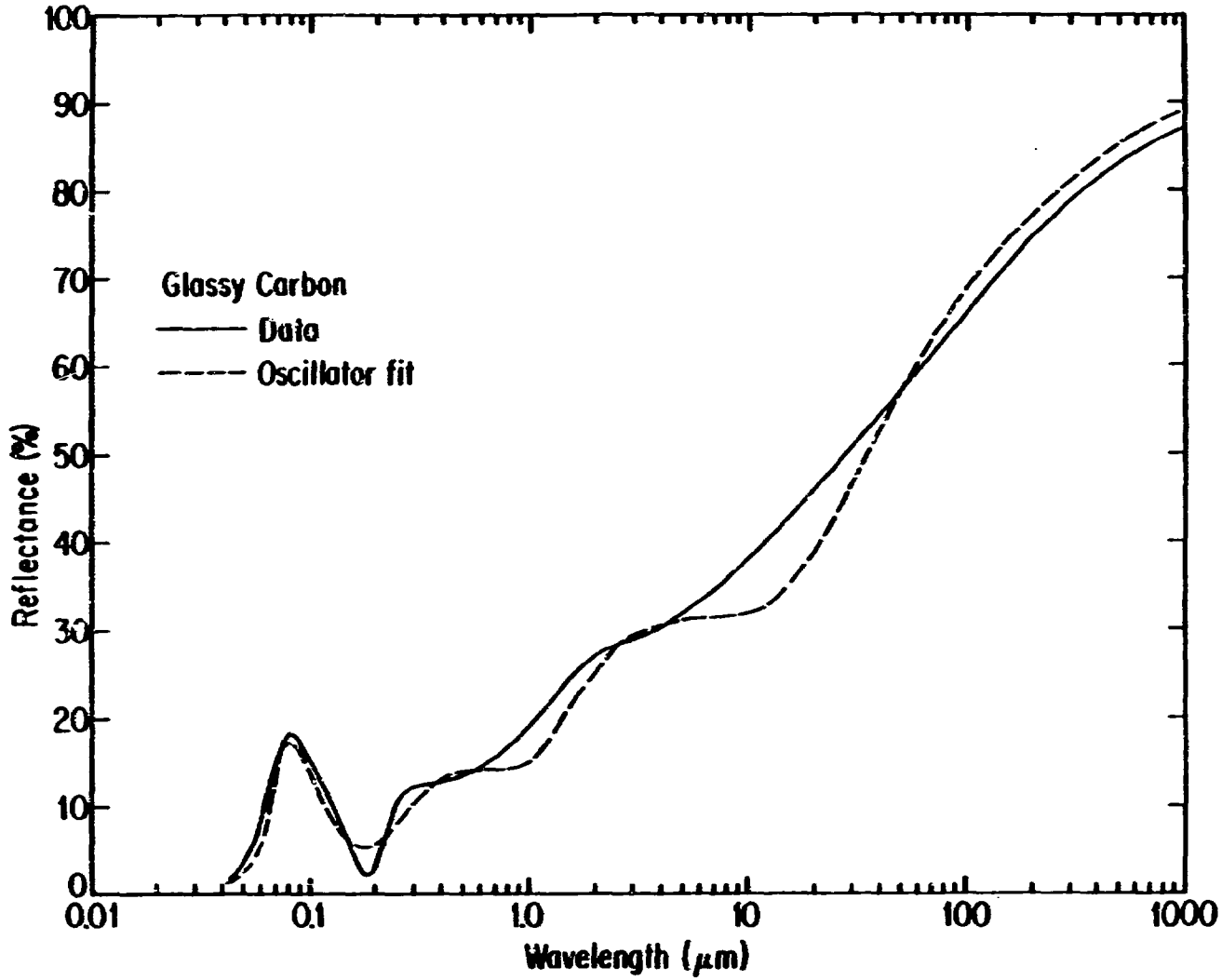

Fig. 33. Oscillator fit of the reflectance of glassy carbon

Table 8. Oscillator parameters for the fit of the reflectance curve of glassy carbon

	Parameter	Value (cm^{-1})
Oscillator 1	ω_{P1}	4000
	ω_1	0.00
	γ_1	1000
Oscillator 2	ω_{P2}	14.5×10^3
	ω_2	5×10^3
	γ_2	9×10^3
Oscillator 3	ω_{P3}	50×10^3
	ω_3	30×10^3
	γ_3	43×10^3
Oscillator 4	ω_{P4}	120×10^3
	ω_4	110×10^3
	γ_4	60×10^3

because the spectral range of the data was not large enough to allow the use of the Kramers-Kronig method.

In all the fits, the oscillator strength parameters (ω_{pj}^2) have been checked against the sum rule (see Kittel, 1976, p. 351 and Wooten, 1972, p. 72):

$$\int_0^\infty \omega\epsilon_2(\omega)\, d\omega = \sum_j \omega_{pj}^2 = \tfrac{1}{2}\pi\omega_p^2 \quad . \tag{41}$$

The plasma frequency ω_p is given by (see Kittel, 1976, p. 289):

$$\omega_p = \frac{4\pi ne^2}{m} \quad , \tag{42}$$

where n is the density of electrons, e and m the charge and the mass of an electron in c.g.s. units. With the assumption that all the four valence electrons of carbon determine ω_p, one obtains:

$$\tfrac{1}{2}\pi\ \omega_p^2 \approx 20.3 \times 10^{32}\ \text{sec}^{-2} \quad .$$

The value of $\sum_j \omega_{pj}^2$ for each case is given in Table 9.
In each of the three cases

$$\sum_j \omega_{pj}^2 < \tfrac{1}{2}\pi\ \omega_p^2 \quad .$$

Table 9. Values of $\sum_j \omega_{Pj}^2$

Material	$\sum_j \omega_{Pj}^2$ (sec^{-2})
Graphite: E ⊥ C	$\sim 4.4 \times 10^{32}$
Graphite: E // C	$\sim 3.3 \times 10^{32}$
Glassy carbon	$\sim 6.2 \times 10^{32}$

This result is expected, since the maximum possible value for n has been chosen for substitution in Eq. (42). Some valence electrons might be sufficiently bound that the sum rule (Eq. 41) is not satisfied over the frequency range of the experiment.

The discrepancy between the experimental and fitted curves observed between λ = 0.3 and 15 μm on Fig. 25. is due to interband transitions which come into play with increasing energy. These transitions gradually increase the reflectance without showing sharp peaks. The Lorentz model used for the fit cannot account well for this phenomenon. The fit of the peak at $\lambda \sim 45$ μm resulted in the sharp drop in the calculated reflectance.

The band structure of graphite as calculated by Mallett (1981) shows narrow band gaps at $\lambda \simeq 0.08$ and 0.25 μm, which account for direct interband transitions, responsible for the sharp peaks observed at those wavelengths. These peaks were easily fitted.

Examination of Figs. 29 and 33 shows that to some extent, the reflectance of the E // C polarization for graphite and that of glassy carbon have the same behavior as the reflectance of the E ⊥ C orientation for graphite. This behavior makes the fit difficult between λ = 0.3 and 15 μm, but the difference between the experimental reflectance and the fit is unimportant because of the low reflectance of the materials considered.

Results obtained by the two methods of analysis for glassy carbon are compared in Table 10 for several wavelengths.

Comparing this Kramers-Kronig analysis with published data, one finds that for the E $\perp$ C orientation of graphite, the optical constants derived agree well with those of Taft and Philipp (1965) (see Table) and Greenaway et al. (1969). At the peak around $\lambda \sim 0.088$ μm, our value of 9.3 for ε_2 is higher than that of Taft and Philipp's (1965) value of ~ 7.0. The difference is due to the values of the parameters used in the short wavelength extrapolations for the Kramers-Kronig analysis (see p. 34).

The optical constants obtained for the E // C orientation of graphite are to our knowledge the only consistent ones available at this writing.

The glassy carbon optical constants agree well with Williams and Arakawa's (1972) results and extend them beyond $\lambda \sim 10$ μm. Differences exist between our results and those published for varouis amporphous carbons as one can readily see in Fig. 18. One exception is the result of Pluchino et al. (1980) (see Fig. 32). The good agreement in this case is worth pointing out, even though the comparison is possible for one wavelength only. Our reflectance measurements were performed on a homogeneous bulk of glassy carbon sample. Pluchino et al. measured the scattered radiation by a single particle, small enough to be homogeneous. It is

Table 10. Results for index n and k obtained by the Kramers-Kronig method and by oscillator fit, in the case of glassy carbon

The indices "OF" and "KK" stand for "Oscillator Fit" and "Kramers-Kronig," respectively.

	Wavelength (μm)						
	0.08	0.15	0.25	1.00	5.00	10.00	100.00
n_{OF}	1.03	1.46	1.40	1.95	2.97	2.88	5.91
n_{KK}	1.04	1.54	1.40	2.15	3.04	3.56	6.09
k_{OF}	0.91	0.38	0.56	0.70	1.15	1.91	5.26
k_{KK}	0.95	0.19	0.74	0.90	1.03	1.54	4.85

Table 11. n and k from this work and those of Taft and Phillip (1965) and Philipp (1977) at the same wavelengths

	Wavelength (μm)							
	.1	.4	.5	.62	1.77	2	5	50
This work								
n	2.5	2.62	2.61	2.7	3.68	3.8	5.2	16
k	0.8	1.28	1.33	1.4	2.4	2.5	3.8	22
Taft and Philipp (1965) and Philipp (1977)								
n	2.4	2.52	2.54	2.6	3.78	3.9	5.1	15.8
k	0.75	1.35	1.36	1.46	2.49	2.6	4.0	22.8

strongly believed that the agreement of our results is due to the homogeneity of the materials on which the experiments were performed. To find optical constants of particles, many workers analyze reflectance data of particles pressed into pellets. Results obtained by this technique are rarely in good agreement for different samples. Chylek et al. (1981) argued that the differences are essentially due to the differing mass concentration of the particles. One reason we have chosen graphite and glassy carbon is because these materials are relatively homogeneous.

13. SMALL PARTICLE EXTINCTION

This chapter deals with the extinction of small carbon particles. The production of the particles and their characterization are presented, and the sample preparation for the extinction measurements shown. Then the measurements leading to the mass calibration and to the extinction are described. Finally, results are presented and discussed.

13.1 Particle Production and Characterization.

Graphite and three other types of carbon have been investigated. These powders are:

1. very fine graphite (Ashbury #250, Dixon),
2. standard lampblack,
3. particles (for solar energy absorption) produced by Hunt (1979) by acetylene pyrolysis at the Lawrence Berkeley Laboratory; those particles are referred to in this work as "LBL Smoke",
4. particles were made by evaporating carbon in an inert gas atmosphere.

The chamber in which these particles were made was evacuated to 2×10^{-4} torr with an oil diffusion pump. The

system was then purged with helium to reduce the partial pressure of oxygen, and reevacuated. Finally the chamber, isolated from the pumping system, was filled with helium, and an arc was struck between carbon electrodes (glassy carbon). The particles were collected on appropriate substrates.

The particles were observed with a "Scanning Electron Microsccpe" (SEM) and/or a "Transmission Electron Microscope" (TEM). For this purpose a small amount of "LBL Smoke," lampblack, or graphite powder was added to methane and the mixture dispersed ultrasonically. The cloudy liquid was then put in a syringe adapted to a Nucleopore membrane filter holder and filtered. The filter retained the individual particles with diameter larger than its pores and also chain-like aggregates of particles. Samples prepared with this technique were observed with the SEM. Results shown in Figs. 34· and 35· confirmed what is commongly observed: spherical shape for most carbon and plate-like shape for graphite (Walker, 1963). The nucleopores used had 0.25 μm diameter pores. Many of the particles presumably had smaller diameter than 0.25 μm.

Smoke made by arc evaporation of bulk glassy carbon was collected directly on grids for observation with TEM. Results showed that in this case, too, the particles are rather spherical, although not as perfect as observed for other particles (see Fig. 36). The heat generated by

Graphite (Dixon, HPN-2)

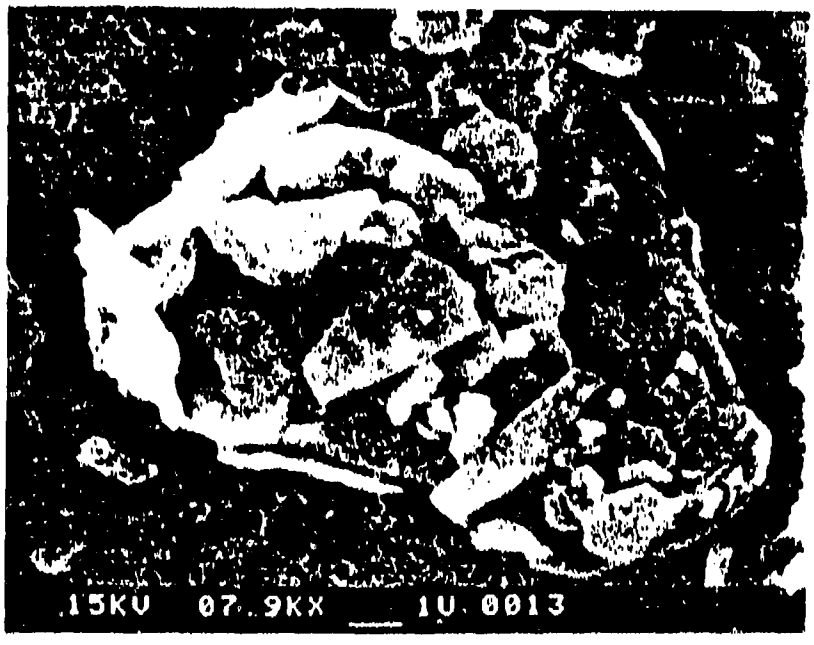

Graphite (Ashbury, Micro #250)

Scanning electron microscope view of two types of graphite particles

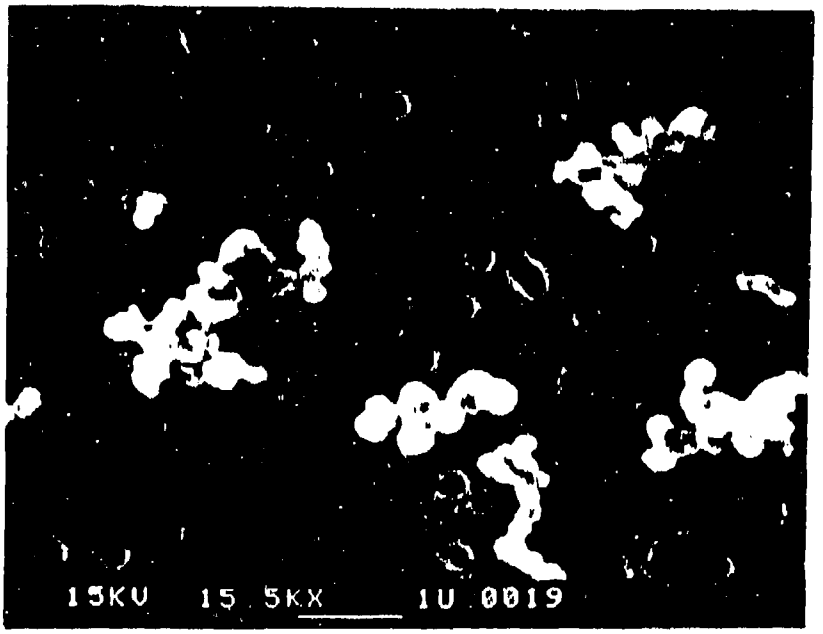

LBL Smoke particles

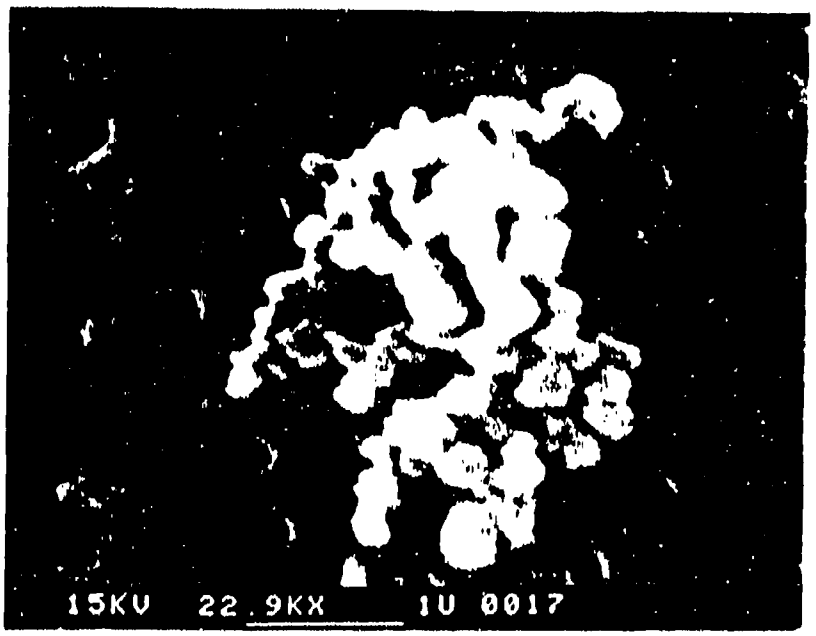

Lampblack particles

Scanning electron microscope view of "LBL smoke" particles and lampblack particles.

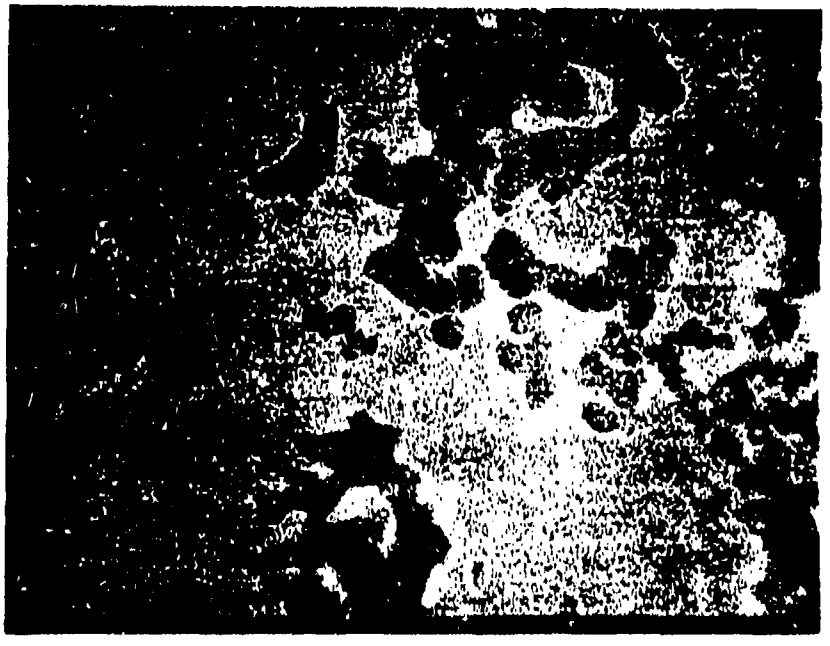

Glassy Carbon particles

Transmission electron microscope view of glassy carbon with magnification 250KX

electrons striking the samples during the observation process is probably responsible for the ragged edges (Walker, 1963).

X-ray powder patterns and electron diffraction patterns observed in the transmission electron microscope showed diffuse bands with little distinction between "LBL smoke," lampblack, and glassy carbon smoke. In contrast, the graphite showed distinct diffraction patterns. It was concluded that the first three are mainly amorphous while the graphite is highly crystalline.

13.2 Sample Preparation.

The transmission measurements from which the extinction was determined required suspension of the particle in one way or another. When they were collected on a usable substrate such as quartz or LiF, no further sample preparation was necessary; otherwise, special particle suspension techniques had to be used.

For extinction measurements from the visible to the mid IR, the KBr pellet technique was used. A small amount of the particulates (typically 50 to 200 μg) was mixed with 0.5 mg of IR quality of KBr in a vial that contained a small steel ball. The mixture was first hand shaken and then shaken for 5 to 10 minutes on a "Wig-L-Bug" dental amalgamator. The mixture was then transferred to an evacuable die connected to a vacuum-pumping system and placed on a

hydraulic press. After evacuating for about two minutes, pressure was applied and slowly increased up to about 2000 lbs per square inch. The vacuum was maintained for two more minutes, then released, as air was slowly admitted to the system. Finally, the pellet was carefully extracted.

For the far IR extinction measurements, polyethylene powder was used as the dispersion medium; 0.1 mg of polyethylene was used in each vial. In this case, shaking a vial caused the mixture to stick to its wall because of electrostatic forces. To circumvent this problem, acetone was added to the mixture. The vial was hand shaken, slightly warmed, and left open overnight to allow the acetone to evaporate. The mixture was then scraped off the container walls and transferred to the KBr die. The die was heated on a hot plate during its evacuation. A gentle hand pressure was exerted on the plunger of the die at the beginning of the heating. Still under evacuation, the die was removed from the hot plate and slowly cooled. The pellet was then carefully removed, with the help of a razor blade, and weighed. If m_1 is the mass of the polyethylene, m_2 the mass of the particles with which the sample preparation was started, and m_3 the mass of the pellet obtained, then:

$$m = \left(\frac{m_2}{m_1}\right) m_3$$

is approximately the mass of particles in the pellet.

13.3 Measurements.

The instruments used to acquire data have been described earlier (see Chapter 12). With the Cary 14, a zero-absorption trace was recorded with two identical sample holders in the two beams. The sample was then inserted in the front beam and a reference blank was placed in the back beam. The spectrophotometer recorded the optical density (OD) as a function of the wavelength. The measuring technique on the Perkin Elmer was the same as on the Cary 14, except that the zero and the 100% lines had to be recorded. The spectra obtained gave intensities which permitted the calculation of the transmission.

The Beckman 11 was used in a one-beam mode. The transmission through the sample and the reference blank was measured separately. The absorption of the particles was found from the ratio of the two transmissions. The calculations of volume-normalized extinction (α) requires knowledge of the mass density σ (mass/area) of the particles. For the pellets used in IR, the mass of particles suspended in a matrix was large enough for weighing with an analytical balance. In the UV, the absorption of carbon particles is so high that a very small quantity of particles must be used to get any transmission. In that case, it was practically impossible to weight the particles; an optical calibration method was used to find σ.

A sufficient quantity of carbon smoke was collected on glass slides and the optical densities (OD) measured in the visible. Each slide was weighed with and without the smoke. Knowing the mass m of the particles on a slide, and the area A of the substrate, $\sigma = m/A$ was computed. Optical density was plotted as a function of σ for several samples of varying thickness, as shown in Fig. 37. The curve shows a leveling off of OD with increasing σ, presumably due to the increasing effect of multiple scattering. In order to avoid the multiple scattering region, the slope of the linear curve at small σ is used to determine a calibration constant (OD/σ) at each wavelength. This calibration can then be used to determine mass densities from optical transmission measurements for samples that are too light for conventional weighing techniques. By calibrating the mass density in the near infrared and the visible, optical measurements on very light samples (i.e., 5 $\mu g/cm^2$) can be extended into the highly absorbing regions of the UV.

13.4 Results and Discussion.

In this section, results of extinction measurements on graphite and amorphous carbon are presented and discussed with respect both to calculations and to other workers' results. This is done first for $\lambda > 0.4$ μm and then for $\lambda \leq 0.4$ μm.

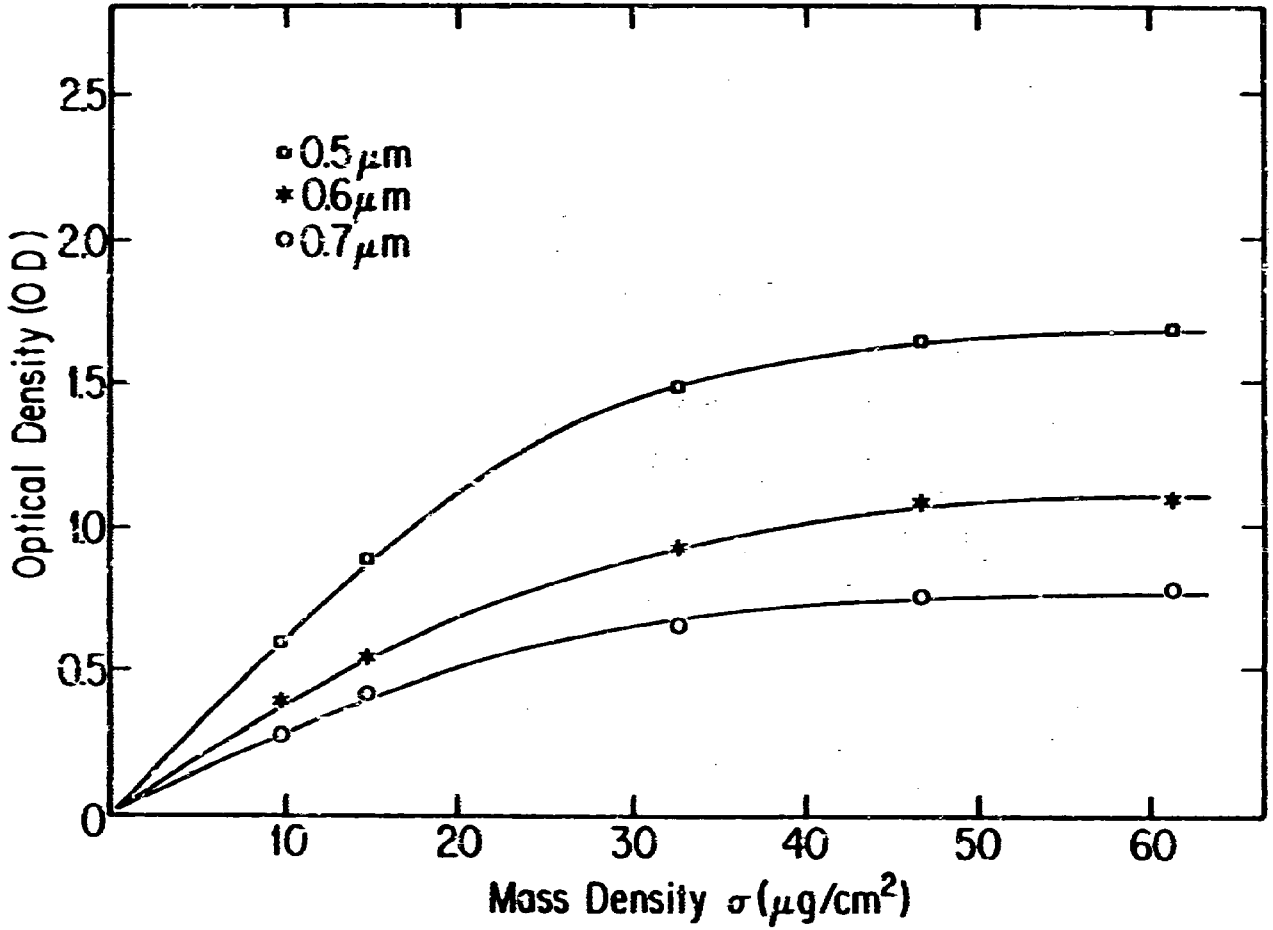

Fig. 37. Variation of the optical density (OD) of glassy carbon, as a function of the mass density σ at various wavelengths

In Fig. 38. are plotted the extinction results from graphite powders (Ashbury micro #250, Dixon HPN-2). On the same figure are plotted two sets of calculations, one based on a continuous distribution of spheres (CS) theory, and the other on a continuous distribution of ellipsoids (CDE).

Although some workers argued that bulk optical properties may not be appropriate for micron-sized particles (Pluchino et al., 1980), the calculations were done using optical constants derived in Chapter 12 with the assumption that the particles are large enough for bulk optical properties to be applicable. A discussion of this point can be found in the review by Huffman (1977, pp. 212-215).

A comparison of the two calculated results shows a substantial difference in strength of the extinction in the infrared region from about $\lambda \sim 1.0$ μm to 100 μm. This provides a quantitative illustration of how shape affects extinction of carbon particles in the infrared.

Visible and Infrared Range

Most of our studies on graphite were done on the Ashbury powder, which was available in large enough quantities to permit the preparation of many samples. Therefore, the discussion of graphite experimental results will be based on the Ashbury sample only.

Three sets of results were obtained (see Fig. 38). From $\lambda \sim 0.4$ μm to 25 μm, extinction of particles in KBr

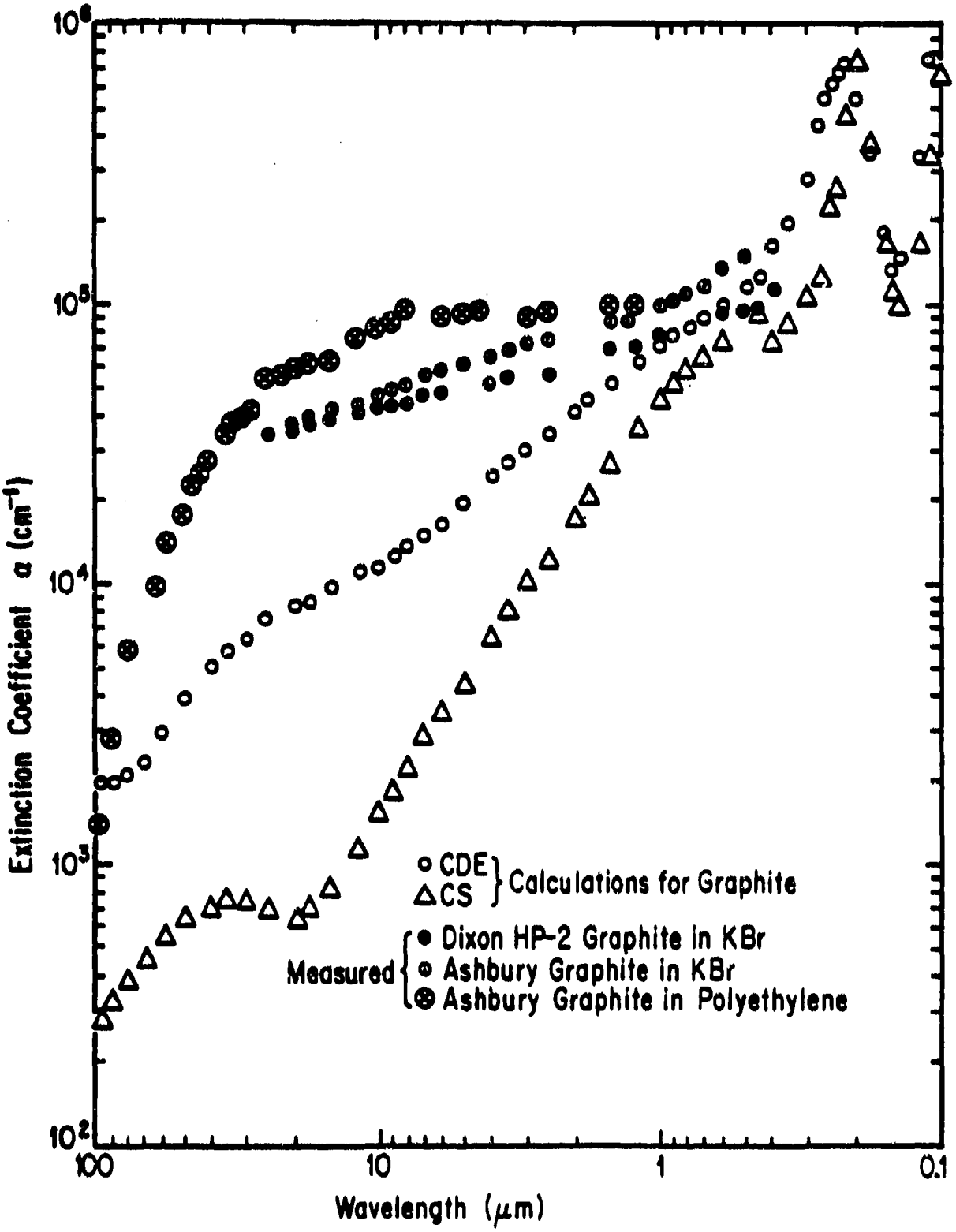

Fig. 38. Experimental extinction for graphite, compared to sphere theory (CS) and to CDE theory

and extinction of particles in polyethylene are shown; above $\lambda \sim 25$ μm, extinction of particles in polyethylene only is presented. The polyethylene sample used from 0.4 μm to 25 μm was obtained from a pellet made by the technique described in the section on sample preparation, then thinned by exerting a slight pressure on the pellet placed between two microscope slides and heated. Comparison of the two results in the $\lambda \sim 0.4$ μm to 25 μm range shows differences which are due to the suspension media used. On the one hand, the carbon particles mixed well with the KBr powder during the vial shaking process; on the other, the polyehtylene and the particles stick to the wall of the vial when shaken, as previously explained.

The observed disagreement of theory and experiment is most likely due to the inappropriateness of the ellipsoid theory. Figure 34. provides evidence that the graphite particles are in fact plate-like particles.

The particle shape is probably responsible for the violation of the sum rule shown in Eq. (40). Indeed, in a very restricted wavelength range (i.e., 5 μm to 50 μm),

$$\int \alpha \, d\lambda = 65 \quad ,$$

exceeding the maximum value which is 30.

Although this investigation was not planned as an illustration of the "shape effect," the comparison of experimental results to one another and to calculations has clearly shown the importance of the shape effect in extinctions.

Extinction of "LBL smoke" and lampblack was also investigated. Experimental results and calculations based on the same theories as for graphite are plotted in Fig. 39. Optical constants derived in Chapter 12 for glassy carbon have been used in the calculation. Extinction of fresh "LBL smoke" from $\lambda \sim 0.6$ μm to 15 μm is pratically the same as predicted by the sphere calculations. This is not surprising since Fig. 35. shows agglomerated spheres. These chains and clusters were probably dispersed in the shaking process.

Pellets made of "LBL smoke" were measured fresh and also two years later; they gave almost exactly the same results as new pellets made of two year old "LBL smoke." Because of the old pellet results, the increase in "LBL smoke" extinction has been assigned to a change in the optical constants of the particles, rather than to the shape effect. The nature of this change is not yet well understood; a graphitization hypothesis has been discounted because x-ray studies of the two-year-old particles did not show any sharp lines.

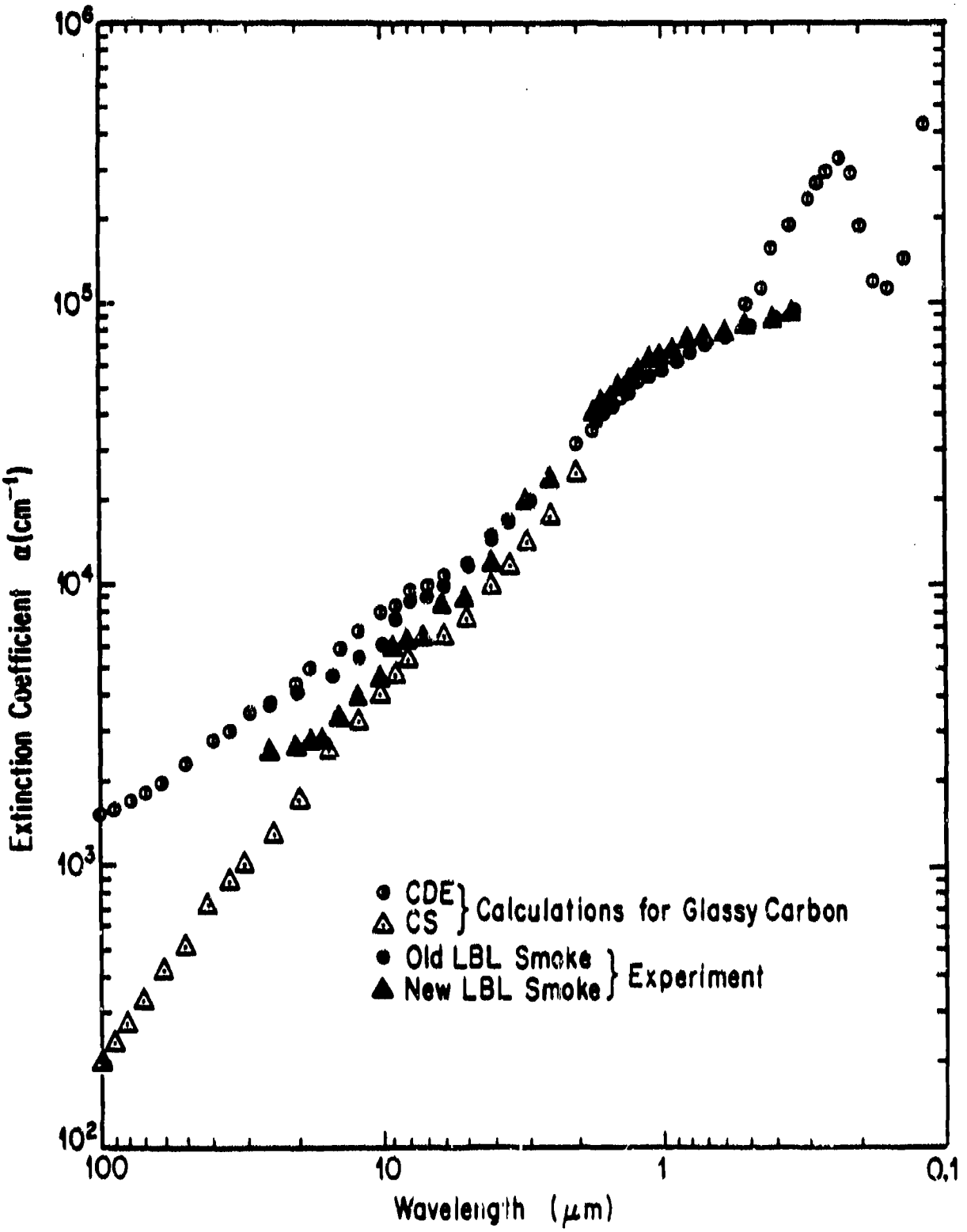

Fig. 39. Experimental extinction for "LBL smoke" with aging effect observed and comparison to sphere theory (CS) and to CDE theory

Figure 40. shows that the lampblack extinction is higher than the highest "LBL smoke" extinction. The lampblack powder used might have experienced the same aging process as the "LBL smoke" and the difference in extinction might be due to a difference in the ages of the particles.

Koike, Hosegawa, and Manabe (1980) measured the extinction of arc evaporated graphite particles and particles produced by burning benzene and xylene in air. The measurements were performed from $\lambda \sim 0.21$ μm to 340 μm on samples prepared with the same techniques as ours. They found humps between $\lambda \sim 5$ μm and 15 μm (Koike et al., 1980). Our data confirmed the presence of these humps (see Figs. 4.5 and 4.6). Koike et al. also found a peak near $\lambda \sim 90$ μm. Neither the data of Blea et al. (1970) nor ours shows this peak. A broad peak found in our calculated result is located around $\lambda \sim 35$ μm and is more apparent in the sphere calculations than in the CDE case (see Fig. 38).

Blea et al. (1970) measured absorption coefficients of black polyethylene over a broad spectral range ($\lambda \sim 2.5$ μm to 3,300 μm). Although their scattered results were assigned to differences in grain size, mass concentration of carbon in polyethylene, and to the form of the carbon, our extinction results from one type of carbon to another are due to differences in the shapes of the particles.

Table 12 shows experimental results of this study and those of other workers at some specific wavelengths.

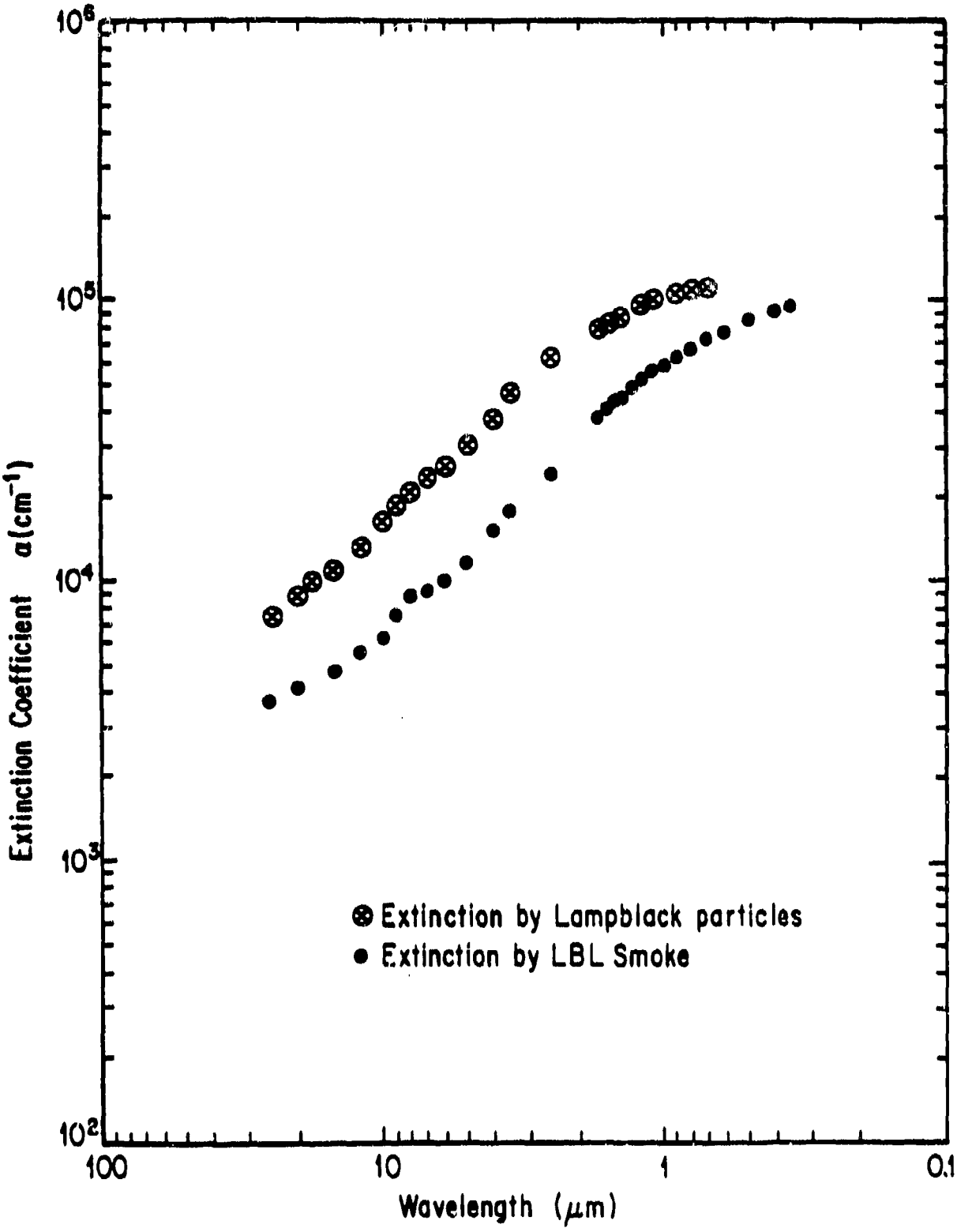

Fig. 40. Comparison of experimental extinctions by "LBL smoke" and by lampblack

Table 12. Measured extinction coefficients at some wavelengths

Authors	Samples	α (cm^{-1}) λ ∿ 0.5 μm	α (cm^{-1}) λ ∿ 5 μm	α (cm^{-1}) λ ∿ 10 μm	Comments
This work	Ashbury Graphite #250	145×10^3	51×10^3	47×10^3	Particles in KBr
	LBL Smoke	83×10^3	11.5×10^3	6.2×10^3	Particles in KBr
Koike et al. (1980)	Arc evaporated graphite (TU)	225×10^3	22.5×10^3	15×10^3	
	Lampblack from benzene (BE)	188×10^3	15×10^3	8.25×10^3	Combustion in air
	Lampblack from xylene (XY)	112.5×10^3	8.25×10^3	6.0×10^3	Combustion in air
Blea et al. (1970)	USIC			22.5×10^3	Black polyethylene
	DOW		∿ 24×10^3	15×10^3	

Ultraviolet Range

For short wavelengths the Rayleigh approximation, on which the sphere and CDE calculations are based, is hardly valid. A switch to Mie calculations is then necessary. Although the particles are not individual spheres or spherical at all (graphite), the calculations can give a rough basis for the evaluation of the experimental results.

Experimental results and calculations are shown in Figs. 41. and 42. for Ashbury graphite and glassy carbon, respectively. It might be surprising that the glassy carbon extinction peak is higher than the graphite one. It has been shown (Rathmann, 1981; Foxvog and Roessler, 1978) that the extinction out of the Rayleigh limit range is radius dependent, and that very fine particles have a higher peak. The graphite used was acquired as a finished powder with rather large particle sizes. The glassy carbon particles were arc-evaporated in helium atmosphere, a technique known for producing very fine particles (Rathmann, 1981). Also the particles were lightly deposited on the substrate to limit their agglomeration.

The graphite particles might obey some kind of sum rule by which the loss of strength in extinction observed between λ = 0.22 μm and 0.24 μm is compensated by the high extinction in the infrared region.

The strength of the experimentally found peak for glassy carbon is rather close to the peak calculated

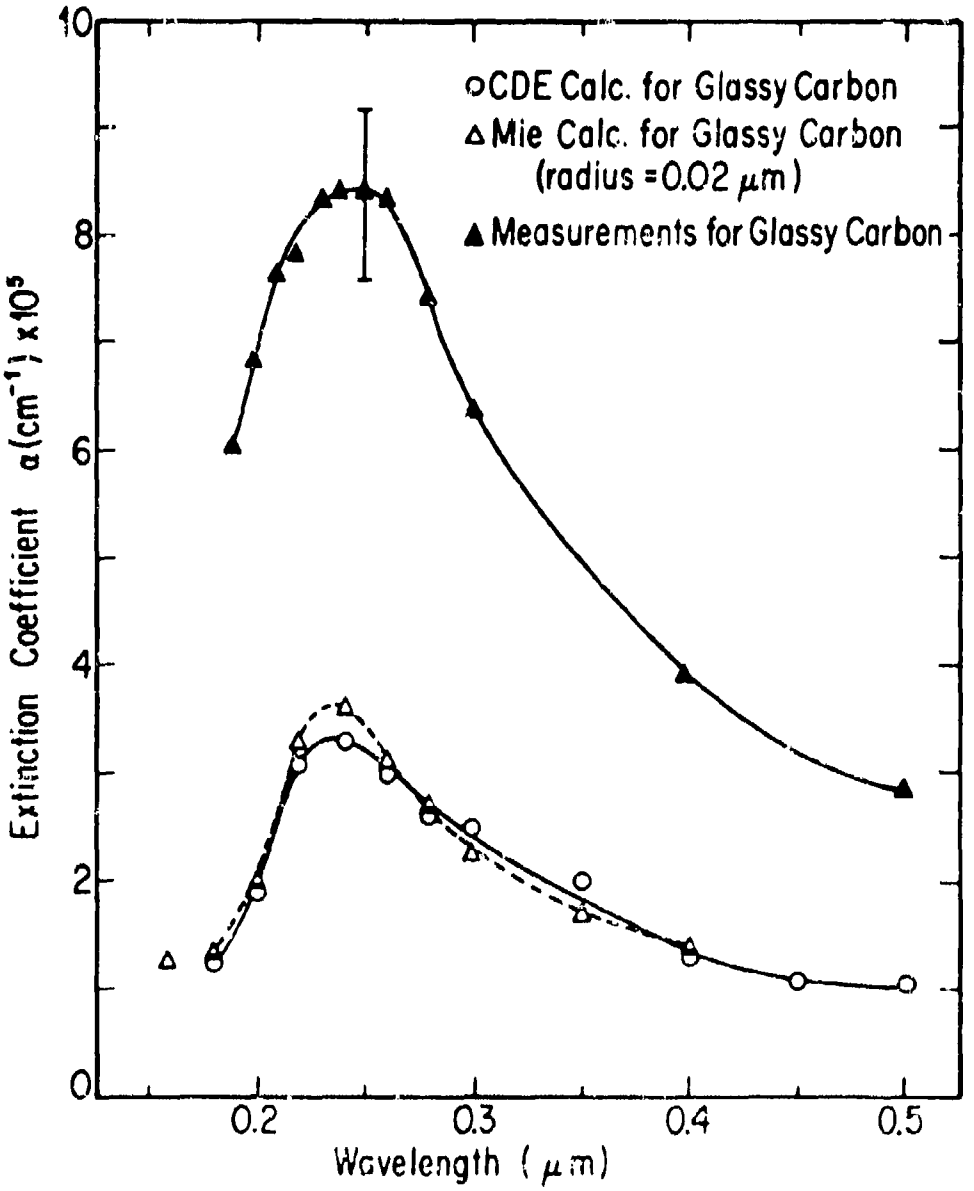

Fig. 41. Comparison of experimental extinction to calculated extinctions for glassy carbon around $\lambda \sim 0.22$ μm

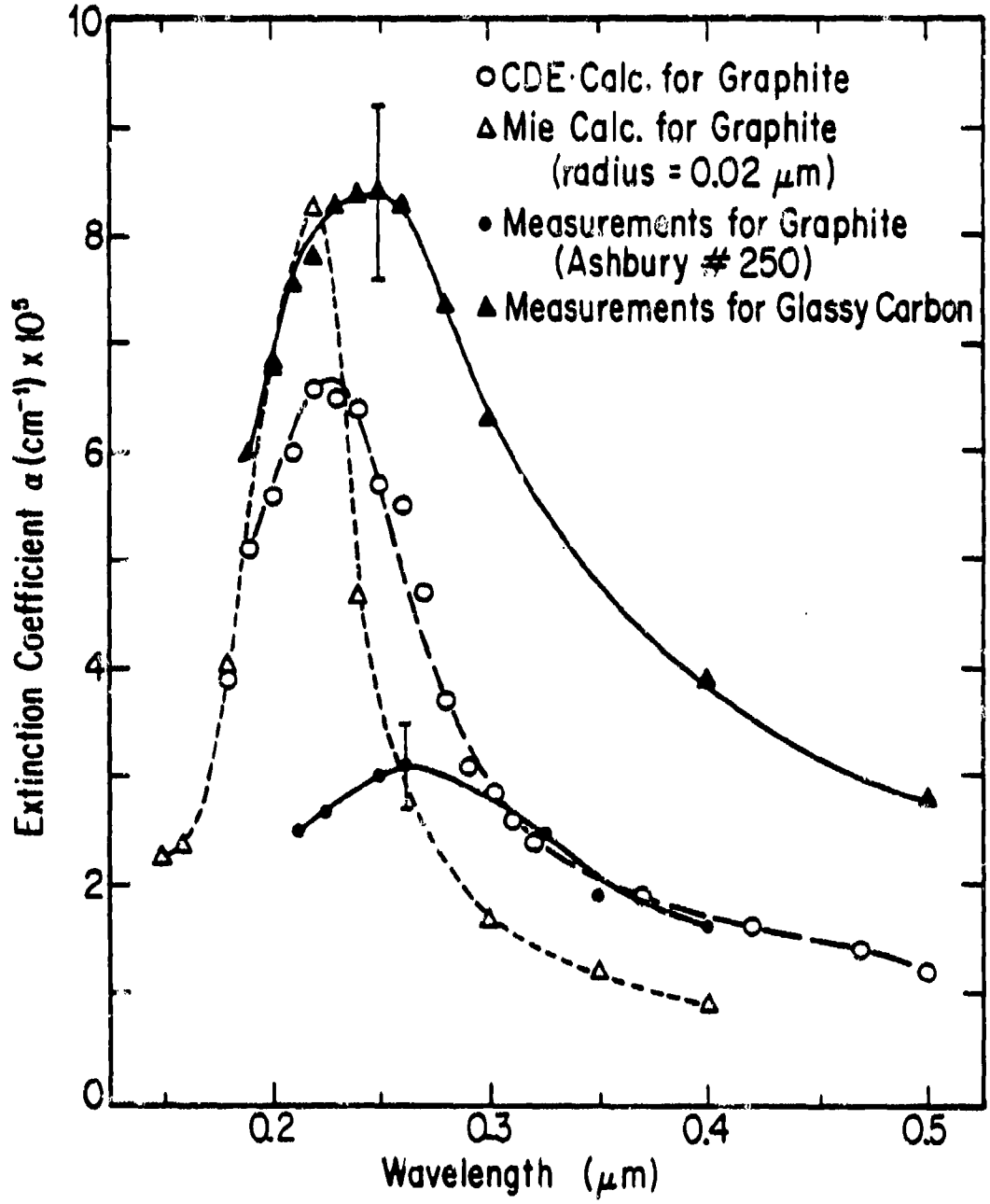

Fig. 42. Comparison of experimental extinctions for graphite and glassy carbon to calculated extinctions for graphite around $\lambda \sim 0.22$ μm

by the Mie method for graphite (see Fig. 42). Although it is known that glassy carbon cannot be significantly altered by heat treatment (Halpin and Jenkins, 1969), the strength of the peak is a good basis for arguing that the particles have graphitized in their production process.

14. SUMMARY AND CONCLUSIONS

Reflectance data for graphite for E ⊥ C orientation and for glassy carbon were compiled from the literature and augmented by our own measurements and/or extrapolations. They were analyzed by the use of the Kramers-Kronig method to yield consistent optical constants over a wide spectral range. For glassy carbon, our results are, at this writing, the only ones available beyond $\lambda \sim 10$ μm.

It was also shown that the homogeneity of the material on which measurements (reflectance, extinction, etc.) are performed is an important factor in obtaining dependable results.

Optical constants obtained for graphite for the E // C orientation by optical and by electron energy-loss methods over a broad (0.05 to 100 μm) spectral range have been combined to give more realistic results than could be provided by each method separately.

Fitting the reflectance data of graphite and glassy carbon to a Drude-Lorentz model was complicated by the existence of interband transitions which increase the reflectance without showing sharp peaks. But except for

the case of E ⊥ C polarization of graphite, the difference between experiment and fit was unimportant because of low reflectances; good results were thus obtained with this method over the spectral range covered.

Differences exist between experimental and calculated extinctions by small carbon particles. High experimentally observed extinctions are either due to a shape effect as observed with graphite, or to an aging process as noticed with the other types of carbon particles. The preparation of small particles by arc evaporation of bulk glassy carbon tends to graphitize the particles, thus enhancing the extinction. This effect was observed around $\lambda \sim 0.22$ μm for particles which were nominally glassy carbon (see Fig. 42).

The poor agreement between experiment and calculations leads to the conclusion that current models are not adequate for predicting extinctions by small carbon particles over a large spectral range. However, the empirical results provided by this work should be useful in designing projects like the solar energy collector conceived by Hunt (1979).

More experimental work should be done in order to reconcile the optical constants for graphite for E // C orientation, as measured by optical and by electron energy-loss techniques. The aging process and the graphitization

of the particles observed in this work need to be studied further and quantified.

Progress in reconciling experimental and theoretical extinctions by small carbon particles will probably depend on how well changes in the particles are understood and incorporated in calculations; it will also depend on the existence of theories which can properly deal with the shape of the particles.

BLANK

APPENDIX B

TABULATION OF THE OPTICAL CONSTANTS OF GRAPHITE AND GLASSY CARBON

Table B-1. Optical constants of graphite for the E ⊥ C polarization

λ (μm)	N	K	λ (μm)	N	K
0.050	0.381	0.313	1.200	3.180	2.000
0.055	0.390	0.543	1.500	3.430	2.180
0.060	0.400	0.850	1.800	3.700	2.430
0.065	0.500	1.150	2.000	3.830	2.520
0.070	0.650	1.330	2.500	4.300	2.750
0.075	0.850	1.700	3.000	4.300	2.950
0.080	1.000	2.000	3.500	4.480	3.330
0.085	1.900	2.450	4.000	4.730	3.550
0.090	2.600	1.650	4.500	5.030	3.730
0.095	2.630	1.350	5.000	5.230	3.830
0.100	2.400	0.900	6.000	5.400	4.030
0.110	2.150	0.500	7.000	5.400	4.450
0.120	1.900	0.130	8.000	5.700	4.950
0.125	1.700	0.100	9.000	5.980	5.250
0.140	1.470	0.130	10.000	6.100	5.550
0.150	1.100	0.160	12.000	6.140	6.850
0.160	0.960	0.280	15.000	6.250	8.000
0.180	0.830	0.650	18.000	6.550	9.000
0.200	0.800	1.200	20.000	6.750	11.000
0.220	0.850	2.000	25.000	7.500	13.000
0.240	1.200	2.400	30.000	8.500	15.500
0.250	1.600	2.450	35.000	10.000	18.500
0.260	2.100	2.650	40.000	11.500	20.500
0.270	2.550	2.450	50.000	16.500	23.500
0.300	2.700	1.700	60.000	20.700	22.000
0.350	2.620	1.360	70.000	22.500	19.300
0.400	2.610	1.240	80.000	21.500	18.900
0.450	2.600	1.250	90.000	20.000	18.800
0.500	2.600	1.370	100.000	18.300	21.300
0.600	2.700	1.360			
0.700	2.750	1.480			
0.800	2.850	1.630			
0.900	2.920	1.740			
1.000	3.000	1.800			

Table B-2. Optical constants of graphite for the E // C polarization

λ (μm)	N	K	λ (μm)	N	K
0.050	0.980	0.360	1.200	1.400	0.100
0.055	0.950	0.420	1.500	1.400	0.100
0.060	0.850	0.480	1.800	1.470	0.100
0.065	0.800	0.600	2.000	1.500	0.100
0.070	0.790	0.780	2.500	1.600	0.150
0.075	0.833	0.833	3.000	1.730	0.150
0.080	0.940	0.950	3.500	1.860	0.150
0.085	0.960	1.05	4.000	1.960	0.150
0.090	1. 30	1.200	4.500	2.060	0.150
0.095	1.150	1.450	5.000	2.200	0.150
0.100	1.300	1.600	6.000	2.350	0.150
0.110	2.200	1.900	7.000	2.410	0.150
0.120	2.700	1.400	8.000	2.400	0.150
0.125	2.800	1.000	9.000	2.398	0.150
0.140	2.550	0.450	10.000	2.396	0.150
0.150	2.230	0.250	12.000	2.330	0.170
0.160	2.100	0.190	15.000	2.250	0.200
0.180	1.600	0.130	18.000	2.150	0.270
0.200	1.220	0.150	20.000	2.050	0.350
0.220	1.100	0.200	25.000	1.930	0.580
0.240	0.990	0.120	30.000	1.920	0.850
0.250	1.000	0.240	35.000	2.000	1.070
0.260	1.050	0.230	40.000	2.080	1.240
0.270	1.120	0.100	50.000	2.200	1.630
0.300	1.250	0.110	60.000	2.300	1.930
0.350	1.370	0.100	70.000	2.430	2.150
0.400	1.400	0.100	80.000	2.540	2.400
0.450	1.370	0.100	90.000	2.630	2.550
0.500	1.330	0.100	100.000	2.700	2.700
0.600	1.300	0.100			
0.700	1.300	0.100			
0.800	1.300	0.100			
0.900	1.300	0.100			
1.000	1.350	0.100			

Table B-3. Optical constants and extinction coefficients of graphite

λ (μm)	$\varepsilon_{1//}$	$\varepsilon_{2//}$	$\varepsilon_{1\perp}$	$\varepsilon_{2\perp}$	α_{CS} (cm^{-1})	α_{CDE} (cm^{-1})
.050	.8308	.7056	.0472	.2385	.7359E+06	.9178E+06
.055	.7261	.7980	-.1427	.4235	.1139E+07	.1341E+07
.060	.4921	.8160	-.5625	.6800	.2062E+07	.1853E+07
.065	.2800	.9600	-1.0725	1.1500	.3511E+07	.2183E+07
.070	.0157	1.2324	-1.3464	1.7290	.3320E+07	.2244E+07
.075	0.0000	1.3878	-2.1675	2.8900	.2322E+07	.2312E+07
.080	-.0189	1.7860	-3.0000	4.0000	.1700E+07	.2318E+07
.085	-.1899	2.0160	-2.3925	9.3100	.1082E+07	.2035E+07
.090	-.379	2.4720	4.0375	8.5800	.9190E+06	.1407E+07
.095	-.7800	3.3350	5.0944	7.1010	.8044E+06	.1254E+07
.100	-.8700	4.1600	4.9500	4.3200	.6652E+06	.1028E+07
.110	1.2300	8.3600	4.3725	2.1500	.3413E+06	.7065E+06
.120	5.3300	7.5600	3.5931	.4940	.1563E+06	.3426E+06
.125	6.8400	5.6000	2.8800	.3400	.1200E+06	.2406E+06
.140	6.3000	2.2950	2.1440	.3822	.1011E+06	.1482E+06
.150	4.9104	1.1150	1.1844	.3520	.1148E+06	.1330E+06
.160	4.3739	.7980	.8820	.5468	.1730E+06	.1822E+06
.180	2.5431	.4160	.2664	1.0790	.3796E+06	.3454E+06
.200	1.4659	.3660	-.8000	1.9200	.7344E+06	.5535E+06
.220	1.170	.4400	-3.2775	3.4000	.4785E+06	.7322E+06
.240	.9657	.2376	-4.3200	5.7600	.2557E+06	.6625E+06
.250	.9424	.4800	-3.4425	7.8400	.2268E+06	.5994E+06
.260	1.0496	.4830	-2.6325	11.1300	.1666E+06	.5377E+06
.270	1.2444	.2240	.5000	12.4950	.1222E+06	.4257E+06
.300	1.5504	.2750	4.4000	9.1800	.1057E+06	.2770E+06
.350	1.8669	.2740	5.0148	7.1264	.8658E+05	.1983E+06
.400	1.9500	.2800	5.2745	6.4728	.7275E+05	.1603E+06
.450	1.8669	.2740	5.1975	6.5000	.9908E+05	.1224E+06
.500	1.7589	.2660	4.8831	7.1240	.9554E+05	.1201E+06
.600	1.690	.2600	5.3856	7.4520	.7552E+05	.9906E+05
.700	1.6800	.2600	5.3721	8.1400	.6609E+05	.8973E+05

Table B-3. Optical constants and extinction coefficients of graphite (continued)

λ (μm)	$\varepsilon_{1//}$	$\varepsilon_{2//}$	$\varepsilon_{1\perp}$	$\varepsilon_{2\perp}$	$\alpha_{CS}(cm^{-1})$	$\alpha_{CDE}(cm^{-1})$
.800	1.6800	.2600	5.4656	9.2910	.5830E+05	.8409E+05
.900	1.6800	.2600	5.4988	10.1616	.5182E+05	.7825E+05
1.000	1.8125	.2700	5.7600	10.8000	.4548E+05	.7150E+05
1.200	1.9500	.2800	6.1124	12.7200	.3626E+05	.6329E+05
1.500	1.9500	.2800	7.0225	14.9548	.2649E+05	.5227E+05
1.800	2.1509	.2940	7.7851	17.9820	.2011E+05	.4572E+05
2.000	2.2400	.3000	8.3185	19.3032	.1723E+05	.4157E+05
2.500	2.5375	.4300	10.9275	23.6200	.1209E+05	.3386E+05
3.000	2.9704	.5190	9.7875	25.3700	.1011E+05	.2988E+05
3.500	3.4371	.5580	8.9815	29.8368	.8095E+04	.2754E+05
4.000	3.8191	.5860	9.7704	33.5830	.6472E+04	.2452E+05
4.500	4.2211	.6180	11.3880	37.5238	.5203E+04	.2180E+05
5.000	4.8175	.6600	12.6840	40.0618	.4371E+04	.1953E+05
6.000	5.5000	.7050	12.9191	43.5240	.3414E+04	.1659E+05
7.000	5.7856	.7230	9.3575	48.0600	.2836E+04	.1536E+05
8.000	5.7375	.7200	7.9875	56.4300	.2226E+04	.1409E+05
9.000	5.7279	.7194	8.1979	62.7900	.1819E+04	.1270E+05
10.000	5.7183	.7188	6.4075	67.7100	.1555E+04	.1176E+05
12.000	5.4000	.7922	-9.2229	84.1160	.1147E+04	.1133E+05
15.000	5.0225	.9000	-24.9375	100.3000	.8307E+03	.9938E+04
18.000	4.5496	1.1610	-38.0975	117.9000	.6990E+03	.8756E+04
20.000	4.0800	1.4350	-75.4375	148.5000	.6323E+03	.8715E+04
25.000	3.3885	2.2388	-112.7500	195.0000	.6926E+03	.7453E+04
30.000	2.9639	3.2640	-168.0000	263.5000	.7743E+03	.6573E+04
35.000	2.855	4.2800	-242.2500	370.0000	.7648E+03	.5825E+04
40.000	2.7888	5.1584	-288.0000	471.5000	.7223E+03	.5128E+04
50.000	2.183	7.1720	-280.0000	775.5000	.6580E+03	.3929E+04
60.000	1.5651	8.8780	-55.5100	910.8000	.5649E+03	.2966E+04

Table B-3. Optical constants and extinction coefficients of graphite (continued)

λ (μm)	$\varepsilon_{1//}$	$\varepsilon_{2//}$	$\varepsilon_{1\perp}$	$\varepsilon_{2\perp}$	$\alpha_{CS}(cm^{-1})$	$\alpha_{CDE}(cm^{-1})$
70.000	1.2824	10.4490	133.7600	868.5000	.4640E+03	.2329E+04
80.000	.6916	12.1920	105.0400	812.7000	.3871E+03	.2105E+04
90.000	.4144	13.4130	46.5600	752.0000	.3279E+03	.1950E+04
100.000	0.0000	14.5800	-118.8000	779.5800	.2813E+03	.1951E+04

Table B-4. Optical constants and extinction coefficients of glassy carbon

λ (μm)	ε_1	ε_2	N	K	α_{CS} (cm^{-1})	α_{CDE} (cm^{-1})
.040	.6932	.1808	.8395	.1077	.3509E+06	.3563E+06
.050	.5189	.2629	.7418	.1772	.4636E+06	.4832E+06
.060	.3323	.5240	.6902	.3796	.8643E+06	.8811E+06
.070	.1395	.9994	.7578	.5594	.1448E+07	.1290E+07
.080	.0558	1.6843	.9330	.9026	.1686E+07	.1433E+07
.090	.7043	2.3895	1.2640	.9452	.1153E+07	.1176E+07
.100	1.6324	2.5728	1.5296	.8410	.7343E+06	.8641E+06
.120	2.7261	1.9411	1.7425	.5570	.3504E+06	.4498E+06
.140	2.8390	.6659	1.6970	.2021	.1160E+06	.1431E+06
.160	1.8971	.4179	1.3856	.1508	.9614E+05	.1037E+06
.180	1.5109	.4472	1.2423	.1800	.1122E+06	.1156E+06
.200	1.3798	.7826	1.2178	.3213	.1838E+06	.1870E+06
.220	1.0962	1.3517	1.1909	.5675	.3044E+06	.3017E+06
.240	1.2475	1.9815	1.3396	.7396	.3226E+06	.3397E+06
.260	1.5744	2.1581	1.4570	.7406	.2692E+06	.3014E+06
.280	1.8439	2.2652	1.5435	.7338	.2298E+06	.2694E+06
.300	2.0453	2.2914	1.5995	.7163	.1998E+06	.2411E+06
.350	2.4116	2.3585	1.7007	.6934	.1523E+06	.1937E+06
.400	2.6026	2.3424	1.7470	.6704	.1242E+06	.1615E+06
.450	2.7368	2.3957	1.7857	.6706	.1148E+06	.1132E+06
.500	2.8268	2.4851	1.8153	.6845	.1044E+06	.1036E+06
.600	3.0359	2.6605	1.8805	.7074	.8777E+05	.8821E+05
.700	3.1521	2.9959	1.9366	.7735	.8042E+05	.8173E+05
.800	3.3749	3.1929	2.0026	.7972	.7033E+05	.7268E+05
.900	3.4084	3.4466	2.0317	.8482	.6557E+05	.6826E+05
.920	3.4229	3.5226	2.0414	.8628	.6493E+05	.6779E+05
.940	3.4242	3.5753	2.0463	.8716	.6418E+05	.6709E+05
.960	3.4615	3.6481	2.0604	.8853	.6322E+05	.6636E+05
.980	3.4258	3.7080	2.0584	.9007	.6306E+05	.6615E+05

Table B-4. Optical constants and extinction coefficients of glassy carbon (continued)

λ (μm)	ε_1	ε_2	N	K	α_{CS} (cm^{-1})	α_{CDE} (cm^{-1})
1.000	3.6452	3.8023	2.1110	.9006	.6014E+05	.6406E+05
1.200	4.1298	4.2824	2.2449	.9536	.4932E+05	.5484E+05
1.400	4.7151	4.6160	2.3784	.9704	.3992E+05	.4644E+05
1.600	5.0430	4.8707	2.4650	.9920	.3416E+05	.4085E+05
1.800	5.4801	5.1030	2.5464	1.0020	.2911E+05	.3596E+05
2.000	5.8491	5.3733	2.6260	1.0231	.2552E+05	.3248E+05
2.500	6.8442	5.6165	2.8016	1.0024	.1815E+05	.2456E+05
3.000	7.2297	5.6681	2.8650	.9892	.1442E+05	.1994E+05
3.500	7.7058	5.9387	2.9525	1.0057	.1194E+05	.1707E+05
4.000	8.1025	6.2812	3.0294	1.0367	.1028E+05	.1515E+05
4.500	8.2643	6.1868	3.0486	1.0147	.8863E+04	.1314E+05
5.000	8.1530	6.2523	3.0354	1.0299	.8140E+04	.1203E+05
6.000	8.5799	7.2198	3.1459	1.1475	.7000E+04	.1090E+05
7.000	8.3985	7.9049	3.1569	1.2520	.6407E+04	.1015E+05
8.000	9.2497	9.4969	3.3546	1.4155	.5529E+04	.9624E+04
9.000	9.5522	10.0839	3.4236	1.4727	.4868E+04	.8774E+04
10.000	10.2428	10.9611	3.5528	1.5426	.4220E+04	.8063E+04
11.000	10.6000	11.6268	3.6286	1.6021	.3777E+04	.7499E+04
12.000	11.0701	12.0562	3.7039	1.6275	.3357E+04	.6887E+04
13.000	11.2024	12.6858	3.7501	1.6914	.3097E+04	.6543E+04
14.000	11.7419	13.4148	3.8451	1.7444	.2786E+04	.6156E+04
15.000	11.8934	13.8275	3.8815	1.7812	.2579E+04	.5826E+04
16.000	12.2703	14.4811	3.9529	1.8317	.2366E+04	.5543E+04
17.000	12.3656	15.1316	3.9942	1.8942	.2217E+04	.5349E+04
18.000	13.0275	15.9965	4.1023	1.9497	.2011E+04	.5101E+04
19.000	13.3952	16.1471	4.1369	1.9516	.1856E+04	.4813E+04
20.000	13.5307	16.5243	4.1766	1.9762	.1745E+04	.4603E+04
21.000	13.6685	17.1490	4.2189	2.0324	.1644E+04	.4469E+04
23.000	14.2323	17.9435	4.3090	2.0821	.1441E+04	.4119E+04
25.000	14.2397	19.1165	4.3633	2.1906	.1308E+04	.3945E+04

Table B-4. Optical constants and extinction coefficients of glassy carbon (continued)

λ (μm)	ϵ_1	ϵ_2	N	K	α_{CS} (cm^{-1})	α_{CDE} (cm^{-1})
27.000	14.7927	20.2703	4.4658	2.2695	.1241E+04	.3684E+04
29.000	14.9539	21.5445	4.5376	2.3740	.1141E+04	.3535E+04
31.000	15.4345	22.3080	4.6131	2.4179	.1041E+04	.3325E+04
33.000	15.4153	23.5677	4.6678	2.5245	.9716E+03	.3223E+04
35.000	16.0055	24.7082	4.7668	2.5917	.8871E+03	.3066E+04
37.000	16.1425	25.7730	4.8246	2.6710	.8277E+03	.2955E+04
39.000	16.6553	26.7136	4.9059	2.7226	.7644E+03	.2819E+04
41.000	16.7579	27.8682	4.9637	2.8072	.7171E+03	.2734E+04
43.000	17.2855	28.7237	5.0403	2.8494	.6662E+03	.2613E+04
45.000	17.5537	29.7915	5.1055	2.9176	.6247E+03	.2527E+04
50.000	18.5925	31.4865	5.2516	2.9978	.5356E+03	.2284E+04
55.000	18.2377	33.8666	5.3246	3.1802	.4800E+03	.2167E+04
60.000	18.7027	36.0256	5.4449	3.3082	.4242E+03	.2024E+04
65.000	17.8914	38.4061	5.4891	3.4984	.3879E+03	.1950E+04
70.000	18.4942	41.9212	5.6707	3.6963	.3400E+03	.1856E+04
75.000	18.1405	43.4166	5.7094	3.8022	.3134E+03	.1766E+04
80.000	18.2833	46.7814	5.8526	3.9965	.2804E+03	.1697E+04
85.000	17.6025	48.9788	5.9012	4.1499	.2592E+03	.1639E+04
90.000	17.3795	51.4302	5.9861	4.2958	.2376E+03	.1577E+04
95.000	15.2082	53.2932	5.9426	4.4840	.2257E+03	.1555E+04
100.000	17.3215	60.8160	6.3465	4.7913	.1893E+03	.1491E+04
105.000	22.4760	64.7425	6.7457	4.7988	.1628E+03	.1363E+04
205.000	43.9262	119.5903	9.2555	6.4605	.4555E+02	.7094E+03
305.000	37.6603	167.3121	10.2264	8.1604	.2396E+02	.5341E+03
405.000	51.2939	222.4011	11.8223	9.4060	.1358E+02	.4039E+03
505.000	54.4501	241.3914	12.2863	9.8236	.1007E+02	.3257E+03
605.000	46.7167	311.0457	13.4397	11.5719	.6728E+01	.2882E+03
705.000	44.1477	352.5256	14.1320	12.4726	.5135E+01	.2522E+03
805.000	49.8105	403.6371	15.1081	13.3583	.3931E+01	.2216E+03
905.000	73.5612	470.0931	16.5737	14.1619	.2975E+01	.1932E+03

BLANK

SELECTED BIBLIOGRAPHY

Abdelrhaman, M., Fumeaux, P., and Suter, P., Solar Energy 22, 45 (1979).

Arakawa, E. T., Williams, M. W., and Inagaki, T., J. Appl. Phys. 48, 3176 (1977).

Blea, J. M., Parks, W. F., Ade, P. A. R., and Bell, R. J., J. Opt. Soc. Am. 60, 603 (1970).

Bohren, C. F., and Huffman, D. R., Absorption and Scattering of Light by Small Particles (New York: John Wiley, 1983).

Carter, J. G., Huebner, R. H., Ham, R. N., and Birkhoff, R. D., Phys. Rev. 137A, 639 (1965).

Chylek, P., Ramaswany, V., Cheng, R., and Pinnick, R. G., Appl. Optics 20, 2980 (1981).

Dalzell, W. H., and Sarofin, A. F., J. Heat Transf. 91, 100 (1969).

Daniels, J., Festenberg, C. V., Raether, H., and Zeppenfeld, K., Springer Tracts in Mod. Phys. 54, 77 (1970).

Day, K. L., and Huffman, D. R., Nature 243, 50 (1973).

Debye, P., Annln. Phys. 30, 59 (1909).

Decker, D., Ph.D. Dissertation, University of California, Riverside (1969).

DiNardo, R. P., and Goland, A. N., J. Opt. Soc. Am. 61, 1321 (1971).

Ergun, S., Nature 213, 135 (1967).

Faxvog, F. R., and Roessler, D. R., Appl. Optics 16, 2612 (1978).

Foster, P. J., and Howarth, C. R., Carbon 6, 719 (1968).

Gouw, T. H., Guide to Modern Methods of Instrumental Analysis (New York: John Wiley, 1972).

Greenaway, D. L., Harbeke, G., Bassani, F., and Tossati, E., Phys. Rev. 178, 1340 (1969).

Hagemann, H. J., Gudat, W., and Kuntz, C., Deutsches Electronen-Synchrotron DESY SR-74/7 (1974).

Halpin, M. K., and Jenkins, G. M., Proc. Roy. Soc. Lond. A 313, 421 (1969).

Howarth, C. R., Foster, P. J., and Thring, M. W., Proceeding of the Third Int. Heat Transf. Conference 5, 122 (1966).

Huffman, D. R., Department of Physics, University of Arizona, Tucson, private communication (1979).

_____, Adv. in Phys. 26, 129 (1977).

_____, Astr. and Space Sci. 34, 175 (1975).

Huffman, D. R., and Bohren, C. F., in Light Scattering by Irregularly Shaped Particles, D. W. Shuerman, ed. (New York: Plenum Press, 1980).

Hunt, A. J., in Topical Meeting on Optical Phenomena Peculiar to Matter of Small Dimensions, Opt. Soc. of America (1980).

_____, in Proceeding of the 13th Intersociety Energy Conversion Engineering Conference, Boston, MA, Aug. 5-10 (1979).

_____, Small Particle Heat Exchangers, Lawrence Berkeley Laboratory Report LBL 7841 (1978).

Jackson, J. D., Classical Electrodynamics, 2nd ed. (New York: John Wiley, 1975).

Janzen, J., J. Coll. Inter. Sci. 69, 436 (1979).

Kerker, M., The Scattering of Light and Other Electromagnetic Radiations (New York: Academic Press, 1969).

Kittel, C., Introduction to Solid State Physics, 5th ed. (New York: John Wiley, 1976).

Klucker, R., Thesis, University of Munich (1971).

Klucker, R., Skibowski, M., and Steinman, W., Phys. Stat. Sol. (B) 65, 703 (1974).

Koike, C., Hasegawa, H., and Manabe, A., Astr. and Space Sci. 67, 495 (1980).

Lee, S. C., and Tien, C. L., in Eighteen International Symposium on Combustion, The Combustion Institute (1981).

Lefevre, J., Astro. Astrophys. 5, 37 (1970).

Lehnam, A. P., and Treherne, D. M., The Observatory 86, 36 (1966).

Mallett, C. P., Phys. C: Solid State Phys. 14, 1213 (1981).

Mie, G., Annln. Phys. 25, 377 (1908).

Miller, R. G., Laboratory Methods in Infrared Spectroscopy (London: Heyden, 1972).

National Academy of Sciences, Understanding Climatic Change, A Program for Action (Washington, DC: NAS, 1975).

Philipp, H. R., Phys. Rev. 16B, 2896 (1977).

Pluchino, A. B., Goldberg, S. S., Dowling, J. M., and Randal, C. M., Appl. Optics 19, 3370 (1980).

Purcell, E. M., Astrophys. J. 158, 433 (1969).

Rathmann, J., Ph.D. Dissertation, University of Arizona, Tucson (1981).

Sato, Y., J. Phys. Soc. Jpn. 24, 489 (1968).

Shobert II, E. I., in Modern Materials, Vol. 4, B. W. Gouser and H. H. Hausner, eds. (New York: Academic Press, 1964).

Steyer, T. R., Ph.D. Dissertation, University of Arizona, Tucson (1974).

Stull, V. R., and Plass, G., J. Opt. Soc. Am. 50, 121 (1960).

Taft, E. A., and Philipp, H. R., Phys. Rev. 138A, 197 (1965).

Tomaselli, V. P., Rivera, R., Edewaard, D. C., and Möller, K. D., Appl. Optics 20, 396 (1981).

Tossati, E., and Bassani, F., Nuovo Cimento 65B, 161 (1970).

Twitty, J. T., and Weiman, J. A., J. Appl. Meteo. 10, 725 (1971).

Twomey, S., and Huffman, D. R., in Light Absorption by Aerosol Particles (Hampton, VA: Spectrum Press, 1982).

van de Hulst, H. C., Light Scattering by Small Particles (New York: John Wiley, 1957).

Venghaus, H., Phys. Stat. Sol. (B) 71, 609 (1975).

_____, Phys. Stat. Sol. (B) 81, 221 (1977).

Walker, P. L., Jr., in Ultrafine Particles, W. E. Kuhn, ed. (New York: John Wiley, 1963).

Wickramasinghe, N. C., Light Scattering Functions for Small Particles (London: Adam Hilger, 1973).

Williams, M. W., and Arakawa, E. T., J. Appl. Phys. 43, 3460 (1972).

Wooten, F., Optical Properties of Solids (New York: Academic Press, 1972).

Zeppenfeld, K., Phys. Lett. 25A, 335 (1967).

*U.S. GOVERNMENT PRINTING OFFICE:1987-[illegible]